

Diss. ETH No. 16989

**Experimental and theoretical investigations
on lipid bilayer permeation**

A dissertation submitted to the
SWISS FEDERAL INSTITUTE OF TECHNOLOGY ZURICH

for the degree of
Dr. sc. ETH Zurich

presented by
ANITA VERENA THOMAE

Dipl. pharm.
born 06.05.1979
citizen of Germany

accepted on the recommendation of
Prof. Dr. Heidi Wunderli-Allenspach, examiner
Prof. Dr. Karl-Heinz Altmann, co-examiner
Dr. Stefanie D. Krämer, co-examiner

Zurich, 2007

Mit dem Wissen wächst der Zweifel.

J. W. von Goethe

Contents

1	Introduction	1
1.1	Membrane permeation as a key process in successful drug delivery	1
1.1.1	The biological membrane: structure and permeation pathways	1
1.1.2	Mechanisms of transbilayer diffusion of molecules	2
1.1.3	Factors influencing lipid bilayer permeation	3
1.1.4	Structure-permeation relationships	7
1.1.5	The influence of the lipid composition on bilayer characteristics	7
1.2	Liposomes as model membranes	8
1.3	Membrane permeation assays	8
1.3.1	Permeation studies with planar lipid bilayers	9
1.3.2	Liposomal permeation assays	9
1.3.3	Artificial barriers for high-throughput screening assays	10
1.4	The Terbium(III) luminescence and permeation assay	11
1.4.1	Terbium(III)-sensitized luminescence	11
1.4.2	The Terbium(III)-permeation assay	12
1.5	Multivariate Analysis	13
1.5.1	Objectives of Multivariate Analysis	13
1.5.2	Principal Component Analysis	14
1.5.3	Cluster Analysis	14
1.5.4	Partial Least Square Analysis	15
1.6	Aim of the thesis	15
2	Materials and Methods	17
2.1	Chemicals and Buffers	17
2.1.1	Chemicals	17
2.1.2	Radiochemicals	17
2.1.3	Lipids	18
2.1.4	Peptides	18
2.1.5	Buffer solutions	18
2.2	Lipid quantification	19
2.2.1	Quantification of lipids by Thin Layer Chromatography	19
2.2.2	Quantification of lipids by High Pressure Liquid Chromatography	19
2.2.3	Enzymatic quantification of lipids	19
2.3	Determination of pK_a values	20
2.3.1	Potentiometric titration	20
2.3.2	UV absorbance measurements	20
2.3.3	^{13}C -NMR measurements	20
2.3.4	pK_a of Stearylamine by Zetapotential measurements	21
2.3.5	Calculation of the molar fractions of the various ionization species	21

2.4	Determination of $\log P_{Oct}$ and $\log D_{pH}$ values	22
2.5	Liposomes	22
2.5.1	Preparation of liposomes	22
2.5.2	Characterization of liposomes	23
2.6	Determination of membrane affinities	23
2.6.1	Equilibrium dialysis	23
2.6.2	Data analysis	24
2.7	Interaction of ACAs with Tb^{3+} in solution	24
2.8	Lipid bilayer permeation	25
2.8.1	Tb(III)-permeation assay	25
2.8.2	Data analysis	25
2.9	Description of the permeation process by a differential equation system	27
2.9.1	Definition of the rate laws	27
2.9.2	Solutions of the differential equation system	28
2.9.3	Estimation of the volumes of the aqueous and lipid phases	28
2.9.4	Relationship between true and apparent rate constants	30
2.10	Multivariate Analysis	30
2.10.1	Source of calculated molecular descriptors	30
2.10.2	Preprocessing of molecular descriptors	31
2.10.3	Settings for the Multivariate Analysis	31
3	Results	33
3.1	Characterization of the test compounds and lipids	33
3.1.1	Determination of pK_a and $\log P_{Oct}$ values of test compounds	33
3.1.2	Determination of the pK_{aM} of stearylamine	36
3.2	Membrane affinity	37
3.2.1	Stability of radiolabeled compounds	37
3.2.2	Affinity to phosphatidylcholine bilayers	38
3.2.3	Influence of cholesterol on membrane affinity	38
3.2.4	Influence of phosphatidylinositol on membrane affinity	40
3.2.5	Influence of stearylamine on membrane affinity	41
3.3	The Tb(III)-permeation assay	42
3.3.1	Interaction of test compounds with Tb^{3+}	42
3.3.2	Characterization of the Tb(III)-permeation assay	45
3.4	Membrane permeation	51
3.4.1	Influence of the solute ionization state on membrane permeation	51
3.4.2	Influence of the lipid bilayer composition on membrane permeation	54
3.5	Structure-permeation relationships	60
3.5.1	„Biomix” lipid composition and verification thereof	60
3.5.2	Permeation profiles with egg phosphatidylcholine and biomix liposomes	60
3.5.3	Multivariate analysis of permeation data	65
3.5.4	Structure-permeation relationships: Conclusions	74
3.5.5	Study design for further investigations	75
3.6	Permeation of peptides across lipid bilayers	78
3.6.1	Peptide characterization	78
3.6.2	Interaction of DPA-labeled peptides with Tb^{3+}	78
3.6.3	Permeation of peptides across egg phosphatidylcholine bilayers	80

3.6.4	pH-Dependent permeation behaviour of DPA- β^3 hVal- β^3 hAla- β^3 hLeu-OH	80
3.6.5	Comparison of the lipid-bilayer permeation of the α - and β -peptides and influence of the molecular weight	82
3.7	Simulations of lipid bilayer permeation	83
3.7.1	Simulation of the influence of P and the translocation rate constants . .	83
3.7.2	Simulation of the influence of the lipid concentration	84
3.7.3	Simulation of the influence of the Tb(III) complex association constant	84
4	Discussion	87
5	Conclusions and Outlook	99
	Bibliography	101
	Acknowledgements	115
	Curriculum vitae	117
	Publication list	119

List of Tables

3.1	pK_a and $\log P_{Oct}$ values of test compounds	33
3.2	Affinity parameters to PhC, PhC/Chol, PhC/PhI, and PhC/StAm membranes . .	38
3.3	Excitation maxima of the Tb(III)-ACA complexes	44
3.4	Influence of the intraliposomal buffer capacity on the $\log Perm_{app}$ of SA	48
3.5	Influence of the buffer type on the permeation coefficient	49
3.6	Influence of the solute ionization state on membrane permeation	51
3.7	Permeation parameters with PhC, PhC/Chol, PhC/PhI, and PhC/StAm membranes	54
3.8	Composition of biomix liposomes	60
3.9	Permeation parameters in PhC and biomix liposomes	62
3.10	Molecular descriptors	68
3.11	Correlations between $\log Perm$ and molecular descriptors	72
3.12	Peptide characterization	79

List of Tables

List of Figures

1.1	Model of lipid bilayer permeation of an amphiphilic molecule	2
1.2	Principle of the permeation rate correction for the unstirred water layer	6
1.3	Phase diagram of lipid/cholesterol membranes	8
1.4	Principle of energy transfer	12
1.5	Principle of the Tb(III)-assay	13
1.6	Principle of Principal Component Analysis	14
2.1	Maple script for the solution of a differential equation system	29
3.1	Salicylic acid derivatives	34
3.2	Halogenated benzoic acid derivatives	34
3.3	Amino benzoic acid derivatives	34
3.4	Heteroaromatic benzoic acid derivatives	35
3.5	Large aromatic carboxylic acids	35
3.6	Determination of the pK_a of SA by ^{13}C -NMR	36
3.7	Stearylamine: Determination of pK_{aM}	37
3.8	Stability of radiolabeled compounds	37
3.9	Membrane affinities to PhC and PhC/Chol 60/40 bilayers	39
3.10	Membrane affinities to PhC and PhC/PhI 70/30 bilayers	40
3.11	Membrane affinities to PhC and PhC/StAm 85/15 bilayers	41
3.12	Interaction of test compounds with Tb^{3+}	42
3.13	Finding of optimal phosphorescence conditions	43
3.14	pH-Dependent excitation spectra of the Tb(III)-SA complex	44
3.15	Kinetics of the complex formation between Tb^{3+} and SA	45
3.16	Kinetic analysis of the permeation curve	46
3.17	Monitoring the pH at the membrane surface	47
3.18	Influence of the solute concentration on the PhC bilayer permeation of SA	49
3.19	Influence of the lipid concentration on the PhC bilayer permeation of SA	50
3.20	Influence of the solute ionization state on membrane permeation	52
3.21	Influence of counterions on the permeation coefficients	53
3.22	Influence of the bilayer state on membrane permeation	54
3.23	Influence of the lipid composition on the membrane permeation of SA	55
3.24	Influence of the lipid composition on the membrane permeation of AA	57
3.25	Influence of the lipid composition on the membrane permeation of OHNA	59
3.26	Verification of biomix composition	61
3.27	Salicylic acid derivatives: Permeation profiles PhC vs. biomix	63
3.28	Halogenated benzoic acid derivatives: Permeation profiles PhC vs. biomix	63
3.29	Amino benzoic acid derivatives: Permeation profiles PhC vs. biomix	64
3.30	Heteroaromatic benzoic acid derivatives: Permeation profiles PhC vs. biomix	64

List of Figures

3.31	Large benzoic acid derivatives: Permeation profiles PhC vs. biomix	65
3.32	Distribution range of parameter values	67
3.33	Correlation between experimental $\log P_{Oct}$ and predicted $\log P_{Oct}$	69
3.34	PCA of X-matrix	70
3.35	PCA of Y-matrix	70
3.36	Cluster dendrogram of the X-matrix	71
3.37	PLS $\log Perm_{PhC}^{AH}$	73
3.38	PLS $\log Perm_{BM}^{AH}$	74
3.39	Study design - Suggested structures	75
3.40	Study design - Distribution range of selected parameters	77
3.41	Interaction of peptides with Tb^{3+}	80
3.42	Permeation of peptides across PhC bilayers	81
3.43	Influence of the pH on the permeation of peptide 3	81
3.44	Influence of the MW on the permeation of α - and β -peptides	82
3.45	Simulation of membrane permeation as function of P and k'_2	83
3.46	Simulation of the influence of the lipid concentration	84
3.47	Simulation of the influence of the complex association constant	85
4.1	Simulation of the permeation profiles of an acidic compound	89
4.2	PermSim - interactive simulation of membrane permeation	96

List of Abbreviations

A	Hydrogen-bond acidity
AA	Anthranilic acid
ABRPOL	Polarizability
AC	Anthracene-9-carboxylic acid
ACA	Aromatic carboxylic acid
Ala	Alanine
Arg	Arginine
B	Hydrogen-bond basicity
CF	5,6-Carboxyfluorescein
CFDA	5-Carboxyfluorescein diacetate
Chol	Cholesterol
CSA	5-Chlorosalicylic acid
DCBA	3,5-Dichlorobenzoic acid
DHB	2,4-Dihydroxybenzoic acid
DPA	Dipicolinic acid
DPPC	Dipalmitoylphosphatidylcholine
EXPP	Experimentally determined octanol/water partition coefficient
HI	Hydrophilicity index
Leu	Leucine
MAA	5-Methylantranilic acid
MIPSA	Polar surface area
MRI	Molecular refractivity
MSA	3-Methylsalicylic acid
MOPS	3-(N-Morpholino)propanesulfonic acid
MV	Molecular volume
MVA	Multivariate analysis
MW	Molecular weight
NHA	Number of hydrogen bond acceptors
NHD	Number of hydrogen bond donors
NROTB	Number of rotatable bonds

List of Abbreviations

Oct	Octanol
OHNA	2-Hydroxynicotinic acid
PC	Principal component
PCA	Pyrazine carboxylic acid
PhC	Phosphatidylcholine
PhE	Phosphatidylethanolamine
PhI	Phosphatidylinositol
PhS	Phosphatidylserine
POL	Polarizabilty
Py	Pyridine
R2	Excess molar refraction
SA	Salicylic acid
StAm	Stearylamine
SUBS	Standardized universal buffer solution
Tb	Terbium
TIE	E-state topological parameter
TPSA	Topological polar surface area
TRIS	Tris(hydroxymethyl)aminomethan
USI	Unsaturation index
UWL	Unstirred water layer
Val	Valine
VIP	Variable importance for the projection

List of Symbols

α	Molar fraction
$[A]$	Solute concentration
A^{2-}	Di-deprotonated species
A^-	Deprotonated species
AH	Net neutral species
AH_2^+	Cationic species
ai	Inner aqueous phase
ao	Outer aqueous phase
c	Weight (in PLS)
D	Distribution coefficient
k	Rate constant
k'	Apparent rate constant
λ_{ex}	Excitation wavelength
λ_{em}	Emission wavelength
li	Inner lipid leaflet
lo	Outer lipid leaflet
MW	Molecular weight
p	Loading
P	Partition coefficient
$Perm$	Permeation coefficient
$Perm^{AH^*}$	Extrapolated permeation coefficient applying the pH-partition hypothesis
Q^2	Predicted variance
r	Liposomal radius
R^2	Explained variance
Rf	Retention factor
t	Score
t_{90}	Time, when 90% of the plateau concentration is reached
T_m	Transition temperature
V_{norm}	Normalization volume

List of Symbols

Summary

The permeation across biological membranes is a key process in successful drug therapy. The diffusion across the lipid bilayer is the most important permeation mechanism of drugs. Methods to distinguish lipid bilayer permeation from other processes are rare and hence, it is not yet understood, how this process is controlled.

The present thesis is focused on the investigation of lipid bilayer permeation combining experimental and theoretical approaches. Liposomes are used to model biological membranes for the investigation of membrane-related processes, i.e. binding to and permeation across the membrane. Membrane affinities were determined using the well-established equilibrium dialysis system, while membrane permeation was tested with the Tb(III)-assay. It is based on the interaction of Tb(III) with aromatic carboxylic acids (ACAs), which results in a characteristic luminescence signal. Thus, the permeation of ACAs into Tb³⁺-loaded liposomes can directly be followed by luminescence measurements. To understand the interplay of the single rate constants, a system of differential equations to model the permeation process was developed and solved numerically.

The characterization of the Tb(III)-assay showed that the complex formation between Tb³⁺ and the ACAs is faster than the permeation process and that the degree of complexation does not affect the permeation rate. The obtained permeation coefficients were independent of the ACA concentration, but increased with increasing lipid concentration. This effect is due to the changed volume ratios in the system and were in agreement with the simulations based on the rate constants of the system.

In total, the permeation profiles of thirteen ACAs were measured with at least two different lipid compositions. For all tested ACAs except of carboxyfluorescein and carboxyfluorescein diacetate we found a significant contribution of the anionic species to the overall permeation rate. The permeation coefficients of the net neutral species ($Perm^{AH}$) were generally higher or equal as compared to the permeation coefficients of the anionic species ($Perm^{A^-}$). The differences between $Perm^{AH}$ and $Perm^{A^-}$ were 12 – 600 resulting in sigmoidal permeation profiles with two plateaus determined by the intrinsic permeation coefficients of the net neutral and anionic species. Due to the low ratio between $Perm^{AH}$ and $Perm^{A^-}$ the permeation of the tested ACAs is controlled by the anionic species at the physiological pH 7.4. These findings are in contrast to the pH-partition hypothesis, which predicts negligible permeation of ionized molecules. The permeation of the anionic species were affected by the buffer composition, but not by the bilayer state, i.e. by the bilayer fluidity.

Membrane permeation has often been directly related to membrane affinity. A decrease of the membrane affinity would thus result in a decreased permeation rate. To test this hypothesis, we determined the affinity and permeation profiles of three representative ACAs with phosphatidylcholine bilayers or membranes of phosphatidylcholine mixed with cholesterol or the charged lipids phosphatidylinositol and stearylamine, respectively. The influence of the lipid composition on the pH-dependent membrane affinity was in accordance with the membrane rigidity and possible electrostatic interactions between the acids and the lipids and was consistent for the different ACAs. However, no direct relationship between the affinity and permeation profiles

Summary

was found. This discrepancy was closer analyzed with numerical simulations of the permeation process based on the single rate constants for partitioning and translocation. The simulations were in line with our experimental findings. Depending on the single rate constants and on the geometry of the system, permeation may correlate positively, negatively or not at all with the respective affinity.

In a pilot study, multivariate analysis techniques were applied to explore the relationship between physicochemical ACA properties and the intrinsic permeation coefficients. While the solute's lipophilicity as expressed by the octanol/water partition coefficient was found to be favorable for lipid bilayer permeation, the hydrogen bond capacities and hydrophilicity parameters of the permeant need to be in an optimal range. The structure-permeation relationship study was, however, limited by the uneven distribution of some of the molecular descriptors and has to be extended in the future.

The Tb(III)-assay was also used to investigate the permeation of twelve α - and β -peptides across egg phosphatidylcholine bilayers. For this purpose, the peptides were coupled to dipicolinic acid which worked as probe for the Tb(III)-assay. The peptides contained two to six amino acids with hydrophobic side chains, except of β -octaarginin, which was used as negative control. The β -peptides permeated faster than their α -analogs, indicating different interactions with lipid bilayer.

Zusammenfassung

Ein Schlüsselprozess für die erfolgreiche Therapie mit Arzneistoffen ist die Arzneistoffpermeation durch biologische Membranen. Neben anderen Transportrouten ist die Diffusion des Arzneistoffes durch die Lipiddoppelschicht der wichtigste Permeationsmechanismus. Es gibt nur wenig Systeme, um ausschliesslich passive Membranpermeation zu testen, was das Verständnis dieses Prozesses erschwert.

Die vorliegende Dissertation untersucht die Permeation von arzneistoffähnlichen Molekülen und kleinen Peptiden durch die Lipiddoppelschicht. Dazu wurden experimentelle und theoretische Ansätze kombiniert. Liposomen dienen als Modelle der biologischen Membran, um membran-bezogene Prozesse wie z.Bsp. Membranaffinitäten und Membranpermeationen zu analysieren. Membranaffinitäten wurden mittels der Gleichgewichtsdialyse bestimmt, welche ein etabliertes Testsystem darstellt. Zur Untersuchung der Membranpermeation kam eine neuartige experimentelle Methode, der Tb(III)-assay, zum Einsatz. Diese Methode basiert auf der Wechselwirkung von Tb(III) mit aromatischen Carbonsäuren (ACAs), welche ein charakteristisches Lumineszenzsignal zur Folge hat. Die Permeation von ACAs in Tb³⁺-gefüllte Liposomen kann daher direkt durch Lumineszenzmessungen verfolgt werden. Um das Verständnis über das Zusammenspiel der einzelnen Geschwindigkeitskonstanten im Gesamtpermeationsprozess zu erleichtern, wurde zusätzlich ein Differentialgleichungssystem aus einem 3-Stufen-Permeationsmodell hergeleitet und numerisch gelöst.

Die Charakterisierung des Tb(III)-assays zeigte, dass die Komplexbildung zwischen Tb³⁺ und den ACAs schneller ist als die Permeation durch die Lipiddoppelschicht. Weiterhin wird die Permeationsrate nicht durch die Komplexbildungskonstante beeinflusst. Die gemessenen Permeationskoeffizienten waren unabhängig von der ACA-Konzentration, stiegen jedoch mit zunehmender Lipidkonzentration. Dies ist durch die veränderten Volumenverhältnisse im System bedingt. Die gemessene Abhängigkeit stimmt überein mit den theoretischen Simulationen, welche auf den verschiedenen Geschwindigkeitskonstanten im System aufbauten.

Die Permeationsprofile von insgesamt 13 ACAs wurden mit mindestens zwei verschiedenen Membranzusammensetzungen gemessen. Die Permeationsrate von allen ACAs ausser Carboxyfluorescein und Carboxyfluoresceindiacetat wurde wesentlich durch die Permeation der ionisierten Molekülspezies beeinflusst. Die Permeationskoeffizienten der ungeladenen Spezies ($Perm^{AH}$) waren 12 bis 600 mal höher oder gleich den Permeationskoeffizienten der anionischen Spezies ($Perm^{A^-}$). Die resultierenden Permeationsprofile verliefen sigmoidal mit zwei Plateaus, die durch die intrinsischen Permeationskoeffizienten der neutralen und anionischen Spezies bestimmt wurden. Bedingt durch den kleinen Unterschied zwischen $Perm^{AH}$ und $Perm^{A^-}$ wird bei physiologischem pH 7.4 die Gesamtpermeationrate durch die Permeation der anionischen Spezies bestimmt. Diese Ergebnisse stehen im Gegensatz zur sogenannten pH-Verteilungs-Hypothese, welche von einer vernachlässigbar kleinen Permeation ionisierter Moleküle ausgeht. Die Permeation ionisierter Moleküle wurde beeinflusst durch die Wahl der Puffer, war jedoch unabhängig von der Fluidität der Lipiddoppelschicht.

Membranpermeation wird oft in direkten Zusammenhang mit der Membranaffinität eines Moleküls gebracht. Demnach würde eine Verminderung der Affinität eine verlangsamte Per-

meation verursachen. Um diese Hypothese zu untersuchen, bestimmten wir die Affinitäts- und Permeationsprofile von drei repräsentativen ACAs mit Phosphatidylcholin-Liposomen und mit Membranen, die eine Mischung aus Phosphatidylcholin und Cholesterol oder den geladenen Lipiden Phosphatidylinositol und Stearylamin enthielten. Der Einfluss der Lipidzusammensetzung auf die pH-abhängige Membranaffinität folgte leicht interpretierbaren Regeln bezüglich der Membranrigidität und elektrostatischen Wechselwirkungen zwischen den Testsubstanzen und den Membranen. Die Effekte der einzelnen Lipide waren ähnlich für die unterschiedlichen ACAs. Es konnte jedoch kein direkter Zusammenhang zwischen den Affinitäts- und Permeationsprofilen gefunden werden. Dieser scheinbare Widerspruch konnte näher analysiert werden durch die numerische Simulation des Permeationsprozesses als Wechselspiel der einzelnen Geschwindigkeitskonstanten für die Verteilung in die Lipiddoppelschicht und den Übertritt zwischen den Lipidschichten. In Abhängigkeit von den Geschwindigkeitskonstanten und den Systemdimensionen kann eine Abnahme der Membranaffinität zu einer Zunahme oder Abnahme der Membranpermeation führen, oder kann auch ohne Effekt bleiben.

In einer Pilotstudie wurde der Zusammenhang zwischen den physikochemischen Eigenschaften der ACAs und ihren Permeationskoeffizienten mittels multivariater Analysetechniken untersucht. Die Lipophilie der Moleküle, welche als Oktanol/Wasser-Verteilungskoeffizient gemessen wurde, war ein begünstigender Faktor für die Membranpermeation. Die Analyse zeigte weiterhin, dass für die Hydrophilie und die Wasserstoffbrückenkapazitäten der Moleküle ein optimaler Bereich existiert. Diese Studie war jedoch limitiert durch die unausgeglichene Verteilung von einigen Eigenschaftsvariablen und sollte deshalb systematisch erweitert werden.

Der Tb(III) assay wurde weiterhin eingesetzt, um die Permeation von zwölf α - und β -Peptiden über Phosphatidylcholinmembranen zu untersuchen. Dazu wurde Dipicolinsäure als Tb(III)-Sonde an die Peptide gekoppelt. Die Peptide bestanden aus zwei bis sechs Aminosäuren mit hydrophoben Seitenketten, ausserdem wurde β -octaarginin als Negativkontrolle getestet. Die Ergebnisse zeigen, dass die β -Peptide schneller permeieren als ihre α -verknüpften Analoga. Dies weist darauf hin, dass β -Peptide anders mit der Lipidmembran in Wechselwirkung treten als α -Peptide.

1 Introduction

1.1 Membrane permeation as a key process in successful drug delivery

1.1.1 The biological membrane: structure and permeation pathways

Theories on the origin of life postulate that liposome-like vesicles were precursors of primitive cellular life. Membranes came first – and provided a closed and regulated internal milieu for the development of life [Deamer, 1997]. At any rate, membranes still maintain this important function and play a central role in the definition of cells and cell compartments as well as the communication between them.

Cell membranes consist of a variety of lipids and proteins. The several hundred lipid species form bilayers of a few nanometer thickness with the apolar lipid acyl chains pointing towards the center of the bilayer and the polar headgroups facing the aqueous phase on either side of the membrane [Alberts et al., 2005; Singer and Nicolson, 1972]. Proteins are embedded in the lipid bilayer, either spanning the membrane or being associated to the inner or the outer lipid leaflet. To our current understanding, the distribution of lipid species and proteins is specific within the lipid bilayers and between the two leaflets. Cell membranes consist of dynamic domains with distinct lipid and protein compositions [Engelman, 2005; Simons and Toomre, 2000]. The lipid bilayer is increasingly realized to function not only as a matrix for embedded proteins but to contribute significantly to protein functions and malfunctions [Cordy et al., 2006; Pinheiro, 2006; Simons and Ehehalt, 2002].

Membranes are not closed boundaries, but regulate the passage of molecules by different mechanisms. The three main pathways of transmembrane solute permeation are (i) simple diffusion, (ii) carrier-mediated diffusion and (iii) active transport [Krämer and Wunderli-Allenspach, 2001]. Electrolytes can in addition permeate via ion-selective pores formed by membrane proteins. Simple diffusion describes the passive movement of solutes through the lipid bilayer following their concentration gradient involving neither carrier nor channel proteins. Carrier-mediated diffusion, instead, describes the facilitated transport of a solute by proteins following its concentration gradient. Active transport comprises all transport processes that require an active binding of the solute to a transporter protein which transports the solute either into the cells or effluxes it from cells, both under energy consumption.

The permeation of drugs across the membrane barrier determines their pharmacokinetic behaviour, which can be critical for the failure or success of a drug. Despite its significance as most important transport mechanism for drugs, lipid bilayer diffusion is poorly understood [Malkia et al., 2004; Kerns, 2001].

1.1.2 Mechanisms of transbilayer diffusion of molecules

The passive diffusion of solutes across the lipid bilayer is described by two theories: The solubility-diffusion model and the flip-flop model. The solubility-diffusion model approximates the biological membrane as a homogeneous barrier [Stein, 1997; Diamond and Katz, 1974]. Lipid bilayer permeation is assumed to follow Fick's first law, which is modified to eq. 1.1 where $Perm$ [$cm \cdot s^{-1}$] is the membrane permeability, P the partition coefficient of the solute, D_m [$cm^2 \cdot s^{-1}$] the diffusion coefficient in the membrane and h [cm] the membrane thickness. Higher partition coefficients lead to a higher concentration gradient within the membrane and thus to an increased permeability.

$$Perm = \frac{D_m \cdot P}{h} \quad (1.1)$$

The solubility-diffusion model was extrapolated to an inhomogeneous membrane by Xiang et al. [1998], assuming that the total solute permeability is limited by the so-called barrier domain, i.e. the region of lowest permeability. This model can provide a sufficient estimate for the transbilayer movement of hydrophilic and hydrophobic solutes [Paula et al., 1998; Stein, 1997; 1986].

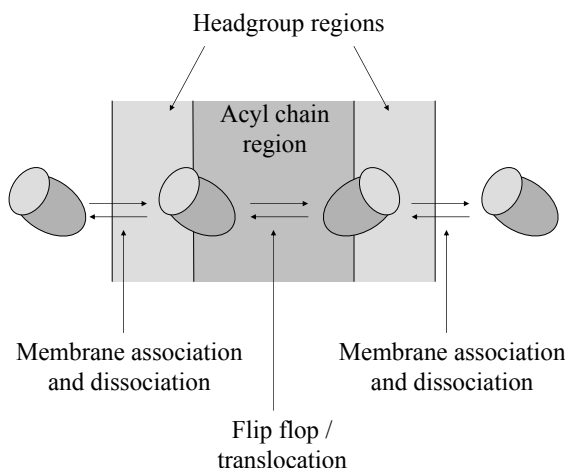


Figure 1.1: Model of lipid bilayer partitioning and permeation of an amphiphilic molecule. The polar headgroup and the hydrophobic acyl chain regions of a lipid bilayer are indicated in light and dark grey, respectively. Four favored positions of an amphiphilic molecule are shown. In the membrane, its hydrophilic moiety (light grey) locates towards the lipid headgroup region and the hydrophobic part (dark grey) orients towards the hydrophobic acyl chains. The molecule partitions between the aqueous phase and the two lipid leaflet and translocates between the two lipid leaflets. The corresponding equilibria are indicated. Adapted from Krämer [2006].

Most drugs, however, hold amphiphilic properties and their permeation behaviour is better described by the flip-flop model [Eytan, 2005; Eytan and Kuchel, 1999] as depicted in Fig. 1.1. After association of the solute to the outer lipid leaflet of the membrane, the translocation from the outer to the inner lipid leaflet is, in contrast to the solubility-diffusion model, considered as distinct flip-flop events and not as diffusion down a gradient. From the inner lipid leaflet

the drugs can dissociate to the inner aqueous phase or flop backwards to the outer leaflet. The permeation can be described by three reversible consecutive reactions as suggested by Lauger et al. [1981] with A_{ao} , the solute A in the outer aqueous phase, A_{lo} and A_{li} the solute in the outer and inner lipid leaflet, respectively, and A_{ai} the solute in the inner aqueous phase (eq. 1.2).



The flip-flop model is more appropriate to describe permeation of drugs than the solubility-diffusion model, since it considers also the anisotropic properties of the lipid bilayer, rather than simplifying it to a lipophilic bulk.

1.1.3 Factors influencing lipid bilayer permeation

For the transbilayer movement of a drug as described in section 1.1.2 the molecule must partition into and translocate across the membrane. These processes are influenced by several factors, which will be discussed in this section. Among the solute properties, the partition coefficient P , the solute charge, the hydrogen bonding capacities, the molecular size and flexibility are the most important variables determining transmembrane diffusion. The electrostatic properties of the lipid barrier affect the permeation process as well as its dynamic properties [Malkia et al., 2004].

Partition coefficient P

According to the rule of Overton [Overton, 1899] the tendency of a solute to cross a biological membrane is directly correlated to the tendency of this solute to enrich in an organic lipophilic solvent. The partition coefficient P is the concentration ratio of a solute species between a hydrophobic and an aqueous phase at equilibrium according to eq. 1.3, where $[A]$ equals the molar concentration of a single solute species in either phase, respectively. It is usually expressed in its logarithmic form, $\log P$ and used to estimate the lipophilicity of a drug [Camenisch et al., 1998; Testa et al., 1996].

$$P = \frac{[A]_{hydrophobic}}{[A]_{hydrophilic}} \quad (1.3)$$

The larger the partition coefficient, the higher the tendency of the solute species to distribute into the lipid phase. When considering all ionized species of a compound the partition coefficient is referred to as distribution coefficient D , which is pH-dependent for ionizable compounds. Although the lipophilicity is usually assigned to a drug, it is rather an interplay of the properties of the drug and the lipid phase and thus dependent on the choice of the lipid phase. The standard lipid phase used is 1-octanol and the octanol/water distribution coefficient at physiological pH is widely applied to estimate membrane permeation [Al-Awqati, 1999; Kubinyi, 1979].

Relationships found between the octanol/water-partition coefficient and Caco-2 cell permeability or the absorbed fraction in humans are linear, sigmoidal or hyperbolic [Krämer, 1999; Camenisch et al., 1996].

Solute charge

From early gastric secretion studies, Brodie and coworkers concluded that only the neutral species of an ionizable solute is able to cross biological membranes [Brodie and Hogben, 1957;

1 Introduction

Shore et al., 1957]. Based on this widely accepted pH-partition hypothesis the transmembrane permeation of charged solutes is assumed to be negligible [Dordas and Brown, 2000; Takanaga et al., 1994; Gutknecht and Tosteson, 1973]. The reason for the poor permeability of lipid bilayers towards ions is desolvation. Before entering the hydrocarbon core, ions will give up some of their hydration water. This is energetically unfavourable and represents the main reason for the low diffusive permeation of ions in lipid bilayers [Cevc, 1990]. The loss of energy can be estimated from the Born equation taking into account the dielectric constants of the membrane interior and water, the ion charge and the ion radius [Disalvo and Simon, 1995]. This estimation, however, simplifies the lipid bilayer to a bulk phase with a very low dielectric constant and considers neither the anisotropic properties of the bilayer nor its flexibility. For instance, the permeability of Na^+ ions as estimated from the Born energy is in the order of $10^{-29} \text{cm} \cdot \text{s}^{-1}$, while molecular dynamics simulations revealed that the permeability was $\approx 14 - 17$ orders of magnitude higher [Wilson and Pohorille, 1996].

Frequently, deviations from the pH-partition hypothesis have been observed [Mashru et al., 2005; Males and Herring, 1999] and were explained by different hypotheses. In general, cell barrier permeation of charged solutes has been assumed to take place through the paracellular route. The paracellular pathway did, however, not provide a plausible explanation for the significant contributions to the transport of two basic drugs across Caco-2 cells as observed by Palm et al. [1999]. Takacs-Novak and Szasz [1999] and Neubert [1989] suggested the formation of neutral ion pairs of the ionic solutes with lipophilic counterions present in the solution. Other studies revealing higher permeation of the ionized species than predicted from the pH-partition hypothesis suggest the presence of an acidic microclimate at the membrane surface leading to a shift of the inflection point in the pH/permeation profile of the permeants, if the pH is measured in the bulk phase [Hogben et al., 1959]. Until today, it is not sufficiently elucidated whether and to which extent the ionized species contribute to lipid bilayer permeation. This knowledge would have significant consequences for the drug discovery process, since most of the drugs in therapeutic use are weak acids or weak bases with pK_a values between 1 and 13. and thus a considerable fraction of the drugs is ionized at the physiological pH 7.4 .

Hydrogen bonding

Lipid bilayers provide a considerable amount of hydrogen bonding groups, the majority of which are hydrogen bond acceptors. These groups are located exclusively in the head group region of the lipids. In order to translocate across the hydrocarbon region of the bilayer the solute must be hydrophobic enough to overcome the energy losses due to the breaking of the hydrogen bonds with water or the lipid head groups. Depending on the hydrogen bonding capacities of a solute this step can present a considerable energy barrier. Accordingly, biological permeation was shown to be significantly affected by the hydrogen bonding capacities of the solutes [Abraham, 2004; Abraham et al., 2002; Goodwin et al., 2001; van de Waterbeemd et al., 1998; el Tayar et al., 1991b].

Solute size

The investigations about the impact of the solute's size on membrane permeation are difficult to analyze, since changes in size are usually combined with changes of other properties, e.g. lipophilicity, hydrogen bond capacity etc. which have an impact on the permeation process on their own. The well-known and widely-applied „Lipinski Rules” deduced from a drug library

with ~ 2000 compounds indicate that among other factors such as hydrogen bonding capacities and lipophilicity of the molecules, drug absorption is likely if the molecular weight is ≤ 500 Da [Lipinski et al., 2001]. The molecular volume is taken into account as an important factor determining the permeation properties also in the solvation equation derived by Abraham [Abraham and Chadha, 1996]. In agreement with the Lipinski rules, Pardridge [1995] showed for the permeability of small molecules through the blood-brain barrier a correlation with $\log P$ up to a molecular size threshold of 400-600 Da. Exceptions of this rule were observed for actively transported molecules. The author suggested that above a certain size threshold the migration of molecules through small mobile defects in the lipid bilayer („kinks”) is sterically hindered.

Molecular flexibility

Veber et al. [2002] showed for a library of 1100 drugs that reduced molecular flexibility favors oral bioavailability in rats. A high molecular flexibility can, however, also be of advantage for the drug permeation, e.g. by a facilitation of internal hydrogen bond formation resulting in the reduction of the hydrogen-bond capacities and an increase of the lipophilicity of the molecule [Pagliara et al., 1999].

Electrostatics of lipid bilayer

Mammalian membranes are typically negatively charged, since the headgroups of the natural lipids are either zwitterionic or anionic. The charge is, however, nonuniformly distributed throughout the bilayer. The charged groups are mostly fixed to the membrane surface while the membrane core is usually free of charge. A complex electric profile is generated over the membrane which is composed of the surface potential and the dipole potential [Cevc, 1990].

The surface potential originates from the negative surface charges, which attract counterions from the membrane surrounding leading to the formation of an electrical double layer at the bilayer/bulk interface. The surface potential is dependent on the charge density as well as on the bulk ionic strength. For natural membranes it is usually several tens of mV and results in an increased local concentration of cations as well as a decreased local anion concentration as compared to the bulk aqueous phase [McLaughlin, 1989].

The dipole potential arises in the region between the aqueous phase and the hydrophobic membrane core. It is estimated to be $\approx +300$ mV towards the membrane interior [Brockman, 1994]. This region is therefore more easily accessible to anions than to cations, possibly counteracting the effect of the surface potential [Meijer et al., 1999].

Fluidity and order of lipid bilayer

Depending on the temperature, lipid bilayers can exist in different phases. The liquid crystal (liquid-disordered) state, which exists at temperatures above the transition temperature T_m , is characterized by a higher fluidity as well as a lower thickness and translational order of the bilayer than the gel (solid-ordered) state, which is formed at temperatures below the T_m . Natural membranes are usually in the liquid crystal state. Higher fluidity of the membrane has been shown to correspond to enhanced permeation rates [Hashizaki et al., 2003; Frezard and Garnier-Suillerot, 1998]. The highest permeation rates, however, were measured at the transition temperature $T = T_m$ [Mouritsen and Zuckermann, 2004].

1 Introduction

Molecular dynamics simulations separate each lipid leaflet into four regions, which differ in their headgroup and tail density, respectively [Bemporad et al., 2005]. Marrink and Berendsen [1996] showed the influence of the membrane density characteristics on its resistance profile. Depending on the physicochemical characteristics of the solute, the maximal permeation resistance is found in different membrane regions.

The unstirred water layer

Passive transport across a membrane barrier comprises not only the transmembrane diffusion, but also diffusion through the stagnant water layers at either side of the membrane. Even by vigorous stirring this layer cannot be completely removed. It is called the unstirred water layer (UWL). For epithelial cells of the gastrointestinal tract the *in vivo* thickness of the UWL is estimated to be 30 – 100 μm [Lennernäs, 1998].

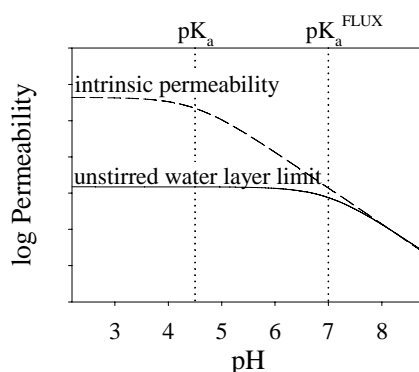


Figure 1.2: Principle of the permeation rate correction for the unstirred water layer phenomenon of an acidic molecule. The solid line shows the observed (experimental) permeation data of an acid. At low pH values the permeation is limited by the diffusion through the UWL. The inflection point (pK_a^{FLUX}) is at higher pH values than the pK_a of the molecule. Based on the assumption of the pH-partition hypothesis the „true” transmembrane permeability (dashed line) and the intrinsic permeability of the neutral species is calculated from the permeation rates at high pH and the pK_a . Modified from Ruell et al. [2003].

The passage of slow-permeating compounds is limited by the membrane permeation, thus the UWL has a minor effect on their permeation rate. Instead, for molecules permeating fast through the lipid bilayer the rate-limiting step can be the passage through the UWL. This might explain the observation that in *in vitro* systems with a considerable UWL similar permeation rates are measured for different highly permeable molecules, i.e. their transport is „diffusion-limited” [Ruell et al., 2003; Avdeef and Testa, 2002]. In this case, the pH/permeation profiles show an inflection point which is for an acid at significantly higher pH values than the pK_a (and for a base vice versa) as illustrated in Fig. 1.2 for an acidic molecule and the measured plateau does not correspond to the intrinsic permeability of the molecule, but to the UWL limit. Based on the pH-partition hypothesis, the measured permeation rates are assumed to be determined by the fraction of the neutral species. Thus, the intrinsic permeation of the neutral species can be extrapolated from the experimental data at high pH, if the pK_a is known (see also eq. 2.24).

1.1.4 Structure-permeation relationships

Many attempts have been made to establish qualitative and quantitative relationships between the molecular structure and transbilayer permeation aiming to predict permeation. A useful guide for medicinal chemists are the Lipinski rules as mentioned in section 1.1.3, predicting that poor absorption of a drug is likely when it has more than 5 hydrogen bond donor groups, more than 10 hydrogen bond acceptor groups, a molecular mass above 500 Da and a $\log P$ bigger than 5 [Lipinski et al., 2001]. A considerable number of quantitative structure-permeation relationship studies have been done confirming the Lipinski rules [Fujikawa et al., 2005; Hansch et al., 2004; Kobayashi et al., 2004; Zhao et al., 2002]. The models obtained can, however, not be considered as universal predictive models, but are strongly depending on the investigated compounds and the permeation systems used. QSAR studies also revealed that the correlation of a single predictor with the permeability usually leads to poor correlations, necessitating the use of sophisticated multivariate analysis methods (see section 1.5).

1.1.5 The influence of the lipid composition on bilayer characteristics

The composition of natural membranes is dependent on their localization and function within the cell. The lipid composition affects various characteristics of the lipid bilayer such as the phase transition behaviour, the fluidity, the stability and its electrostatic properties [Barenholz and Cevc, 2000].

Lipids show thermotropic polymorphism. The chain melting temperature (transition temperature T_m), which is characteristic for each lipid, separates the solid-ordered state from the liquid-disordered state. In mixtures of different lipids the phase behaviour is more complex. It can be characterized by phase diagrams as shown for a binary mixture of phosphatidylcholine/cholesterol in Fig. 1.3. The phase boundaries are not only a function of temperature, but also of the lipid ratio. In the case of non-ideally mixing lipids the coexistence of different phases was observed [Vaz, 1995].

The phase diagram of binary mixtures of phosphatidylcholine/cholesterol (Fig. 1.3) is of special interest since it shows the appearance of a new phase, the liquid-ordered phase. Up to 10 % Chol the phase diagram shows a depression of the chain melting temperature and a narrow coexistence region of solid-ordered (*so*) and liquid-disordered (*ld*) state. With higher amounts of Chol the so-called liquid-ordered (*lo*) state is formed [Miao et al., 2002]. This intermediate phase is characterized by the high acyl chain order of the solid-ordered and the freedom of lateral diffusion present in the liquid-disordered state [Ipsen et al., 1987]. Beyond a critical temperature there are no further phase transitions reported and it cannot be distinguished between liquid-disordered and liquid-ordered phase.

The fluidity of the bilayer decreases with increasing lipid chain saturation and total chain length. Cholesterol has diverse effects on membrane fluidity, it typically decreases fluidity at the level of the chain ends but lowers the average chain order near the headgroups.

Apart from the bilayer fluidity, the bilayer composition will obviously affect the surface potential as described in section 1.1.3, which is dependent on the electronic properties of the lipid headgroup. Changes of the headgroup will also influence the interactions between the headgroups based on hydrogen bonds or electronic interactions.

Interestingly, the different lipid species are not randomly distributed but are laterally ordered in dynamic domains [Kahya et al., 2004; Mouritsen and Jorgensen, 1997]. The lipid species will influence the domain size and hence the dynamic bilayer heterogeneity [Mouritsen and Jorgensen,

1994].

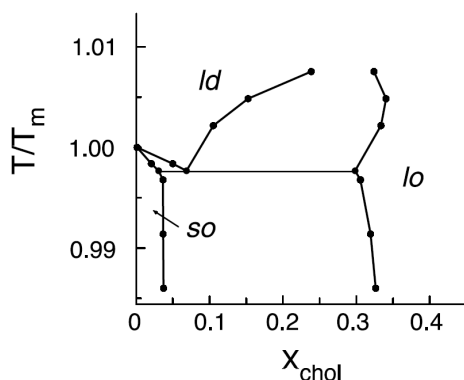


Figure 1.3: Theoretical phase diagram of lipid/cholesterol membranes as determined from Monte Carlo simulations. x_{chol} , molar fraction of cholesterol; T_m , transition temperature; *so*, solid-ordered state; *ld*, liquid-disordered state; *lo*, liquid-ordered state. The full lines represent the phase boundaries. Between them, the different phases coexist. Beyond the critical point which is extrapolated to $T \approx 1.01 \cdot T_m$ and $x_{chol} \approx 0.3$ the *ld* and *lo* phases cannot be distinguished from each other. Adapted from Miao et al. [2002]

1.2 Liposomes as model membranes

Liposomes are spherical vesicles consisting of one or several concentric bilayers. After the first description of the phenomenon that lipids spontaneously form closed bilayer membranes in aqueous surroundings [Bangham et al., 1965], liposomes gained quickly in importance as models for cellular membranes. The abundance of available lipids and preparation techniques has resulted in the possibility to produce liposomes custom-tailored to specific needs.

Concerning their biomimetic qualities liposomes are superior to any other artificial membrane or bulk lipids and thus the ideal tool to model biological membranes wherever biomembranes are too complex. Liposomes are also a valuable alternative to octanol in partition studies. A standard method to determine affinities to liposomal membranes has been established by Pauletti and Wunderli-Allenspach [1994] and has been widely applied since then [Marenchino et al., 2004; Krämer, 2001]. Membrane proteins can be reconstituted into liposomes to study the protein in its natural environment or to explore e.g. the role of the lipid surrounding [Rigaud et al., 1995]. These proteoliposomes are used e.g. for investigations on multidrug-transporters such as P-glycoprotein [Ambudkar, 1995; Bucher et al., manuscript submitted]. Liposomes prove valuable to understand the organization and domain formation within the lipid bilayer [Kahya et al., 2004] and facilitate the understanding of budding processes such as endo- and exocytosis [Holopainen et al., 2000]. Liposomes have also been used for membrane permeation studies (section 1.3.2).

1.3 Membrane permeation assays

During the last decades the need of exploring a solute's ability to pass membrane barriers has led to the development of a variety of permeation assays. For the assessment of intestinal drug

permeability, epithelial cell culture models such as Caco-2 cells are routinely used [Artursson et al., 2001] and provide good estimates about the fraction of drug absorbed in humans after oral administration. Depending on the specific characteristics of the cell line, their use allows not only the investigation of passive diffusion but also of active transport processes, paracellular transport and efflux systems. This versatility is, however, of disadvantage for the exclusive investigation of simple diffusion across the lipid bilayer. To gain insight into the process of passive diffusion across lipid bilayers the use of artificial lipid membranes is considered to be more informative than cell culture models since any other permeation process can be excluded *a priori*.

The ideal *in vitro* transbilayer permeation assay should provide a physiological barrier, i.e. a lipid bilayer, and a high lipid/permeant ratio avoiding unspecific effects on the membrane by high solute concentrations. Furthermore, it should be applicable to a wide range of compounds and be automatable to allow high-throughput screening. In practice, such an ideal assay has proven difficult to develop. This section provides an overview of *in vitro* permeation assays commonly used to study exclusively passive lipid bilayer permeation.

1.3.1 Permeation studies with planar lipid bilayers

Early permeation studies were done using planar lipid bilayers [Gutknecht and Tosteson, 1982; 1973]. For instance, a solution containing 1.5% lipids in dodecane, is spread over an aperture in a Teflon partition to form the so-called black lipid membranes (BLM) upon evaporation of the organic solvent [Ti Tien and Ottova-Leitmannova, 2000]. Alternatively, two lipid monolayers formed at a water/air interface are mounted on either aperture side, thus allowing the formation of asymmetric bilayers [Krylov et al., 2001]. The formation of BLM may be followed optically or electrically by monitoring its resistance. The bilayer separates two aqueous compartments, which are accessible for probes and sampling, respectively. Ag/AgCl- or calomel electrodes are placed in either of the aqueous compartments and membrane resistances are calculated from current/voltage curves.

Drawbacks of this technique are the relative instability of the membranes and the distances between the membrane and the probes and hence, the unstirred water layer represents a relevant diffusion-limiting barrier of 100-200 μm width for permeating solutes.

1.3.2 Liposomal permeation assays

In unilamellar liposomes, the lipid bilayer separates two different aqueous compartments allowing to study the permeation of solutes across the liposomal membrane. Liposomes are more stable than BLM and the unstirred water layer can be neglected since the liposomal diameter is in the range of a few nm (small unilamellar vesicles) until several micrometer (giant vesicles) and the interliposomal distance is usually small, depending on the liposome concentration.

The intraliposomal compartment is, however, not directly accessible to physical probes, which is the main drawback of liposomes as compared to BLM. A couple of methods to separate the liposomes from the outer aqueous phase, such as ultracentrifugation or size-exclusion chromatography, are risky concerning the disturbance of the permeation equilibrium, and thus, might lead to erroneous results. Furthermore, the formation of asymmetric bilayers is not straightforward with conventional liposome preparation methods.

The permeation across liposomal membranes can, however, be followed using fluorescence or UV/VIS changes of the permeant or an intraliposomal probe upon the permeation of solutes. A variety of permeation assays is based on the self-quenching characteristics, of e.g.

carboxyfluorescein [Hashizaki et al., 2006; Silvander et al., 1998; Weinstein et al., 1977] or calcein [Straubinger et al., 1983]. The fluorescent dye is entrapped into liposomes at self-quenching concentrations. Upon leakage the dye is diluted in the outer aqueous compartment leading to an increase of the fluorescence signal. By this method, the influence of different conditions such as temperature, lipid composition or membrane-disrupting agents on the liposome permeability can be investigated. These studies are, however, limited to a small choice of fluorescent dyes. The same constraint applies to assays based on membrane-induced quenching of fluorescent dyes, such as Rhodamine 123 [Eytan et al., 1996].

Another approach to avoid additional separation steps is the entrapment of non-permeating reaction partners in the intraliposomal lumen. Upon permeation of the solute, the reaction results in a fluorescence or UV/VIS signal. Using this approach, the permeation of anthracyclines was investigated with DNA-containing liposomes. The fluorescence of anthracyclines is quenched upon intercalation into the DNA [Frezard and Garnier-Suillerot, 1998; 1991]. The application of these permeation assays is, however, limited by the solute structure. The FluorosomeTM technique (GLSynthesis, Inc., Worcester, MA) combines the use of different impermeable fluorescence markers [Fix and Melchior, 2002], and thus claims to be suitable for any drug. So far there is, however, no publication available objectively evaluating the fluorosome technique and giving insight into the markers used.

Recently a very promising approach was introduced by Flaten et al. [2006a;b]. By several centrifugation and freeze-thawing cycles a tight layer of fused liposomes was deposited on a filter support avoiding the use of organic solvent. It is assumed that the liposomes fill the pores of the filter and form an additional layer on top of it. The filter-liposome layer separates two aqueous compartments, which are accessible for solute sampling by, e.g. UV/VIS. This method combines the advantage of using lipid bilayers with the possibility for automation and bears thus the potential to be used for high-throughput screenings instead of the rather unphysiological artificial barriers described in section 1.3.3. The possibility of storage of the phospholipid filter barriers for up to two weeks is an additional benefit for high-throughput screening. This assay should be applicable to a wide range of structurally diverse drugs.

Another very interesting approach utilizes impermeable shift reagents to distinguish solutes in the outer and inner aqueous compartment by nuclear magnetic resonance (NMR) techniques [Alger and Prestegard, 1979]. Even though this experimental set-up should be widely applicable for the determination of permeation coefficients, only few NMR permeation studies have been published until today [Males and Herring, 1999; Males et al., 1998].

1.3.3 Artificial barriers for high-throughput screening assays

The need of fast high-throughput permeation measurements resulted in the development of PAMPA (Parallel Artificial Membrane Permeability Assay) [Kansy et al., 1998]. A filter membrane is impregnated with an organic lipid solution, e.g. 10% *w/v* egg lecithin in dodecane. The filter membrane is used to separate an aqueous solution containing a test compound from an aqueous buffer initially free of the molecule [Avdeef and Testa, 2002]. The test compound is quantified in the acceptor compartment by spectroscopic methods. Every step is automatable, which is the enormous advantage of PAMPA. Today, it is commercially available and usually run in a 96-well plate format. Permeation data, however, have to be corrected for the phenomenon of the unstirred water layer [Ruell et al., 2003]. Since its first publication PAMPA has been used and modified many times, aiming to create a lipid barrier close to physiological membranes, e.g. of the gastrointestinal barrier [Sugano et al., 2001] or the blood-brain barrier [Di et al., 2003], and

to decrease the amount of organic solvent. However, the main limitation of PAMPA, which is the nature of the lipid barrier comprising rather a bulk lipid-solvent phase than a physiological lipid bilayer, is not overcome yet.

In a recent study a PAMPA-like permeation assay is reported which is composed of a hydrated cellophane membrane and a lipophilic membrane of pure n-octanol in a nitrocellulose matrix [Loftsson et al., 2006]. It was developed to simulate both the membrane resistance and the diffusion resistance in the unstirred water layer of a biological membrane. As for PAMPA, the nature of the lipid barrier deviates significantly from a biological membrane.

1.4 The Terbium(III) luminescence and permeation assay

1.4.1 Terbium(III)-sensitized luminescence

Due to their special luminescent properties lanthanides such as Terbium (Tb) and Europium have attracted a considerable interest as luminescence probes in biomedical studies [Elbanowski and Makowska, 1996], immunoassays [Blomberg et al., 1999], analytical procedures [Ocana et al., 2001; Egorova et al., 2001; Egorova and Beltyukova, 1999] and enzyme activity assays [Bemquerer et al., 2002]. The ligation of lanthanides by an appropriate chromophore leads to the indirect excitation of the energy acceptor molecule by energy transfer from an energy donor molecule [Martin and Richardson, 1979].

The principle of energy transfer as it has first been described by Förster [1948] is illustrated in Fig. 1.4. Upon excitation of the donor molecule from the ground state S_0 ($S_0 \rightarrow S_1$), the excited singlet state S_1 has three deactivation pathways: (i) fluorescence emission ($S_1 \rightarrow S_0$), (ii) non-radiative transition to the triplet state T_1 by intersystem crossing (ISC) under spin inversion and (iii) nonradiative deactivation to the ground state. The excited triplet state T_1 has also three deactivation pathways: (i) phosphorescence emission to the ground state ($T_1 \rightarrow S_0$), (ii) nonradiative transition and excitation of the acceptor ground state by *energy transfer* and (iii) nonradiative deactivation to the ground state of the donor ($T_1 \rightarrow S_0$). The different deactivation pathways are in competition. At room temperature phosphorescence is seldom observed in aqueous solutions since nonradiative deactivation of the triplet state is usually faster than radiative deactivation. If a suitable acceptor is present, the energy transfer rate can, however, compete with the nonradiative deactivation rate and an energy transfer from the donor molecule to the acceptor molecule can occur [Zhu and Kok, 1997]. Upon energy transfer the donor-acceptor complex can be excited with the excitation wavelength of the donor and will emit light of the emission wavelength of the acceptor. Energy transfer can only occur if the distances between donor and acceptor molecule are in the 10-70 Å range and if the lowest excitation triplet energy of the donor is higher than the energy of the ground state of the acceptor [Selvin and Hearst, 1994].

Since the process of light absorption, intersystem crossing, energy transfer and light emission has a longer lifetime than the radiative deactivation of the excited singlet state to the ground state of the donor ($S_1 \rightarrow S_0$, i.e. fluorescence of the donor) the signal of the donor-acceptor complex can be measured with a time delay of several μs . This temporal resolution allows to eliminate the direct fluorescence of the donor as well as any other background signal with a short fluorescence life time. Additionally, the time-resolved mode enhances the analytical signal as it is integrated during a longer time than in the fluorescence mode. Furthermore, lanthanides show large Stokes shifts and narrow emissions bands, which is advantageous for the analytical precision.

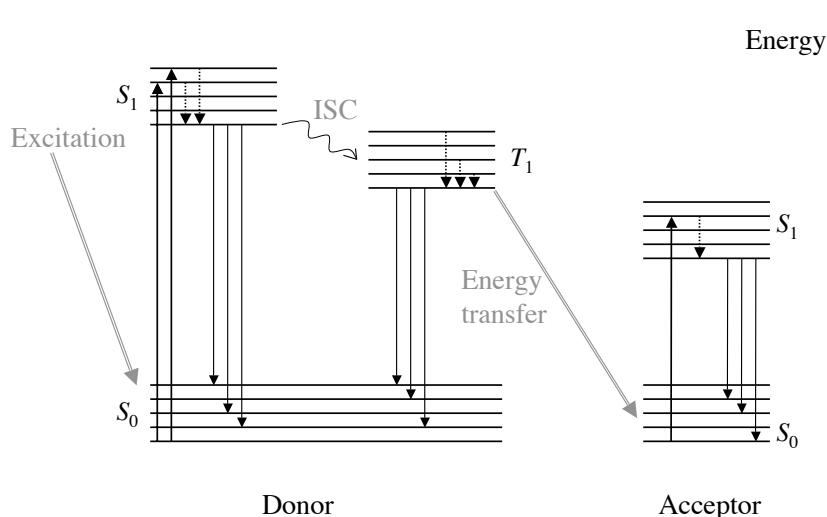


Figure 1.4: Principle of energy transfer - simplified Jablonski diagram: Upon excitation of the donor molecule ($S_0 \rightarrow S_1$) it can be deactivated to the triplet state T_1 by intersystem crossing (ISC). The excited triplet state T_1 can transfer the energy to the ground state of the acceptor. The excited singlet state S_1 of the acceptor is deactivated by radiative emission to the ground state ($S_1 \rightarrow S_0$). Thus, the signal of the acceptor-donor-complex is recorded with the excitation wavelength of the donor and the emission wavelength of the acceptor. Other possible pathways of deactivation: see text. For clarity, nonradiative deactivations to the ground states are not shown in this figure. Modified from Gomez-Hens and Aguilar-Caballo [2002].

1.4.2 The Terbium(III)-permeation assay

Tb(III)-loaded liposomes were first used in membrane fusion studies by Wilschut et al. [1980]. Two liposome population loaded with either Tb^{3+} or dipicolinic acid are mixed in the presence of e.g. fusion-inducing agents. Upon fusion of the vesicles and mixing of the aqueous contents Tb^{3+} and dipicolinic acid form a luminescent complex, and thus, vesicle fusion is registered as fluorescence increase.

The idea of Tb(III)-containing liposomes was exploited by Krämer and Wunderli-Allenspach [2003] to design a novel permeation assay. It is based on the chelation of Tb^{3+} by aromatic carboxylic acids (ACA) resulting in a characteristic luminescence signal as described in section 1.4.1. The permeation of ACA into the interior of the Tb^{3+} -loaded liposomes can thus directly be monitored by luminescence measurements as shown in Fig. 1.5 avoiding the need of an additional separation step. Extraliposomal Tb^{3+} is removed by size exclusion chromatography prior to the permeation studies. The assay has originally been developed to investigate the ability of the cell-penetrating peptide TAT(44-57) to permeate lipid bilayers without energy consumption at physiological pH [Krämer and Wunderli-Allenspach, 2003]. For this purpose two TAT peptide sequences were coupled to N-(4-carboxy-3-hydroxyphenyl)maleimide via a cystein residue. The carboxy-hydroxyphenyl-maleimide group functioned as probe interacting with Tb^{3+} . The Tb(III)-assay was characterized concerning the entrapped concentration of Tb^{3+} (5 to 7 mM) and the Tb^{3+} leakage. It was demonstrated that extraliposomal Tb^{3+} was negligible for several hours, which is in agreement with the data published by Wilschut et al. [1980]. Hydroxylation

of entrapped Tb^{3+} , however, limits the stability of Tb^{3+} -loaded liposomes to 24 h.

Since Tb^{3+} interacts with a wide range of ACAs, the Tb(III)-permeation assay presents an ideal tool to study the permeation not only of ACA-labeled peptides but also of ACAs which exhibit drug-like properties and to investigate different aspects of lipid bilayer permeation.

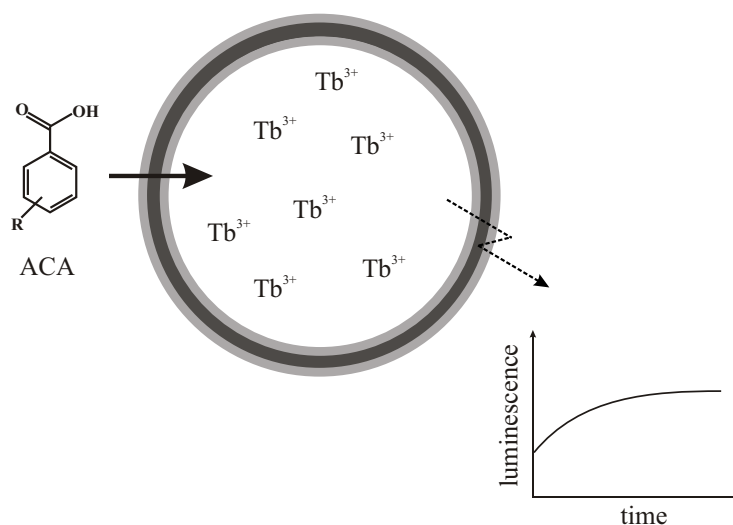


Figure 1.5: Principle of the Tb(III)-assay. Tb^{3+} -loaded liposomes are incubated with an aromatic carboxylic acid (ACA). Upon ACA permeation, Tb^{3+} is ligated by the ACA resulting in a characteristic luminescence signal. Extraliposomal Tb^{3+} is removed by size exclusion chromatography prior the permeation measurement.

1.5 Multivariate Analysis

1.5.1 Objectives of Multivariate Analysis

Multivariate Analysis (MVA) comprises a set of techniques to analyse large and complex data sets with multiple variables. The main objectives of MVA are to reduce and condense the data mass to the relevant information, to identify correlations within the data matrices and to classify clusters, i.e. objects with similar variable properties in the data set. This allows to develop model of reduced complexity which describes the original data and might even predict the behaviour of additional objects.

During the last decades MVA was developed as powerful tool to explore large and multidimensional data series and is widely used in different fields, such as psychology, economic sciences, chemistry, agricultural sciences and ecology [Erikson et al., 2001]. Furthermore, MVA is also used in drug design and development for the establishment of quantitative structure activity relationships [Deconinck et al., 2006; Norinder et al., 1999; Winiwarer et al., 1998].

In this application area MVA aims to effectively predict target properties which are difficult to obtain experimentally, e.g. human jejunal absorption [Winiwarer et al., 1998], from physico-chemical compound parameters which are easier to measure or could even be calculated, such as the polar surface area.

The term MVA summarizes a variety of different analysis methods. Within this thesis, Principal Component Analysis, Cluster Analysis and Partial Least Square Analysis were used and will

be introduced in the following.

1.5.2 Principal Component Analysis

Principal Component Analysis (PCA) aims to reduce a data matrix of v dimensions (variables) and o objects to a new data matrix M of x dimensions with $x \leq v$. The informations of the variables are extracted into new variables, the principal components (PC) or factors. The PCs represent the eigenvectors of the systems, and can be interpreted as regression lines in the multidimensional space spanning the maximum variance of the data. By definition, the single PCs are perpendicular to each other, and thus independent of each other. The PCs form the axes of a new low-dimensional coordinate system. Each data point can be projected onto the eigenvector. This projection value is the *score* t of a data point. The contribution of the original variables for the PCs is apparent from their *loadings* p to the PCs. Geometrically, the loading value of a variable corresponds to the cosine of the angle between the variable and the PC. The higher the loading, the bigger is the influence of the variable [Erikson et al., 2001; Kramer, 1998]. Fig. 1.6 gives an overview of the parameters used.

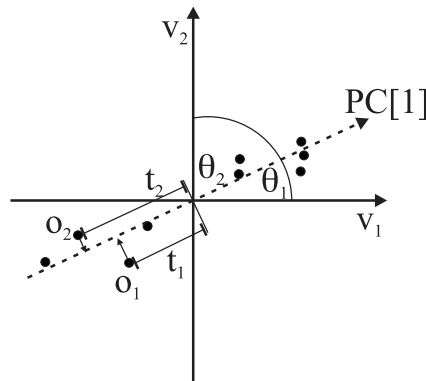


Figure 1.6: Principle of Principal Component Analysis PCA. In this example, a dataset is shown with $o = 9$ and $v = 2$. The eigenvector (PC [1]) spans the maximal variance of the data matrix. The projections of each observation on the PC are the scores t . The contribution of the original variables to the location of the PC is measured as the cosine of the angle between v and the eigenvector (loading p). In this case, a 2-dimensional dataset is reduced to a 1-dimensional dataset and v_1 has a higher loading value p than v_2 .

A graphical PCA result combines thus two parts, a score plot and a loading plot. Observations with similar variable values display similar scores and thus, groups of similar observations are easily identified as groups in the score plot, while observations that are substantially different from the others and show extreme values can be detected as outliers. The variables responsible for these similarities can be identified in the loading plot. Similar loadings of variables indicate correlations between them, i.e. collinearity.

1.5.3 Cluster Analysis

The objective of cluster analysis (CA) is to divide a series of objects into groups whereas the objects within one group, i.e. within one cluster are more similar to each other than to those in other

groups. The measure for similarity is the distance between two data points in the multidimensional system, with smaller distances representing larger similarity [Migliavacca, 2003]. The similarity measure used in this work is the Euclidian distance, which is the length of a straight line between two objects. The result of a CA is usually presented in form of a dendrogram.

1.5.4 Partial Least Square Analysis

Partial Least Square Analysis (PLS) is a regression extension of PCA and aims to detect a relation between an X-matrix (predictor variables) and a Y-matrix (response variables). It is the method of choice for constructing predictive models when the number of variables is high and the variables could be collinear. For each matrix, a PCA is carried out, considering however the scores of the other matrix in an iterative way. The scores and loadings of each resulting matrix are related to each other by weights c [Kramer, 1998; Geladi and Kowalski, 1986]. Thus, the Y-matrix can finally be predicted from the scores and loadings of the X-matrix.

PLS is especially useful when the number of variables is similar to or higher than the number of observations. Caution should, however, be taken, that overfitting of the model is avoided by careful selection of the variables.

1.6 Aim of the thesis

The present thesis aims at gaining insight into the process of lipid bilayer permeation. Liposomes are used as membrane models to investigate membrane-related processes, i.e. binding to and permeation across the membrane.

The major part of this study explores the permeation behaviour of aromatic carboxylic acids (ACA). A series of 13 acids with drug-like physicochemical properties was chosen and characterized concerning their dissociation behaviour and their hydrophobicity as expressed by the octanol/water partition coefficient (section 3.1). The membrane affinities of three representative ACAs were determined by equilibrium dialysis [Pauletti and Wunderli-Allenspach, 1994] in various liposomal systems, including net neutral membranes and charged membranes. By varying systematically the membrane composition the influence of single lipids on the membrane affinities of the test compounds could be explored (section 3.2). To investigate the process of membrane permeation, the Tb(III)-permeation assay as introduced by Krämer and Wunderli-Allenspach [2003] was utilized. It was further developed to measure in a broader pH range, i.e. between pH 2 and 7 and to increase the signal specificity. The Tb(III)-assay was characterized concerning its dependency of the buffer capacity and Tb(III) complexation constant, of the lipid and solute concentrations and the formation of pH-gradients (section 3.3).

Since most therapeutic drugs are predominantly ionized at the physiological pH 7.4, it is of high importance to understand the influence of the solute ionization state on lipid bilayer permeation (section 3.4.1). The effect of changes in the membrane barrier was studied by changing the lipid bilayer composition in the same manner as for the membrane affinity (section 3.4.2). This allows a direct comparison of the lipids effects on affinity and permeation and insight in the interplay of the two processes. To explore the influence of the solute structure on membrane permeation the permeation profile of all 13 ACAs was determined using two different liposome systems (section 3.5). The structure-permeation relationship was investigated as a multifactorial process by means of multivariate analysis.

1 Introduction

In addition to small drug-like compounds, the permeation of peptides across the liposomal membranes was investigated as a function of the peptide size and secondary structure (section 3.6).

The last part of this study presents a theoretical simulation of the lipid bilayer permeation based on a three-step-permeation model (section 3.7). The model is interpreted as a differential equation system which is solved numerically. The results allow to understand the interplay of the different processes and to explain the experimental data.

2 Materials and Methods

2.1 Chemicals and Buffers

2.1.1 Chemicals

Anthranilic acid (AA, #10680), 5-chlorosalicylic acid (CSA, # 26320), 3,5-dichlorobenzoic acid (DCBA, #35321), 2-hydroxy nicotinic acid (OHNA, #55966), salicylic acid (SA, #84210), and TbCl_3 hexahydrate (#21290-3) were purchased from Fluka (Buchs, Switzerland). Anthracene-9-carboxylic acid (AC, #S59065), 2,4-dihydroxy-benzoic acid (DHB, # D10, 940-1), 5-methyl-anthranilic acid (MAA, #419443), 3-methylsalicylic acid (MSA, #167037) and pyrazine carboxylic acid (PCA, #P5, 610-0), were from Aldrich (Steinheim, Germany). Dipicolinic acid (DPA, # D0759) was supplied by Sigma (Buchs, Switzerland). 5,6-Carboxyfluorescein (CF, #C-194) was from Molecular Probes (Eugene, OR) and 5-carboxyfluorescein diacetate (CFDA, #C1361) was from Invitrogen (Basel, Switzerland). All other chemicals used were of analytical grade. All chemicals were stored according to the specifications of the supplier.

2.1.2 Radiochemicals

^{14}C -salicylic acid (^{14}C -SA, #NEC263) was purchased from Perkin Elmer (Boston, MA). Sigma (Steinheim, Germany) supplied ^{14}C -anthranilic acid (^{14}C -AA, #30455-7), and ^{14}C -2-hydroxy nicotinic acid (^{14}C -OHNA, #1140) was supplied from ARC (St.Louis, MO).

Stability and purification of the radiolabeled compounds

Prior to the partitioning experiments the purity of all radiolabeled compounds was tested by Thin Layer Chromatography (TLC). A sample of the compound (1 μl) was spotted on silicagel 60 aluminum sheets (Merck, Poole, UK). The mobile phase was glacial acetic acid/ methanol/ water (1/40/60 v/v) for all compounds [Secretariat, 1997]. After developing the chromatograms for 10 cm and drying, the sheets were cut into ten strips of 1 cm each. The strips were mixed with 3 ml UltimaGold Scintillation cocktail (#6013329, Perkin Elmer, Boston, MA) and counted with the Beckmann Liquid Scintillation counter LS 7800 (Beckmann, Fullerton, CA). *R_f* values of the radiolabeled compounds were compared with the *R_f* values of the corresponding unlabeled compounds obtained under the same conditions but with detection of fluorescence extinction. Radiochemicals were considered to be pure if only one peak was detected with an *R_f* value comparable to the *R_f* of the unlabeled compound.

^{14}C -OHNA was found to be not pure (see section 3.2.1) and was purified prior to each partitioning experiment by TLC. The required amount of ^{14}C -OHNA was spotted on a TLC and developed for 10 cm under the same conditions as described above. After developing the sheet was cut between cm 3 and 7, where the pure compound was expected. ^{14}C -OHNA was eluted from the sheet with methanol by rotation in a small flask. Silica was removed by filtration of

2 Materials and Methods

the solution through a 0.22 μm filter. Afterwards, methanol was evaporated and the pure ^{14}C -OHNA remaining in the flask was dissolved with the respective liposome suspension used for the partitioning experiment.

2.1.3 Lipids

Egg phosphatidylcholine (PhC) grade 1, phosphatidylethanolamine (PhE), phosphatidylinositol (PhI) and phosphatidylserine (PhS) were supplied by Lipid Products (Nutfield, UK). Cholesterol (Chol, #C-8667) was from Sigma (Steinheim, Germany) and Stearylamine (StAm, #74750) was purchased from Fluka (Buchs, Switzerland). Di-palmitoyl-phosphatidylcholine (DPPC, #850355) was from Avanti Polar Lipids (Alabaster, AL). *N*-(fluorescein-5-thiocarbamoyl)-1,2-dihexadecanoyl-sn-glycero-3-phosphoethanolamine triethyl-ammonium salt (fluorescein DHPE, #F362) was from Molecular probes (Leiden, The Netherlands). All lipids were stored at -20°C .

2.1.4 Peptides

The peptides were prepared by solid phase peptide synthesis on Wang resin using Fmoc-protecting group strategy as described in Gardiner et al. [2006]. The 2,6-pyridinedicarboxyl moiety was introduced in its benzyl-protected form in the final coupling step of the synthesis. Cleavage from the resin, and subsequent benzyl-deprotection with Pd-C (10% w/w) in methanol under a hydrogen atmosphere gave the crude peptides. Pure samples ($\geq 98\%$) were obtained by reverse phase HPLC.

2.1.5 Buffer solutions

Various buffers were prepared for equilibrium dialysis and permeation experiments.

- Standardized universal buffer solutions (SUBS) [Pauletti and Wunderli-Allenspach, 1994]
For the stock solution A 7 g citric acid monohydrate, 3.54 g boric acid, 3.5 ml phosphoric acid 85 %, 343 ml NaOH 1 M were dissolved in water to a final volume of 1 l. Solution A has to be stored in a plastic bottle under N_2 . For 100 ml buffer 20 ml solution A were mixed with 0.5 M HCl to adjust the pH to a value between 2 and 12. To reach a constant ionic strength of 230 mmol/kg and a physiological osmolality, 3.2 M NaCl was added.
If not indicated otherwise, standardized universal buffer solutions (SUBS) were used for all permeation and equilibrium dialysis experiments. SUBS cannot be used to record the luminescence spectra of free Tb^{3+} since the phosphate leads to a precipitation of free Tb^{3+} .
- 3-(*N*-Morpholino)propanesulfonic acid (MOPS)
For 200 mM MOPS 46.25 g of the 3-(*N*-Morpholino)propanesulfonic acid sodium salt (MW 231.2 g mol^{-1}) were dissolved in water. The buffer was adjusted to pH 6.8 with 0.5 M NaOH before diluting to the final volume of 1 l.
MOPS was used to record the luminescence spectra of free Tb^{3+} , the ACAs and the peptides.
- TRIS buffer
For 200 mM TRIS buffer 31.52 g of Tris(hydroxymethyl)aminomethan hydrochloride (MW 157.60 g mol^{-1}) were dissolved in water. The buffer was adjusted to pH 6.8 with

NaOH before diluting to the final volume of 1 l.

To study the influence of counterions, 130 mM NaCl were added to obtain a similar ionic strength as in SUBS buffer.

2.2 Lipid quantification

2.2.1 Quantification of lipids by Thin Layer Chromatography

After preparation of liposomes containing at least two different lipids, the amounts of the single lipids were quantified by TLC according to Krämer et al. [2002] on silicagel 60 aluminum sheets (Merck, Poole, UK). Mobile phases were chloroform/methanol/acetic acid/water (60/50/1/4 v/v) for the separation of the polar lipids and heptane/diethyl ether/acetic acid (60/40/2 v/v) for the neutral lipids. Liposome samples in triplicates and at least five reference solutions were spotted on the same TLC sheet in equal volumes. After the chromatograms were developed and dried, they were impregnated with an aqueous solution of 3% cupric acetate and 8% phosphoric acid. The dried sheets were exposed to 180°C for 7 min to char the lipids. Constant heating conditions were crucial to get reproducible results. Heating time had to be extended to 30 min for the quantification of StAm. The TLC sheets with the dark lipid spots were scanned and subsequently analyzed by the computer program ImageJ (National Institutes of Mental Health, Bethesda, Maryland, release beta 1.30q) using the Gel Plotting Macro. The dark spots were converted to density peaks, which were quantified by their area under the curve (AUC). Relationships between the AUCs and the lipid amounts of the reference spots followed either an exponential or a saturation function as described in Krämer et al. [2002] and were analyzed using the solver tool of Microsoft Excel:mac.

2.2.2 Quantification of lipids by High Pressure Liquid Chromatography

For the partitioning studies it is essential to determine the exact amount of lipids (see eq. 2.18). Therefore, the lipids were quantified by HPLC according to a method of Singh et al. [2005] on a Hitachi Elite LaChrome HPLC (Hitachi High-Technologies Corporation, Japan). The mobile phase was prepared by mixing an ammonium phosphate buffer (50 mM, pH 2.7, pH adjusted with 85% phosphoric acid) and methanol in the ratio 15:85 (v/v). Standard stock solutions of the lipids PhC, Chol and PhI (1.0 mg/ml) were prepared using methanol. The different calibration samples (n=5) were obtained by dilution of the stock solution with the mobile phase. The samples (injection volume 50 µl) were run on a BDS Hypersil C₈ column (# 7342, Thermo Electron Corporation, Waltham, MA) with the dimensions 150 x 4.6 mm, 5 µm particle size, 130 Å pore size. The elution time was 20 min (isocratic) and the column temperature was 60°C, the mobile phase flow rate was 2.0 ml/min. The UV detector was set to 205 nm.

2.2.3 Enzymatic quantification of lipids

Lipids were quantified by an enzymatic reaction using the Wako Kit PL B (# 999-54006, Wako, Neuss, Germany). To dissolve the liposomes, 10 µl of liposome suspension containing ~ 4 mM or about 3 mg lipids per ml were incubated with 40 µl Triton X-100 at 65°C for 5 min. After cooling the dissolved liposomes on ice, 1.5 ml of enzyme reagent (corresponding to 1.17 mg enzyme) contained in the kit were added and incubated at 37°C for 10 min under vigorous

shaking. Absorbance was read at 505 nm. Calibration samples were prepared as the liposomes, using 10 μ l of choline standard (3 mg/ml; MW 139.63) instead of liposomes.

Lipid quantification by enzymatic reaction was not sufficiently accurate and thus, quantification by HPLC was favored for determining the lipid concentration.

2.3 Determination of pK_a values

2.3.1 Potentiometric titration

The pK_a values of the studied ACAs were determined potentiometrically at 25°C using the PCA 101 instrument from Sirius Analytical Instruments (Forest Row, UK) according to Avdeef [1993]. Titrations were done in triplicates in 0.15 M KCl with 0.5 M HCl and 0.5 M KOH, respectively. The pK_a values were calculated from the titration curves with the pKaLOGP software (Sirius Analytical Instruments, Forest Row, UK). Due to the high precision and rapidness of this method it was used for all studied ACAs except the compounds with a solubility ≤ 0.3 mg/ml. The pK_a values of the latter (i.e. Anthracene-9-carboxylic acid) were determined by UV absorbance measurements as described in section 2.3.2.

2.3.2 UV absorbance measurements

Changes of the ionization state of a compound are often associated with changes in the UV absorbance of the molecule. The pH of 0.01 mM solutions of the respective ACA were adjusted to the desired pH values and the UV absorbance spectra were taken on a Cary-1E UV-VIS spectrophotometer (Varian, Middelburg, Netherlands). Changes in the spectra were analyzed as a function of the pH and the pK_a was estimated according to eq. 2.1,

$$Abs_{pH} = \alpha^{AH} \cdot Abs^{AH} + \alpha^{A^-} \cdot Abs^{A^-} \quad (2.1)$$

with Abs^{AH} and Abs^{A^-} being the extrapolated absorbance values for the single ionization species and Abs_{pH} the absorbance measured at the respective pH. α^{AH} and α^{A^-} are the molar fractions of the respective ionization species as calculated in section 2.3.5. The determination of the pK_a by this method is less accurate than the determination by potentiometric titration.

2.3.3 ^{13}C -NMR measurements

To test, whether NMR-spectroscopy could be applied to assign pK_a values to particular acidic or basic moieties in a molecule, the pK_a value of salicylic acid was determined by ^{13}C -NMR measurements as a first pilot experiment. The respective SA solutions corresponding to ~ 1 mg SA in 0.5 ml final sample volume were adjusted to the desired pH with 0.5 M HCl and 0.5 M KOH. ^{13}C -NMR spectra were recorded on a Bruker 400 UltraShield with 1024 scans. Peaks were assigned manually to the functional groups and the chemical shifts of each functional groups were analyzed as a function of pH according to eq. 2.2,

$$\delta_{pH} = \alpha^{AH} \cdot \delta^{AH} + \alpha^{A^-} \cdot \delta^{A^-} \quad (2.2)$$

with δ^{AH} and δ^{A^-} representing the extrapolated chemical shifts for the single ionization species and δ_{pH} the chemical shift measured at the respective pH. α^{AH} and α^{A^-} are the molar fractions of the respective ionization species as calculated in section 2.3.5.

The high signal/noise ratio of the ^{13}C -NMR spectra was due to the low solubility ($\leq 2\text{mg/ml}$) of the compound.

2.3.4 pK_a of Stearylamine by Zetapotential measurements

Liposomes containing egg PhC and 30 mol% StAm were diluted to a final lipid concentration of 3 mg/ml in SUBS of different pH. The zetapotential ζ of the liposome suspensions were measured with a Zetasizer 3000 HSA (Malvern Instruments, Malvern, UK) in triplicates. The pK_{aM} of Stearylamine in the liposomal membrane was determined by fitting ζ as a function of pH as described with eq. 2.3,

$$\zeta = \alpha^{StAm} \cdot \zeta^{StAm} + \alpha^{HStAm^+} \cdot \zeta^{HStAm^+} \quad (2.3)$$

$$\text{with } \alpha^{StAm} = \frac{1}{1 + 10^{pK_{aM} - pH}} \quad (2.4)$$

$$\text{and } \alpha^{HStAm^+} = 1 - \alpha^{StAm} \quad (2.5)$$

ζ^{StAm} and ζ^{HStAm^+} denote the extrapolated ζ of the single ionization species.

This method could be applied to any lipid capable of forming liposomes. The determined dissociation constant is an apparent pK_{aM} in the membrane environment.

2.3.5 Calculation of the molar fractions of the various ionization species

The pK_a values were used to calculate the molar fractions of the net neutral (AH) and deprotonated (A^-) species of a monoprotic acid according to eqs. 2.6 and 2.7:

$$\alpha^{AH} = \frac{1}{1 + 10^{pH - pK_a}} \quad (2.6)$$

$$\alpha^{A^-} = 1 - \alpha^{AH} = \frac{1}{1 + 10^{pK_a - pH}} \quad (2.7)$$

For amphiprotic compounds the fractions of fully deprotonated, mono-protonated and di-protonated (AH_2^+) species were determined as follows (eqs. 2.8– 2.10):

$$\alpha^{A^-} = \frac{10^{-pK_a^{AH_2^+/AH}} - pK_a^{AH/A^-}}{10^{-2pH} + 10^{-pH - pK_a^{AH_2^+/AH}} + 10^{-pK_a^{AH_2^+/AH}} - pK_a^{AH/A^-}} \quad (2.8)$$

$$\alpha^{AH} = \frac{10^{-pH - pK_a^{AH_2^+/AH}}}{10^{-2pH} + 10^{-pH - pK_a^{AH_2^+/AH}} + 10^{-pK_a^{AH_2^+/AH}} - pK_a^{AH/A^-}} \quad (2.9)$$

$$\alpha^{AH_2^+} = \frac{10^{-2pH}}{10^{-2pH} + 10^{-pH - pK_a^{AH_2^+/AH}} + 10^{-pK_a^{AH_2^+/AH}} - pK_a^{AH/A^-}} \quad (2.10)$$

For clarity, the fully deprotonated (A^{2-}), mono-deprotonated (AH^-) and di-protonated (AH_2)

species of the diprotic molecule DPA were calculated as follows (eqs. 2.11– 2.13:

$$\alpha^{A^{2-}} = \frac{10^{-pK_a^{AH_2/AH^-}} - pK_a^{AH^-/A^{2-}}}{10^{-2pH} + 10^{-pH-pK_a^{AH_2/AH^-}} + 10^{-pK_a^{AH_2/AH^-}} - pK_a^{AH^-/A^{2-}}} \quad (2.11)$$

$$\alpha^{AH^-} = \frac{10^{-pH-pK_a^{AH_2/AH^-}}}{10^{-2pH} + 10^{-pH-pK_a^{AH_2/AH^-}} + 10^{-pK_a^{AH_2/AH^-}} - pK_a^{AH^-/A^{2-}}} \quad (2.12)$$

$$\alpha^{AH_2} = \frac{10^{-2pH}}{10^{-2pH} + 10^{-pH-pK_a^{AH_2/AH^-}} + 10^{-pK_a^{AH_2/AH^-}} - pK_a^{AH^-/A^{2-}}} \quad (2.13)$$

2.4 Determination of $\log P_{Oct}$ and $\log D_{pH}$ values

Partition coefficients of the ACAs in n-octanol/0.15 M KCl were determined potentiometrically with the PCA 101 instrument (Sirius Analytical Instruments, Forest Row, UK) with at least four different volume ratios r between 0.05 and 20 of organic (octanol), V_{Oct} , and aqueous (0.15 M KCl), V_{KCl} , phase [Avdeef, 1993]. The $\log P_{Oct}$ values were fitted with SigmaPlot 8.0 (SPSS Inc., Chicago, IL) according to eq. 2.14 [Krämer et al., 1998b]:

$$p_0K_a - pK_a = \log \left(10^{\log P^{AH}} \cdot r + 1 \right) - \log \left(10^{\log P^{A^-}} \cdot r + 1 \right) \quad (2.14)$$

$$\text{with } r = \frac{V_{Oct}}{V_{KCl}} \quad (2.15)$$

where $p_0K_a - pK_a$ is the difference between the apparent dissociation constant in the respective octanol/KCl system and the dissociation constant of the solute in 0.15 M KCl. The term $p_0K_a - pK_a$ is positive if the solute has a higher affinity to the octanol phase at pH values below its dissociation constant (i.e. usually for an acid) and vice versa.

The distribution coefficient at a particular pH is calculated according to eq. 2.16:

$$\log D_{pH} = \log(10^{\log P^{AH}} \cdot \alpha_{pH}^{AH}) \quad (2.16)$$

2.5 Liposomes

2.5.1 Preparation of liposomes

Liposomes were prepared by extrusion [Krämer and Wunderli-Allenspach, 2003; Hope et al., 1985]. In brief, for the preparation of Tb^{3+} -containing liposomes, 0.2 mmol $TbCl_3$ hexahydrate and 100 mg of the respective lipids (PhC, PhC/Chol, PhC/PhI, PhC/StAm, biomix¹) were dissolved in methanol and dried to a film in a round flask at least 20 K above the transition temperature (T_c) of the lipids. The film was rehydrated at the same temperature in a total of 3 ml water to form multilamellar liposomes which were subjected to five cycles of freezing and thawing and subsequent extrusion at temperatures $\geq 10 K$ above T_m of the lipids through double-stacked

¹The term „Biomix” represents a mixture of the lipids PhC, Chol, PhI and PhE (see section 3.5.1). The lipids were premixed in a stock solution in Methanol/Chloroform. 2.5 ml of this stock solution (corresponding to 100 mg of total lipids) were mixed with 0.2 mmol dissolved $TbCl_3$ hexahydrate.

Nucleopore polycarbonate membranes with an average pore diameter of 200 nm (Corning, Ac-
ton, MA). Liposomes containing Chol, StAm and the biomix liposomes were extruded through
membranes with 800 and 400 nm pores prior to the extrusion through 200 nm pores.

External Tb^{3+} was separated from the liposomes on a Sephadex G-25 PD-10 desalting column
(Amersham Biosciences, Freiburg, Germany) with 0.2 M NaCl, water or the appropriate buffer.
The collected fraction contained about 15 to 20 mg lipids/ml. The local concentration of Tb^{3+} in
the liposomal lumen was between 5 and 7 mM [Krämer and Wunderli-Allenspach, 2003]. Tb^{3+} -
containing liposomes were used within a few hours.

Liposomes for partition studies were prepared without Tb^{3+} as described above, omitting the
separation step at the end. The Tb^{3+} -free liposomes were stored at 4°C and used within three
days.

2.5.2 Characterization of liposomes

The average size and the size distribution of all liposome preparations were analyzed by dynamic
light scattering with a Zetasizer 3000 HSA (Malvern Instruments, Malvern, UK). The Tb^{3+} -
containing liposomes showed an average mean hydrodynamic diameter between 140 and 180
nm and Tb^{3+} -free liposomes between 120 and 200 nm, depending on the lipid composition. The
polydispersity indices of both types of liposomes were ≤ 0.2 corresponding to a size variance of
maximal 45% assuming a monomodal size distribution. Tb^{3+} -free StAm-containing liposomes
showed higher polydispersity indices (≤ 0.4 , corresponding to a size variance of 63%). All
liposome preparations were further characterized by their zeta potential ζ at pH 6.8 using the
Zetasizer 3000 HSA (Malvern Instruments, Malvern, UK). ζ was $5 \pm 4mV$ for PhC and PhC/Chol
liposomes and $5 \pm 4mV$ and $23 \pm 4mV$ for PhC/PhI 94/6 (mol/mol) and PhC/PhI 70/30 liposomes,
respectively. For Tb^{3+} -containing PhC/StAm 85/15 liposomes ζ was $20 \pm 4mV$, while it was
 $40 \pm 4mV$ for Tb^{3+} -free PhC/StAm 85/15 liposomes. Except for PhC/StAm liposomes, ζ of
 Tb^{3+} -containing liposomes were similar to the values of the corresponding Tb^{3+} -free liposomes,
indicating that the binding or adsorption of Tb^{3+} to the membrane surface was negligible.

For liposomes containing charged lipids, the experimental pH values of the permeation and
partitioning experiments were corrected for the estimated difference (ΔpH) between the bulk
pH (pH_{bulk}) and the pH of the stationary buffer layer at the membrane surface ($pH_{at\ membrane}$)
according to Krämer et al. [1998a], eq. 2.17:

$$\Delta pH = pH_{bulk} - pH_{at\ membrane} = -\frac{F \cdot \zeta}{2.303 \cdot R \cdot T} \quad (2.17)$$

with ζ , the experimentally determined zeta potential; F , the Faraday constant and R , the gas
constant.

2.6 Determination of membrane affinities

2.6.1 Equilibrium dialysis

The affinity of radiolabeled compounds to liposomal membranes was determined by a standar-
dized equilibrium dialysis system [Pauletti and Wunderli-Allenspach, 1994]. The pH was ad-
justed with buffer as indicated, the concentration of radiolabeled solutes was 10^{-7} M and the
lipid concentrations were 3 mg/ml (SA and AA, pH 2-6) and 30 mg/ml (SA and AA, pH ≥ 7),

OHNA all pH). Equilibrium dialysis cells were from Dianorm (Munich, Germany) with a volume of 1 ml for lipid concentrations of 3 mg/ml and 0.2 ml for lipid concentrations of 30 mg/ml. The two cell chambers were separated by a cellulose membrane (*MW* cut-off 10000, Dianorm, Munich, Germany) that was preconditioned in phosphate buffer pH 7.4 for at least 30 min prior to the experiments. One chamber was filled with the liposome suspension containing the radiolabeled ACA while the other chamber contained buffer of the respective pH. The dialysis cells were rotated at ~ 5 rpm for 5 h at the indicated temperature. After collection of the chamber contents the pH was measured immediately at the respective incubation temperature using an Beckmann Φ 71 pH meter in combination with a Mettler Toledo InLab423 microelectrode (# 52000124, Mettler Toledo, Greifensee, Switzerland). Triplicates of 200 μ l or 30 μ l were mixed with 3 ml UltimaGold Scintillation cocktail (# 6013329, Perkin Elmer, Boston, MA) and counted with the Beckmann Liquid Scintillation counter LS 7800 (Beckmann, Fullerton, CA).

2.6.2 Data analysis

The distribution coefficients were calculated according to Pauletti and Wunderli-Allenspach [1994] using eq. 2.18:

$$D = \frac{(c_{LB} - c_B) \cdot V_{LB}}{c_B \cdot V_{Lipids}} + 1 \quad (2.18)$$

where c_{LB} is the molar solute concentration in the liposome-containing chamber and c_B in the buffer chamber. The symbol V_{LB} denotes the sample volume of the liposome suspension and V_{Lipids} the volume of the lipophilic phase, i.e. the lipid bilayers. This volume was calculated from the lipid concentrations in the dialysis cells, which were determined with an enzymatic choline quantification assay or by HPLC as described in section 2.2, and a density of 1.0 g/ml for the lipids [Huang and Mason, 1978]. The pH-dependent distribution of the solutes between the lipid bilayer and the aqueous phase was fitted according to eq. 2.19:

$$\log D = \alpha^{AH} \cdot 10^{\log P^{AH}} + \alpha^{A^-} \cdot 10^{\log P^{A^-}} + \alpha^{AH_2^+} \cdot 10^{\log P^{AH_2^+}} \quad (2.19)$$

where P^{AH} is the partition coefficient of the net neutral, P^{A^-} of the deprotonated solute and $P^{AH_2^+}$ of the di-protonated solute. The molar fractions of the different ionization species were calculated as described in section 2.3.5.

2.7 Interaction of ACAs with Tb^{3+} in solution

The interactions of the ACAs with Tb^{3+} were determined using an LS50B luminescence spectrometer (Perkin Elmer, Boston, MA). Excitation and emission spectra were recorded with a time delay of 0.05 ms, gate time of 1 ms, cycle time of 20 ms and at 1 flash per cycle to filter out any signal from other sources than the free and complexed Tb^{3+} . The slit widths for the excitation and emission monochromators were set to 10 nm. The concentration of Tb^{3+} was 0.5 mM and the concentrations of the ACAs were between 1 and 2 μ M. The pH of the solutions was adjusted with either 20 mM TRIS (pH 6.8) or with 0.5 M HCl and 0.5 M KOH, respectively.

2.8 Lipid bilayer permeation

2.8.1 Tb(III)-permeation assay

The entry kinetics of the ACAs and the studied peptides into the aqueous liposomal lumen containing Tb^{3+} were determined by luminescence measurements on a Synergy HT plate reader (Bio-Tek Instruments, Winooski, VT) [Thomae et al., 2005]. The liposomes were diluted in SUBS (see section 2.1.5) or as indicated. For experiments with SUBS containing TRIS, the pH was adjusted after the addition of TRIS. The pH was stable during all kinetic measurements. All solutions were equilibrated at 25°C. At time zero, 10 to 20 μ l of 0.1 to 1 mM ACA or peptide solution were added to the wells of a 96-well plate (Corning # 3915) containing each 200 μ l of the diluted liposomes. The final lipid concentration was between 2 and 3 mg/ml, the total Tb^{3+} concentration about 0.1 mM and the ACA or peptide concentrations from 5 to 100 μ M. Under these conditions the kinetics were independent of the ACA and liposome concentrations. The samples were excited at the wavelength resulting in the highest signal of the complex, i.e. between 230 and 318 nm, and Tb^{3+} luminescence was recorded every 30 s at 545 nm with a time delay of 0.05 ms, gate time of 1 ms, cycle time of 20 ms and at 1 flash per cycle. The time delay was set to filter out any signal from other sources than Tb^{3+} . The assays were run for one to two hours. Kinetics with rate constants $\geq 3 \text{ min}^{-1}$ were determined with an SX18-MC stopped-flow instrument (Applied Photophysics, Leatherhead, UK) under similar conditions but without time delay or with a fluorescence spectrometer LS50B (Perkin Elmer, Boston, MA) equipped with a stopped-flow device. To estimate the concentration ratio of SA in the inner and outer aqueous compartments of the Tb^{3+} -containing liposomes at the permeation equilibrium, the partitioning of ^{14}C -SA between Tb^{3+} -containing PhC liposomes and SUBS at pH 7 was determined by equilibrium dialysis as described below and compared to the partitioning in Tb^{3+} -free liposomes. The total SA concentration was 0.06 mM in the liposome-containing chamber. The ratio of the SA concentrations of the inner and outer compartments was about 1.5, the estimated association constant of a 1:1 SA- Tb^{3+} complex 10^2 M^{-1} .

2.8.2 Data analysis

Data were analyzed with the solver tool of Microsoft Excel:mac and with SigmaPlot. The luminescence/time curves ($I(t) = f(t)$) were fitted with a monoexponential (eq. 2.20) and a biexponential function (eq. 2.21), respectively.

$$I(t) = I_{max} - (I_{max} - I_0) \cdot e^{-k \cdot t} \quad (2.20)$$

$$I(t) = I_{max_I} + I_{max_{II}} - \left((I_{max_I} - I_0) \cdot e^{-k_I \cdot t} + (I_{max_{II}} - I_0) \cdot e^{-k_{II} \cdot t} \right) \quad (2.21)$$

where I_{max} denotes the maximal luminescence of the respective exponential, I_0 the luminescence at time 0, i.e. the intersection with the ordinate, and k the rate constant of the respective exponential. Indices in eq. 2.21 refer to the fast (*I*) and the slow (*II*) process. For the determination of permeation coefficients the biexponential eq. 2.21 was used, and apparent permeation coefficients $Perm_{app}$ were calculated from k_I and the liposomal radius r as follows (eq. 2.22):

$$Perm_{app} = k_I \cdot \frac{r}{3} \quad (2.22)$$

where $r/3$ is used as an approximation for the ratio between the total inner aqueous volume of the liposomes and the total membrane area [Paula et al., 1998]. The radius r was estimated from

2 Materials and Methods

the hydrodynamic mean diameter of the liposomes as determined by dynamic light scattering (see section 3.1).

Intrinsic permeation coefficients of the net neutral ($Perm^{AH}$), deprotonated ($Perm^{A^-}$) and diprotonated ($Perm^{AH_2^+}$) were fitted from the $\log Perm_{app}/pH$ profiles according to eq. 2.23.

$$\log Perm_{app} = \log \left(\alpha^{AH} \cdot 10^{\log Perm^{AH}} + \alpha^{A^-} \cdot 10^{\log Perm^{A^-}} + \alpha^{AH_2^+} \cdot 10^{\log Perm^{AH_2^+}} \right) \quad (2.23)$$

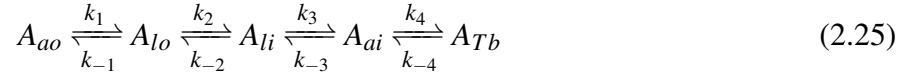
The pH-partition hypothesis neglects the permeation of the net charged species when estimating membrane permeation. To test the hypothesis for the studied ACAs, $\log Perm^{AH^*}$ values were extrapolated for each $\log Perm_{app}$ value according to eq. 2.24:

$$Perm^{AH^*} = Perm_{app} / \alpha^{AH} \quad (2.24)$$

2.9 Description of the permeation process by a differential equation system and numerical solution thereof

2.9.1 Definition of the rate laws

Permeation kinetics were simulated based on the rate constants of the equilibria for partitioning and translocation as described in eq. 2.25, which is in agreement with the model for membrane permeation by Lauger et al. [1981].



A_{ao} denotes the solute A in the outer aqueous phase, A_{lo} and A_{li} designate the solute in the outer and inner lipid leaflet, respectively, and A_{ai} stands for the solute in the liposomal lumen. The luminal solute ligated to entrapped Tb^{3+} in the liposomes is given by A_{Tb} . The partitioning into the membrane is described by the rate constants k_1 and k_{-3} , whereas k_{-1} and k_3 are the dissociation rate constants. The ratios k_1/k_{-1} and k_{-3}/k_3 equal the partition coefficient P . The translocation rate constants are defined as k_2 and k_{-2} . The rate constant k_4 describes the 1:1 complex formation between free A and Tb^{3+} and k_{-4} the dissociation of the complex.

The following conditions were considered for the membrane permeation model described in eq. 2.25:

(i) the complex formation (k_4) is faster than the overall permeation process as shown in section 3.3.2. Control experiments revealed that under our experimental conditions the complex formation had no influence on the overall permeation coefficients (see section 3.3.2). Simulations including the equilibrium for the complex formation revealed a range where k'_4 and k'_{-4} were indeed without effect on the permeation coefficients (see section 3.7.3). Thus, both k_4 and k_{-4} were not included in the simulations, if not indicated otherwise.

(ii) The bilayer is symmetrical and the inner and outer leaflets have equal volumes and thus (eq. 2.26),

$$k_2 = k_{-2} \quad (2.26)$$

(iii) As the aqueous and lipid volumes are not equal the rate constants in eq.2.25 have to be normalized for a reference volume V_{norm} according to the general eq. 2.27,

$$k' = k \cdot \frac{V_{norm}}{V_x} \quad (2.27)$$

with V_{norm} as the reference volume for normalization and V_x the volume of the respective origin phase in the experimental setup. The normalization of the rate constants are described in detail in section 2.9.4

With these considerations the rate laws for eq. 2.25 can be written as (eq. 2.28):

$$\begin{aligned} d[A_{ao}]/dt &= -k'_1 \cdot [A_{ao}] + k'_{-1} \cdot [A_{lo}] \\ d[A_{lo}]/dt &= k'_1 \cdot [A_{ao}] - (k'_{-1} + k'_2) \cdot [A_{lo}] + k'_{-2} \cdot [A_{li}] \\ d[A_{li}]/dt &= k'_2 \cdot [A_{lo}] - (k'_{-2} + k'_3) \cdot [A_{li}] + k'_{-3} \cdot [A_{ai}] \\ d[A_{ai}]/dt &= k'_3 \cdot [A_{li}] - k'_{-3} \cdot [A_{ai}] \end{aligned} \quad (2.28)$$

2.9.2 Solutions of the differential equation system

To solve the differential equation system eqs. 2.28 numerically a simulation algorithm was implemented as command line version in ANSI-C and in Java [Thomae et al., submitted]. The differential system of equations can also be solved using mathematical toolkits, such as Maple. The Maple script with example settings is shown in Fig. 2.1. The results of the possible solutions were not significantly different for the three approaches.

The numerical solution of the differential equations revealed triexponential equations of the form (eq. 2.29),

$$[A_x(t)] = a \cdot e^{-qt} + b \cdot e^{-rt} + c \cdot e^{-st} + d \quad (2.29)$$

where $[A_x(t)]$ represents the concentration of the solute A in phase x at time t and q, r, s are composed of the single rate constants k'_1 to k'_{-3} .

To compare the overall permeation rates, i.e. $d[A_{ai}]/dt$, we introduced t_{90} , the time when 90% of the plateau value of the maximal luminal permeant concentration $[A_{ai}(t \rightarrow \infty)]$ is reached. It has to be noted that an increase in t_{90} reflects a decrease in the permeation rate. Choosing the time point t_{50} instead of t_{90} led to similar results for the comparison of the different settings.

2.9.3 Estimation of the volumes of the aqueous and lipid phases

Assuming that liposomes are spheres, the total volume of one average liposome, $V_{liposome}$, was calculated according to eq. 2.30:

$$V_{liposome} = \frac{1}{6} \pi \cdot d^3 \quad (2.30)$$

with d corresponding to the hydrodynamic diameter as obtained by dynamic laser light scattering (see section 3.1). The volume of the inner aqueous phase (V_{inner}) and of the lipid bilayer ($V_{bilayer}$) of one average liposome were calculated from d and the bilayer thickness h according to eqs. 2.31 and 2.32, respectively. According to Huang and Mason [1978] the bilayer thickness h equals $\sim 4 \text{ nm}$.

$$V_{inner} = \frac{1}{6} \pi \cdot (d - 2h)^3 \quad (2.31)$$

$$V_{bilayer} = V_{liposome} - V_{inner} \quad (2.32)$$

With the amount of lipids [mg] used for the assay the total lipid volume, V_{lipids} , was approximated with a lipid density $\rho = 1.0 \text{ g} \cdot \text{ml}^{-1}$ [Huang and Mason, 1978]. The number of liposomes $N_{liposomes}$ resulted from eq. 2.33.

$$N_{liposomes} = \frac{V_{lipids}}{V_{bilayer}} \quad (2.33)$$

The total volume of inner aqueous phase, V_{ai} , is related to $N_{liposomes}$ as follows (eq. 2.34):

$$V_{ai} = N_{liposomes} \cdot V_{inner} \quad (2.34)$$

The volume of the outer aqueous phase, V_{ao} , is calculated from the total sample volume (V_{total}) as shown in eq. 2.35.

$$V_{ao} = V_{total} - (N_{liposomes} \cdot V_{liposome}) \quad (2.35)$$


```

##### 1
# a maple script for the simulation of a permeation process 2
# by using a differential equation system 3
# 4
# Knud Zabrocki <zabrocki@physik.uni-halle.de> 5
# 27/02/2006 6
# 7
# Distributed without any warranties whatsoever. 8
# 9
##### 10
restart; 11
##### 12
## INPUT 13
# initiate start concentration 14
Aao0:=1; 15
Alo0:=0; 16
Ali0:=0; 17
Aai0:=0; 18
# set rate constants 19
k1:=1.0; 20
k2:=100; # k-1 21
k3:=1; # k2 22
k4:=1; # k-2 23
k5:=100; # k3 24
k6:=10; # k-3 25
##### 26
## SOLUTION PROCEDURE 27
# solve the equation system 28
SS:=dsolve({ 29
diff(Aao(t),t)=-k1*Aao(t)+ k2*Alo(t) ,Aao(0)=Aao0, 30
diff(Alo(t),t)= k1*Aao(t)-(k2+k3)*Alo(t) +k4*Ali(t) ,Alo(0)=Alo0, 31
diff(Ali(t),t)= k3*Alo(t)-(k4+k5)*Ali(t)+k6*Aai(t) ,Ali(0)=Ali0, 32
diff(Aai(t),t)= k5*Ali(t)-k6*Aai(t) ,Aai(0)=Aai0}, 33
{ Aao(t), Alo(t), Ali(t), Aai(t) }); 34
##### 35
## OUTPUT 36
# plot a 2D-graph 37
plot([rhs(SS[1]),rhs(SS[2]),rhs(SS[3]),rhs(SS[4])],t=0..50); 38
##### 39

```

Figure 2.1: Maple script for a numerical solution of eq. 2.28. The parameters were set to representative examples. # signs indicate programmer’s comments. Note that the nomenclature of the equations is different from the one used in eq. 2.28 due to software restrictions.

The total volume of all outer (V_{lo}) or inner (V_{li}) lipid leaflets, respectively, was estimated by eq. 2.36:

$$V_{li} \approx V_{lo} \approx \frac{V_{lipids}}{2} \quad (2.36)$$

With the standard conditions of the permeation assay, i.e. $d \sim 200nm$ and $c_{lipid} \sim 2mg/ml$, eq. 2.30-2.36 reveal the following volume ratios (eq. 2.37):

$$V_{ao} : V_{lo} : V_{li} : V_{ai} = 98.6 : 0.1 : 0.1 : 1.2 \approx 1000 : 1 : 1 : 10 \quad (2.37)$$

The indices have the same meaning as in eq. 2.25.

2.9.4 Relationship between true and apparent rate constants

As the volumes of the aqueous and lipid phases are not equal (eq. 2.37) in the permeation assay, the true rate constants k have to be transformed into apparent rate constants k' . Considering the partition coefficient P and applying the volume ratios described above the ratios of k'_1/k'_{-1} and k'_3/k'_{-3} can be calculated with eqs. 2.38 to 2.40.

$$P = \frac{k_1}{k_{-1}} \quad (2.38)$$

$$= \frac{k_{-3}}{k_3}$$

$$\frac{k'_1}{k'_{-1}} = P \cdot \frac{V_{lo}}{V_{ao}} \quad (2.39)$$

$$= P \cdot \frac{1}{1000}$$

$$\frac{k'_{-3}}{k'_3} = P \cdot \frac{V_{li}}{V_{ai}} \quad (2.40)$$

$$= P \cdot \frac{1}{10}$$

$$= 100 \cdot \frac{k'_1}{k'_{-1}}$$

Normalization to V_{ao} according to eq. 2.27 revealed the apparent rate constants (eq. 2.41 - 2.44) for a symmetrical bilayer, i.e. $V_{lo} = V_{li}$, with equal conditions in the outer and inner aqueous phases.

$$k'_1 = k_1 \quad (2.41)$$

$$k'_{-1} = \frac{k'_1 \cdot V_{ao}}{P \cdot V_{lo}} \quad (2.42)$$

$$= k'_3$$

$$k'_2 = k'_{-2} \quad (2.43)$$

$$= k_2 \cdot \frac{V_{ao}}{V_{lo}}$$

$$k'_{-3} = \frac{V_{li}}{V_{ai}} \cdot P \cdot k'_3 \quad (2.44)$$

$$= \frac{V_{ao}}{V_{ai}} \cdot k'_1$$

2.10 Multivariate Analysis (MVA)

2.10.1 Source of calculated molecular descriptors

The 2D structure (neutral form) of the 13 compounds used in this study were converted into their SMILES code using the JMEMoleculareditor (courtesy of Peter Ertl, Novartis, Basel, Switzer-

land). MILOGP and MIPSAs (see Table 3.10 for explanation of the abbreviations) were calculated from the Molinspiration Property Calculation Services [Free online Cheminformatics Services, 2006]. ALOGP, IALOGP, KOWWIN, XLOGP, MIPSAs, USI, HI, TIE and MRI were calculated with the ALOGPS 2.1 and PClient software [Tetko et al., 2005] from VCCLAB [Tetko, 2006]. POL was computed with SPARC v3.1 [University of Georgia, 2006]. The commercial available software Absolv Predictor was used to obtain A, B, ABRPOL, R2, VX (ADME Boxes v 3.0, Pharma Algorithms, Toronto, Canada).

2.10.2 Preprocessing of molecular descriptors

Since the results of PCA and PLS modeling are scale-dependent, all variable values were mean-centered and scaled for unit variance according to eq. 2.45 with the average value \bar{x} and the standard deviation σ . For each variable, the resulting values x_{mc} had uniform average values $\bar{x}_{mc} = 0$ and $\sigma_{mc} = 1$.

$$x_{mc} = \frac{x - \bar{x}}{\sigma} \quad (2.45)$$

2.10.3 Settings for the Multivariate Analysis

PCA and PLS were performed using the software SIMCA-P 11.0 (Umetrics, Umeå, Sweden). The significant number of principal components (PC) was obtained using the default significance test settings of the software. For each model, a confidence region of 95% was calculated. All scores were within this interval.

Throughout the whole analysis, cross validation (CV) was used. With CV, some observations are kept out of the model development, then the deleted observations are predicted by the model and compared with the actual values. This process is repeated several times until every observation has been omitted once. The prediction error sum of squares (*PRESS*) is the sum of the squared differences between observed and predicted values for the data kept out of the model fitting.

For each model, the explained variance R^2 and the predicted variance Q^2 are displayed. R^2 is the fraction of the sum of squares (*SS*) i.e. the percent of variation which is explained by the extracted components. R^2 is a measure of how well the model fits the data. Q^2 is the fraction of the total variation that can be predicted by the extracted components according to cross validation, which is computed as (eq. 2.46):

$$Q^2 = 1.0 - \frac{PRESS}{SS} \quad (2.46)$$

A large Q^2 ($Q^2 \geq 0.5$) indicates good predictability. In the PLS modelling, the importance of the variables both to explain X and to correlate to Y is summarized as variable influence in the projection (VIP). Variables with $VIP \geq 1$ are the most relevant for determining Y, while VIP values ≤ 0.5 indicate irrelevant variables [Erikson et al., 2001].

For the computation of the dendrograms we used a statistical computing software called R [R Development Core Team, 2006]. The hierarchical cluster analysis was performed by the `hclust` function using as input an euclidean distance matrix of the various molecular descriptors.

3 Results

3.1 Characterization of the test compounds and lipids

3.1.1 Determination of pK_a and $\log P_{Oct}$ values of test compounds

Potentiometric titration

The pK_a values of the investigated ACAs as determined by potentiometric titration and UV measurements are shown in Table 3.1. Due to methodological limitations, $pK_a \leq 2$ and ≥ 12 were not determined.

ACA	abb.	pK_{a1}	pK_{a2}	$\log P_{Oct}^{AH}$
salicylic acid	(SA)	2.75 ± 0.01	–	2.44
2,4-dihydroxybenzoic acid	(DHB)	3.17 ± 0.01	8.65 ± 0.03	1.93
3-methylsalicylic acid	(MSA)	2.72 ± 0.07	–	3.04
5-chlorosalicylic acid	(CSA)	2.40 ± 0.08	–	3.09
3,5-dichlorobenzoic acid	(DCBA)	3.18 ± 0.02	–	3.61
anthranilic acid	(AA)	2.15 ± 0.11	4.76 ± 0.01	1.20
5-methylanthranilic acid	(MAA)	2.29 ± 0.08	5.10 ± 0.03	1.32
2-hydroxynicotinic acid	(OHNA)	4.97 ± 0.01	–	-0.13
pyrazine carboxylic acid	(PCA)	2.60 ± 0.03	–	-0.01
dipicolinic acid	(DPA)	2.07 ± 0.08	4.57 ± 0.02	0.62
anthracene-9-carboxylic acid	(AC)	4.5 ^a	–	1.15 ^b
5,6-carboxyfluorescein	(CF)	4.33 ± 0.33	6.38 ± 0.06	1.31
5-carboxyfluorescein diacetate	(CFDA)	3.83 ± 0.14	4.58 ± 0.01	2.27

Table 3.1: pK_a and $\log P_{Oct}$ values of ACAs investigated. If not indicated otherwise, values were obtained by potentiometric titration. abb., abbreviation.

^aas determined by UV measurements

^bas determined by shake-flask method

The salicylic acid derivatives (Fig. 3.1) had $\log P_{Oct}^{AH}$ values, i.e. $\log P_{Oct}$ of the net neutral species, of ~ 2 to ~ 3 . Introducing further hydroxy groups as in DHB led to a decrease of the affinity to the octanol phase, while the addition of the unpolar methyl group led to an increase of $\log P_{Oct}^{AH}$. MSA and SA had similar pK_a values indicating that the methyl group did not change

3 Results

the acidity of the carboxy group. The carboxy group in DHB (pK_{a1}), however, had a weaker acidity as compared to the other two. This is probably due to the positive mesomeric effect of the second hydroxy group, which leads to an increased electron density in the mesomeric system.

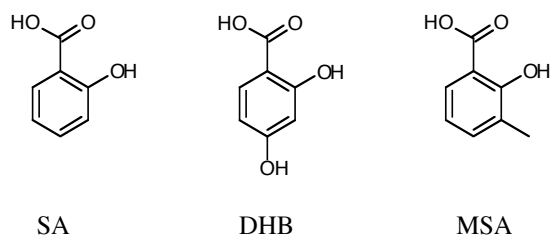


Figure 3.1: Structures of the tested ACAs: Salicylic acid derivatives. Salicylic acid (SA), 2,4-dihydroxybenzoic acid (DHB), 3-methylsalicylic acid (MSA).

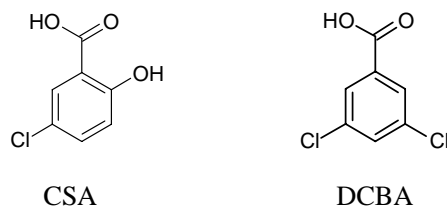


Figure 3.2: Halogenated benzoic acid derivatives: 5-Chlorosalicylic acid (CSA), 3,5-dichlorobenzoic acid (DCBA).

Halogenation at the aromatic ring (Fig.3.2) increased the affinities of the ACAs to octanol, e.g. the affinity of CSA is five times higher than that of its unhalogenated analog SA. The acidity of the halogenated ACAs was slightly increased as compared to their analogs, due to the negative inductive effect of the electron-withdrawing chlorine atoms.

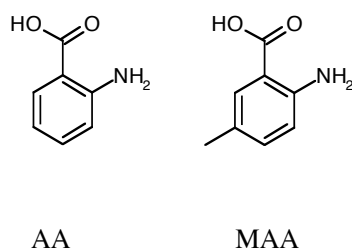


Figure 3.3: Amino benzoic acid derivatives: Anthranilic acid (AA), 5-methylanthranilic acid (MAA).

The introduction of amine groups at the benzene ring (Fig. 3.3) instead of the hydroxy group led to a decrease in the hydrophobicity of the compounds. The P_{Oct}^{AH} of AA, the amino analog of SA, is e.g. 15 times lower than the corresponding value of SA. This corresponds to 1.2 log units. Substitution of the benzene ring with apolar methyl groups led to an increase in hydrophobicity

3.1 Characterization of the test compounds and lipids

as found for the salicylic acid derivatives.

The amino benzoic acid derivatives display two pK_a values. In the literature, the higher pK_a value was assigned to the dissociation equilibrium of the carboxy group and the lower pK_a has been shown to correspond to the dissociation equilibrium of the amine group [Robinson and Briggs, 1957]. Thus, the amino benzoic acid derivatives can exist as net neutral, positively and negatively charged species. In a pH range between the pK_a values the uncharged species is predominating. Since the two pK_a values are close to each other (≤ 3 pH units) the uncharged species is assumed to be in equilibrium with the zwitterionic form [Pagliara et al., 1997]. The acidity of the carboxy function was significantly decreased as compared to the acidity of the salicylic acid derivatives.

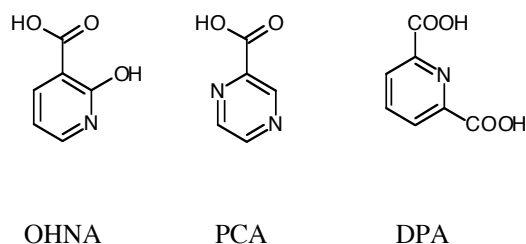


Figure 3.4: Heteroaromatic benzoic acid derivatives: 2-Hydroxynicotinic acid (OHNA), pyrazine carboxylic acid (PCA), dipicolinic acid (DPA).

Exchanging the benzene ring with the pyridine or pyrazine ring (Fig. 3.4) led to drastic changes in both, hydrophobicity and acidity. The P_{Oct}^{AH} of the heteroaromatic ACAs is around 200 times, i.e. 2.3 log units, lower than that of their non-heteroaromatic analogs. The determined pK_a of OHNA corresponds to the values described in literature for the pyridinium group of nicotinic acid (2.10 carboxy group, 4.63 pyridinium group, [Allan, 2006]). The pK_a of the carboxy function is probably ≤ 2 and thus out of the experimental range. Between \sim pH 2 and 5 the zwitterionic form is assumed to be the predominating species of OHNA. The pK_a of PCA cannot be assigned to a functional group. Experimental data indicate, however, that the predominating species at $pH \leq pK_a$ has in general a higher lipophilicity than at $pH \geq pK_a$ indicating that at pH values $\geq pK_a$ the net neutral species is present.

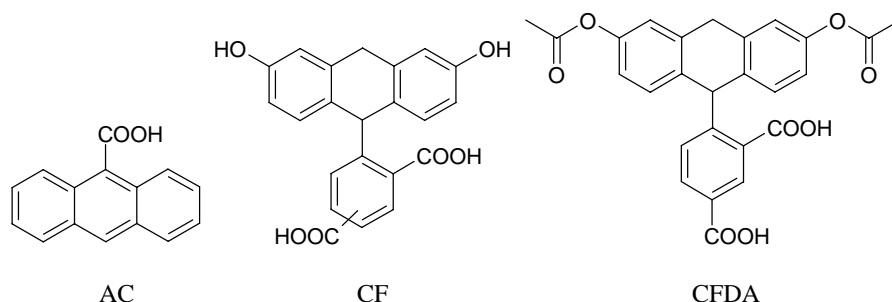


Figure 3.5: Large ACAs: Anthracene-9-carboxylic acid (AC), 5,6-carboxyfluorescein (CF), 5-carboxyfluorescein diacetate (CFDA)

Even though the large ACAs CF and CFDA have a large conjugated aromatic system, their

3 Results

lipophilicity is not increased as compared to the SA derivatives, probably because also the number of polar groups is increased. Esterification of two polar hydroxy groups increased the lipophilicity of CF 10fold (CFDA). The two pK_a values of CF and CFDA can be assigned to the two carboxy functions. The $\log P_{Oct}$ of AC is unexpectedly low. It has to be noted that due to the low solubility of AC the $\log P_{Oct}$ has been determined by the shake-flask method.

Determination of dissociation constants by ^{13}C -NMR measurements

The dissociation constant of SA was determined by ^{13}C -NMR measurements as described in section 2.3.3. The chemical shift δ of the carboxy function is shown as a function of pH in Fig. 3.6. The determined chemical shifts corresponded very well to the values described [London, 1980] with $\sim 172.5\text{ ppm}$ for the neutral species and $\sim 175.5\text{ ppm}$ for the dissociated species. The pK_a value as determined by ^{13}C -NMR was 2.68 which is in good agreement with the pK_a value as determined by potentiometric titration (2.75, Table 3.1).

However, the assignment of the chemical shifts to the functional groups is essential for the determination of the pK_a by ^{13}C -NMR. Since the solubility of the ACAs studied here was low leading to a high signal/noise ratio and a difficult peak assignment no further dissociation constants were determined with this method.

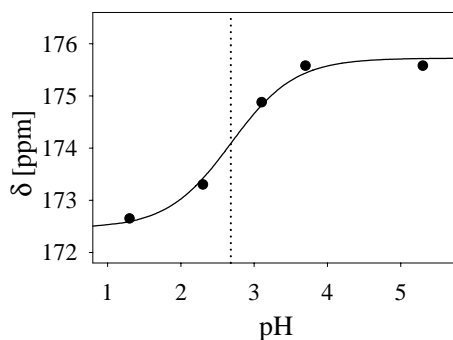


Figure 3.6: Determination of the pK_a of SA by ^{13}C -NMR at T 25°C: ●, measured δ . The full line represents the fit according to a Henderson-Hasselbalch function (eq. 2.2); the dotted line shows the fitted pK_a 2.68.

3.1.2 Determination of the pK_{aM} of stearylamine

The dissociation constant of StAm in the lipid bilayer environment was determined as described in section 2.3.4 by zetapotential measurements. The zetapotential ζ of PhC/StAm (70/30, mol/mol) liposomes increased with decreasing pH of the buffer used for the liposome dilution as shown in Fig. 3.7. The pK_{aM} of StAm was determined based on a Henderson-Hasselbalch function (eq. 2.3) using 25 mV and 0 mV as estimates for the ζ of the completely protonated StAm ζ^{HStAm^+} and the neutral StAm ζ^{StAm} , respectively. StAm is a base, curve fitting revealed a pK_{aM} of 9.7, which is in good agreement with the values found by Ptak et al. [1980] with ^{13}C -NMR measurements (~ 9.5). Thus, for the pH-range investigated in the permeation experiments ($\text{pH} \leq 7$), StAm is $\geq 99.9\%$ protonated.

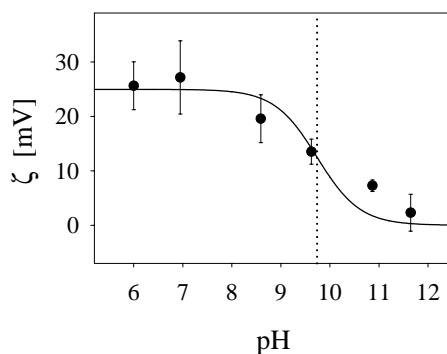


Figure 3.7: Determination of the pK_{aM} of stearylamine at T 25°C: ●, measured zeta potential ζ ; error bars, standard deviation ($n = 3$). The full line represents the fit according to eq. 2.3; the dotted line shows the fitted pK_{aM} 9.7.

3.2 Membrane affinity

3.2.1 Stability of radiolabeled compounds

The stabilities of ^{14}C -SA, ^{14}C -AA, and ^{14}C -OHNA were tested by TLC as described in section 2.1.2. The results of the TLCs are shown in Fig. 3.8. ^{14}C -SA and ^{14}C -AA show only one peak each (R_f 0.9 for both, SA and AA) that corresponds to the R_f -value as determined by TLC with the corresponding unlabeled compounds (R_f 0.9 for both SA and AA). Thus, these compounds can be considered as pure, no further purification step was necessary for the determination of the membrane affinities.

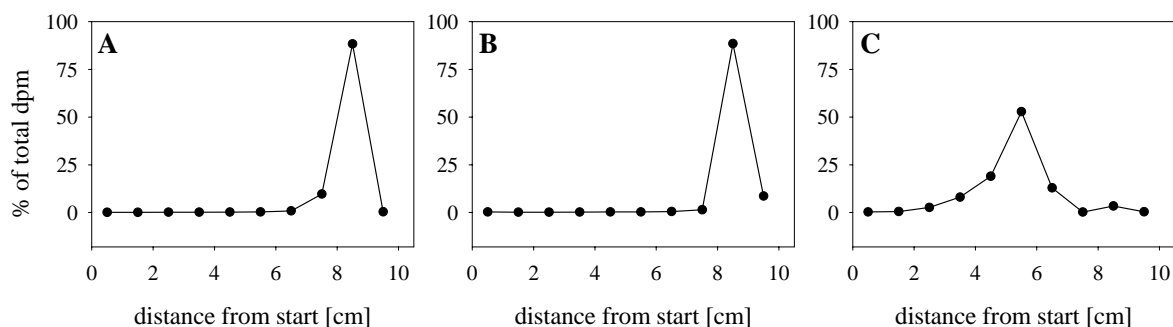


Figure 3.8: Stability of radiolabeled ACAs as determined by TLC. TLC sheets were developed for 10 cm and cut into stripes of 1 cm each. The graphs show the measured radioactivity (●, in % of total measured radioactivity) per stripe. The mobile phase was glacial acetic acid/ methanol/ water (1/40/60 v/v). (A) ^{14}C -SA; (B) ^{14}C -AA; (C) ^{14}C -OHNA

With ^{14}C -OHNA two peaks were found, a main peak (R_f 0.6) and a second peak (R_f 0.9). The R_f of the main peak corresponds to the R_f determined with the unlabeled compound (R_f 0.6). The second peak can be assigned to an impurity with a higher lipophilicity than OHNA. Even if the percentage of the impurity is small ($\approx 4\%$), it could lead to significant errors in the determi-

nation of the membrane affinity due to its higher lipophilicity. Thus, the membrane affinities of ^{14}C -OHNA were determined only after its purification by TLC as described in section 2.1.2.

3.2.2 Affinity to phosphatidycholine bilayers

The membrane affinities of the test compounds, expressed as $\log D$, were determined by equilibrium dialysis between pH 1.5 and 7.5. The $\log D$ values were pH-dependent, following Henderson-Hasselbalch functions. The experimental data at T 25°C are shown in Fig. 3.9 (open symbols) together with the fitted distribution profiles according to eq. 2.19. The fitted $\log P$ values of the different ionization species are shown in Table 3.2. There was no significant difference to the partition data determined at T 37°C (data not shown). Comparing the net neutral species (AH), SA had the highest PhC membrane affinity, $\log P_{\text{PhC}}^{\text{AH}}$ was 2.59. The membrane affinity of the net neutral species of AA was three times lower as compared to SA, $\log P_{\text{PhC}}^{\text{AH}}$ was 2.08. The $\log P_{\text{PhC}}^{\text{AH}}$ of OHNA was ≤ 1 . The membrane affinities of OHNA were in general low leading to a high scattering of the data, hence $\log P$ values were not fitted in any of the tested systems. The membrane affinities of the anionic species (A^-) of SA and AA were ~ 55 and 90 times lower than those of the corresponding neutral species ($\log P_{\text{PhC}}^{\text{A}^-}$ 0.85 and 0.13, respectively). The affinity of the di-protonated species AH_2^+ of AA was similar to the affinity of the net neutral species.

		PhC	PhC/Chol 60/40	PhC/PhI 70/30	PhC/StAm 85/15
SA	$\log P^{\text{AH}}$	2.59 ± 0.03	2.23 ± 0.02	2.41 ± 0.04	2.59 ± 0.04
	$\log P^{\text{A}^-}$	0.85 ± 0.04	0.51 ± 0.06	0.00 ± 0.07	1.60 ± 0.02
AA	$\log P^{\text{AH}_2^+}$	1.97 ± 0.08	n.d.	n.d.	n.d.
	$\log P^{\text{AH}}$	2.08 ± 0.02	1.66 ± 0.03	1.74 ± 0.06	1.83 ± 0.03
	$\log P^{\text{A}^-}$	0.13 ± 0.04	0.02 ± 0.08	-0.40 ± 0.32	1.06 ± 0.04

Table 3.2: Membrane affinity parameters of SA and AA in different liposomal systems at T 25°C. Fitted values \pm estimated standard errors are shown. The membrane affinities of all ionization species of OHNA were too low to be fitted reliably.

3.2.3 Influence of cholesterol on membrane affinity

To investigate the influence of Chol on the membrane affinity of the three ACAs, equilibrium dialysis experiments were performed with either PhC/Chol 90/10, PhC/Chol 75/25 or PhC/Chol 60/40 (% mol/mol) liposomes. The comparison of the distribution profiles obtained with PhC/Chol 60/40 liposomes and PhC liposomes is shown in Fig. 3.9, left panel. The fitted $\log P$ values at all tested PhC/Chol ratios are shown in Fig. 3.9, right panel. The $\log P$ values of all ionization species at 40% (mol/mol) Chol are given in Table 3.2. The $\log P^{\text{AH}}$ and $\log P^{\text{A}^-}$ of SA decreased with increasing amounts of Chol, except at 10% Chol, which had no effect. For both ionization species, the affinity to the PhC/Chol 75/25 bilayers was ~ 1.3 times reduced and the affinity to PhC/Chol 60/40 liposomes was about two times lower than to PhC liposomes.

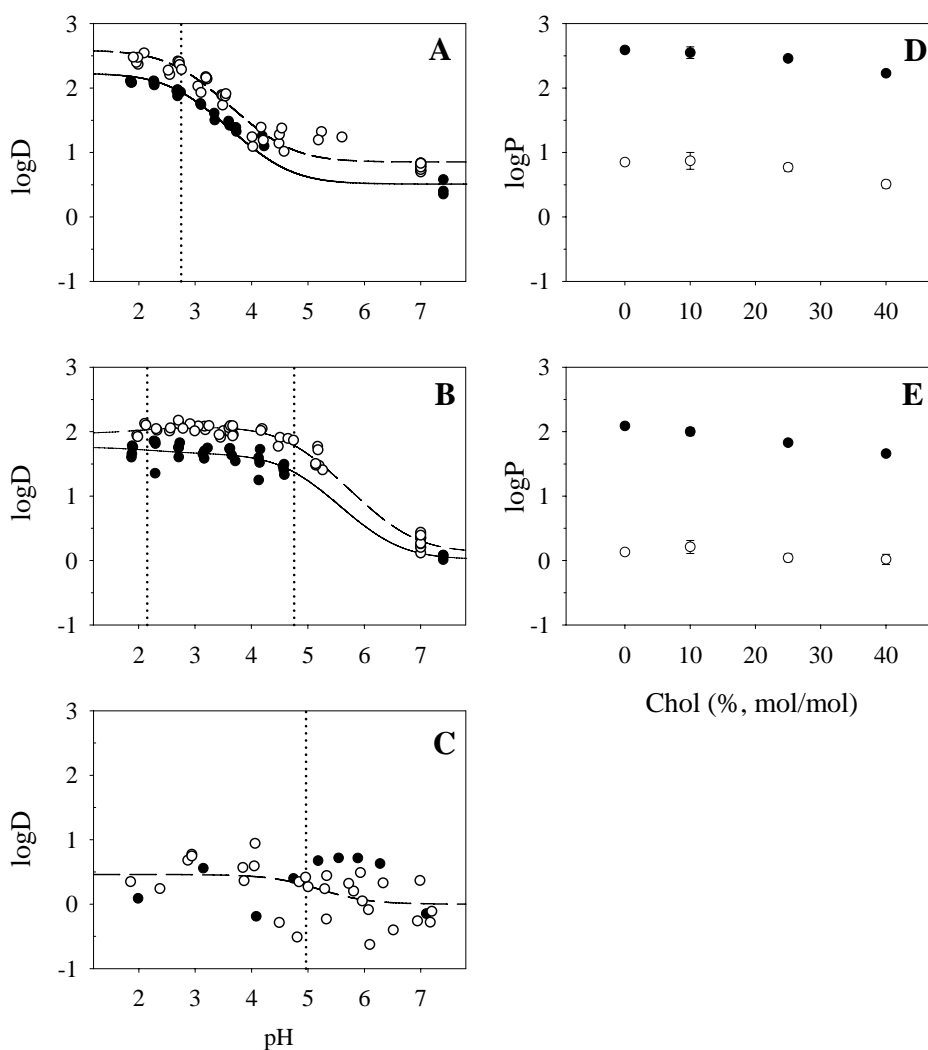


Figure 3.9: Affinity to PhC and PhC/Chol bilayers. (left panel) Membrane affinity of (A) SA, (B) AA and (C) OHNA to PhC (\circ) and PhC/Chol 60/40 (\bullet) liposomes at T 25°C. $\log D/\text{pH}$ profiles were fitted based on the Henderson-Hasselbalch equation with the titrated pK_a of the respective acid (dotted lines) and considering the partitioning of all ionization species (PhC, dashed line; PhC/Chol 60/40, solid line). (right panel) Fitted $\log P$ values (error bars, estimated standard errors) of the different ionization species (\bullet , $\log P^{AH}$; \circ , $\log P^{A^-}$) for (D) SA and (E) AA in PhC and all tested PhC/Chol liposomes. Data are from 2 or 3 independent experiments.

The influence of Chol on the membrane affinity of the net neutral and the anionic forms of AA was similar as for SA. The membrane affinities of the cationic species AH_2^+ of AA are not well defined as the respective pK_a is at the very low end of the experimental pH range. In addition, at this pH the pK_a of PhC ($pK_a \approx 2$) affects the membrane characteristics [Pauletti and Wunderli-Allenspach, 1994].

3.2.4 Influence of phosphatidylinositol on membrane affinity

To explore the influence of the negatively charged PhI on the membrane affinity, equilibrium dialysis experiments were performed with PhC/PhI 70/30 liposomes. Fig. 3.10 and Table 3.2 show the distribution profiles and the fitted $\log P$ values.

The membrane affinity of neutral SA to PhC/PhI 70/30 liposomes was reduced by a factor of 1.5 as compared to PhC liposomes. The affinity of the anionic species was decreased by a factor of 7. The membrane affinity of the net neutral form of AA was reduced by a factor of 2 and P^{A^-} decreased by the factor 3.5 in PhC/PhI 70/30 bilayers as compared to PhC liposomes. As mentioned above, the membrane affinities of OHNA were too low to allow the analysis by curve fitting.

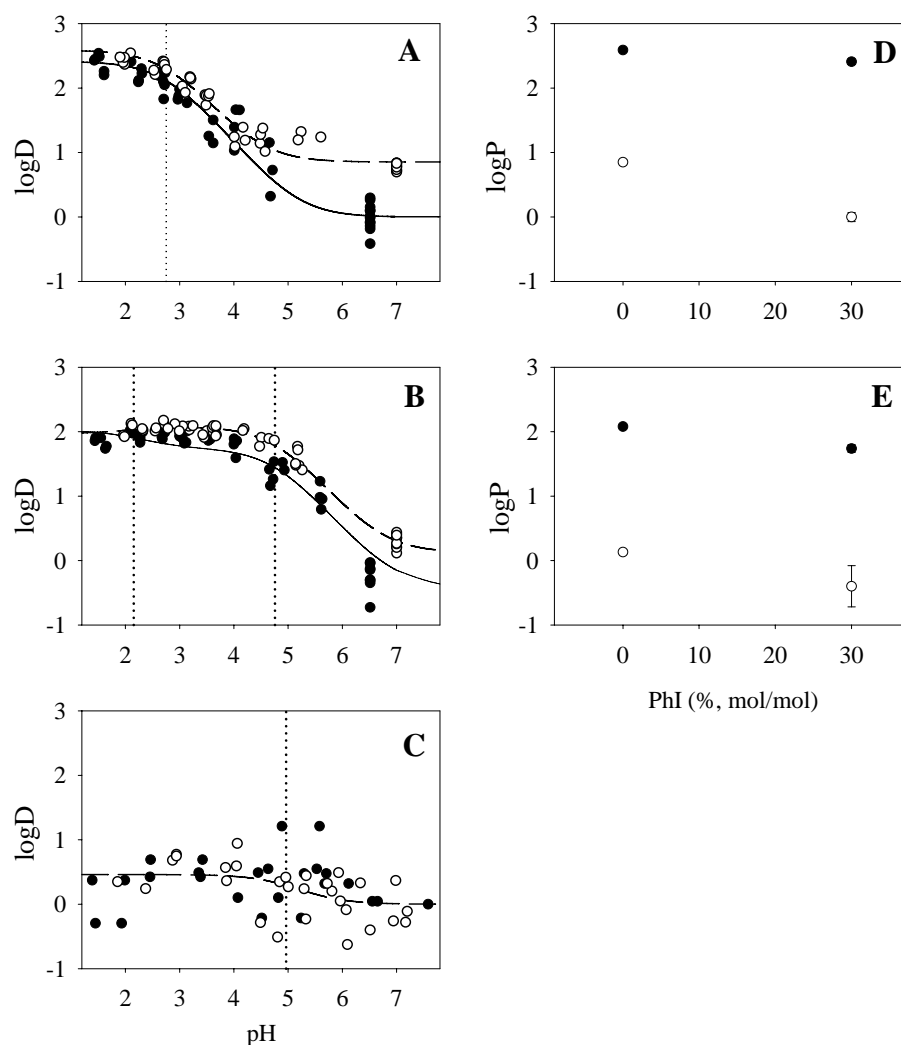


Figure 3.10: Affinities to PhC and PhC/PhI bilayers. (left panel) Membrane affinities of (A) SA, (B) AA, and (C) OHNA to PhC (\circ) and PhC/PhI 70/30 bilayers (\bullet) at T 25°C. $\log D$ /pH profiles were fitted as described in Fig. 3.9 (PhC, dashed line; PhC/PhI 70/30, solid line). (right panel) Fitted $\log P$ values of the different ionization species (\bullet , $\log P^{AH}$; \circ , $\log P^{A^-}$) for (D) SA and (E) AA in PhC and PhC/PhI 70/30 liposomes. Data are from 2 or 3 independent experiments.

3.2.5 Influence of stearylamine on membrane affinity

The influence of the positively charged lipid StAm on the membrane affinity was investigated using PhC/StAm 85/15 liposomes. The distribution profiles and fitted $\log P$ values are shown in Fig. 3.11 and Table 3.2. The partition coefficients of the SA and AA anions were increased 5.5 and 8.5 times, respectively, with 15% of the positively charged StAm as compared to PhC bilayers. The membrane affinity of the net neutral species was decreased by a factor 2. The membrane affinity of the positively charged species of AA was not well defined but was clearly lower than in the PhC liposome system. Note that data were best fitted allowing a deviation of the inflection points of the distribution profiles of SA and AA (inflection point around pH 6) from the titrated pK_a by + 0.8 and + 1.4 pH units, respectively.

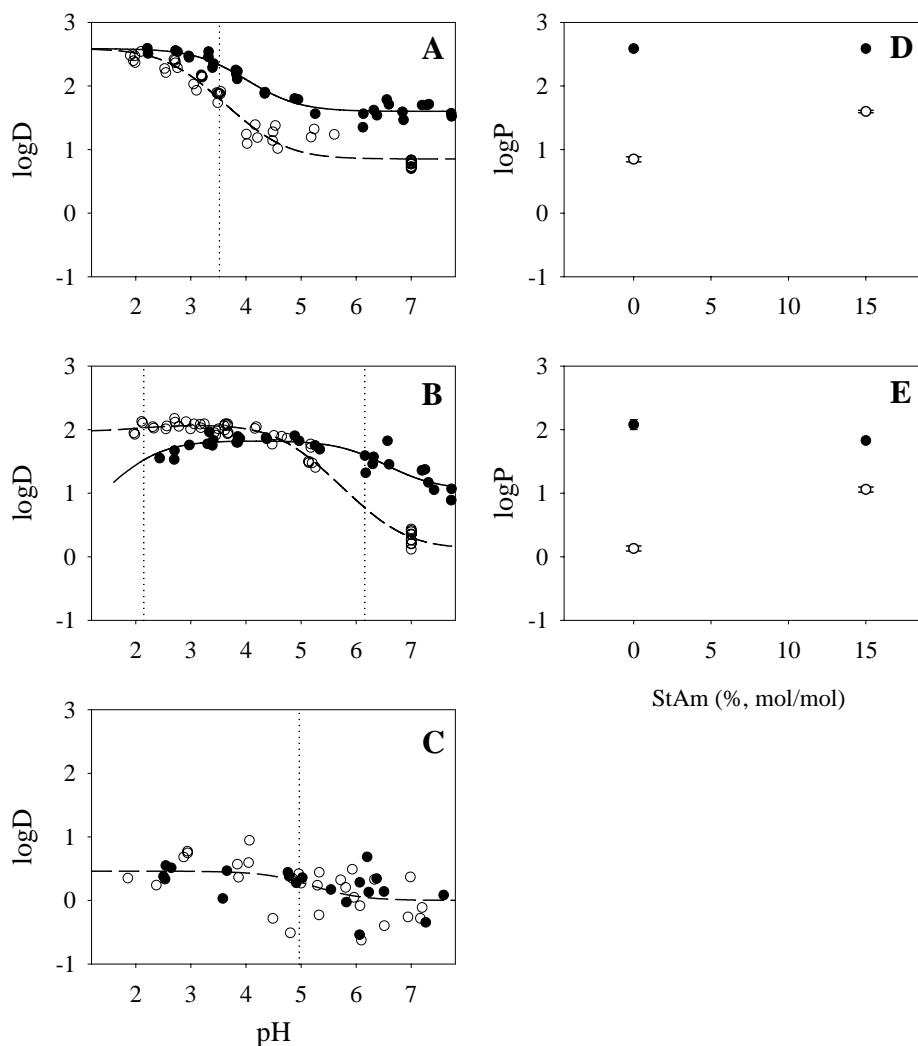


Figure 3.11: Membrane affinities to PhC and PhC/StAm 85/15 bilayers. (left panel) Membrane affinities of (A) SA, (B) AA, and (C) OHNA to PhC (\circ) and PhC/StAm 85/15 bilayers (\bullet) at T 25°C. $\log D$ /pH profiles were fitted as described in Fig. 3.9 (PhC, dashed line; PhC/StAm 85/15, solid line). (right panel) Fitted $\log P$ values of the different ionization species (\bullet , $\log P^{AH}$; \circ , $\log P^{A^-}$) for (D) SA and (E) AA in PhC and PhC/StAm 85/15 liposomes. Data are from 2 or 3 independent experiments.

3.3 The Tb(III)-permeation assay

3.3.1 Interaction of test compounds with Tb³⁺

Types of interaction

The fluorescence spectrum of Tb³⁺ shows two excitation peaks: a main peak at ≤ 230 nm and a side peak at 275 nm. There are three narrow emission bands at 490 nm, 545 nm and 585 nm as shown in Fig. 3.12. The basic principle of energy transfer has been explained in section 1.4.1.

Upon their interaction with Tb³⁺ the ACAs investigated can be divided into two groups. If the emission bands of Tb³⁺ are at higher wavelengths, i.e. at lower energy levels than the emission bands of the ligating ACA, Tb³⁺ acts as energy acceptor. Upon excitation of the complex at a wavelength corresponding to the excitation maximum of the ACA, energy is transferred from the ACA to the ligated Tb³⁺, resulting in an increase of the Tb³⁺ signal as shown in Fig. 3.12A with SA as ligand. In this way interact the ACAs SA, DHB, MSA, CSA, DCBA, AA, MAA, OHNA, PCA and DPA, i.e. all ACAs with one aromatic or heteroaromatic ring, since their excitation maxima are below ~ 400 nm.

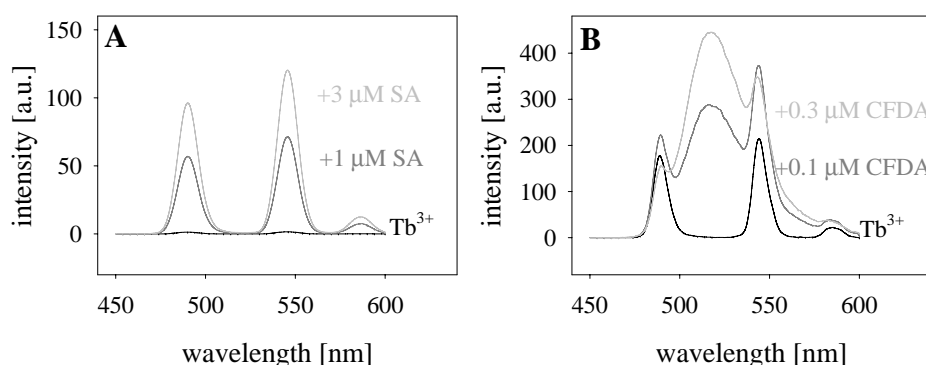


Figure 3.12: Interaction of ACAs with Tb³⁺. Spectra were recorded with 0.5 mM Tb³⁺ and different concentrations of (A) SA (λ_{ex} 318 nm) and (B) CFDA (λ_{ex} 230 nm) in 20 mM MOPS, pH 6.5 at T 25° under luminescence conditions (see below). (A) Tb³⁺ (energy acceptor) with and without SA (energy donor). Upon excitation of SA (λ_{ex} 318 nm) the Tb³⁺ signal increases. (B) Tb³⁺ (energy donor) with and without CFDA (energy acceptor). Upon excitation of Tb³⁺ (λ_{ex} 230 nm) the Tb³⁺ signal decreases (λ_{em} 490 nm) and a new peak arises at the emission maximum of the ligand (λ_{em} 517 nm).

If, however, the excitation bands of the ligand are at similar or higher wavelengths than the emission bands of Tb³⁺, Tb³⁺ acts as an energy donor. Upon excitation of the complex at a wavelength corresponding to the excitation maximum of Tb³⁺ (230 nm), the energy is transferred from Tb³⁺ to the ligand. This results in a decrease of the Tb³⁺ signal at the emission wavelength below the ligand excitation maximum, while simultaneously a new peak arises at a wavelength

corresponding to the emission peak of the ligand as shown in Fig. 3.12B with CFDA as ligand. In excess of Tb^{3+} , both effects are dependent on the ligand concentration. This interaction was found for the ACAs with conjugated aromatic systems (AC, CF, CFDA), since their excitation maxima are above 400 nm. With AC no formation of a new peak was found, and thus only the decrease of the Tb^{3+} signal was recorded.

Optimal phosphorescence conditions

Since the ACAs used show fluorescence on their own and the energy transfer to or from the Tb(III) is not quantitative, the quality of the spectra obtained under fluorescence conditions is poor and the signal is not selective for the ACA-Tb(III)-complex. The lifetime of the ACA-Tb(III)-complex signal is, however, longer than the lifetime of the ACA fluorescence signal [Maji et al., 2003], which is due to the process of intersystem crossing and energy transfer as described in section 1.4.1. The signal selectivity could thus be improved by recording the complex signal under phosphorescence conditions, i.e. with a time delay following the excitation flash.

Figure 3.13A shows the signal of the SA-Tb(III)-complex as recorded under fluorescence conditions and with different time delays (see caption for details). While with increasing time delay the unspecific signals decay very fast, the signal of the complex (λ_{em} 490, 545, 585 nm) is initially increased due to the longer integration time of the signal when changing from the fluorescence mode into the phosphorescence mode and decays considerably slower. This is indicated in Fig. 3.13B with λ_{em} 516 nm as unspecific background signal and λ_{em} 545 nm as specific signal of the complex. With increasing time delay the unspecific and specific signal as well as the ratio specific/unspecific signal decrease. The optimal time delay was determined to be 0.05 ms, reducing completely any unspecific signal while providing a good quantum yield of the SA-Tb(III)-complex. All permeation experiments were therefore recorded with a time delay of 0.05 ms.

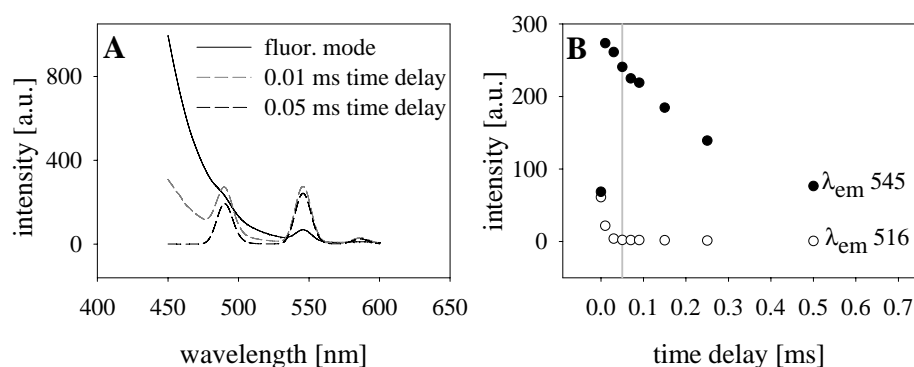


Figure 3.13: Optimal phosphorescence conditions. Spectra of 0.5 mM Tb^{3+} with 0.005 mM SA in 20 mM MOPS pH 6.8 were recorded with λ_{ex} 318 nm at T 25°C. (A) Spectra recorded with different time delays after the excitation flash. The fluorescence mode (fluor. mode) corresponds to no time delay. (B) Decay of the SA-Tb(III)-complex signal (●, λ_{em} 545 nm) in comparison with the decay of an unspecific signal (○, λ_{em} 516 nm as representative example). The straight grey line indicates the phosphorescence conditions providing an optimal ratio between specific/unspecific signal (0.05 ms).

pH-Dependency of excitation spectra

The excitation maxima of the ACA-Tb(III)-complexes were pH-dependent as shown in Fig. 3.14 with the SA-Tb(III)-complex as a representative example. Decreasing the pH from ~ 7 to ~ 3 shifts the excitation maximum to shorter wavelengths by ~ 18 nm and decreases the quantum yield of the signal.

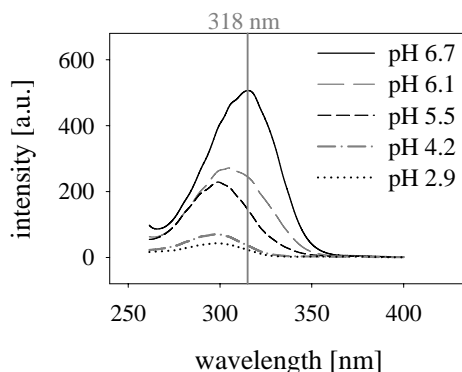


Figure 3.14: pH-dependent excitation spectra of the SA-Tb(III)-complex: $\lambda_{em} = 545$ nm, $c_{Tb^{3+}} = 0.5$ mM, $c_{SA} = 0.05$ mM, T 25°C. The full grey line indicates the excitation maximum at pH 7 ($\lambda_{ex} = 318$ nm). With decreasing pH of the solution the excitation maxima are blue-shifted and the quantum yields are reduced.

Table 3.3 shows the excitation maxima of the different ACAs as a function of the pH. For the larger ACAs the excitation maximum of the ACA-Tb(III) complex (corresponding to the excitation maximum of Tb^{3+}) was never pH-dependent, however, the quantum yield decreased with decreasing pH.

ACA	Excitation maxima λ_{ex}				
	pH 7	pH 6	pH 5	pH 4	pH 3
SA	318	308	300	300	300
DHB	307	298	289	289	289
MSA	316	305	305	305	305
CSA	327	327	312	312	312
DCBA	280	280	280	287	287
AA	318	318	318	318	318
MAA	328	328	328	328	263
OHNA	312	312	312	312	312
PCA	272	272	272	272	272
DPA	272	272	272	272	272

Table 3.3: Excitation maxima λ_{ex} [nm] of the test compounds in complex with Tb^{3+} at different pH with $\lambda_{em} 545$ nm, T 25°C.

3.3.2 Characterization of the Tb(III)-permeation assay

Kinetics of the complex formation

The interaction of Tb^{3+} and SA was determined at pH 7.0 in the absence of liposomes under stopped-flow conditions (Fig. 3.15). Kinetic data were fitted with the biexponential function eq. 2.21 revealing rate constants of $6\ s^{-1}$ for the fast phase and $0.5\ s^{-1}$ for the slow phase. In comparison to the kinetics of lipid bilayer permeation as determined with the Tb(III)-assay, the rate constant of the slow phase was four times higher than the rate constants of the fastest permeation kinetics, i.e. of CF at low pH, in the egg PhC liposome system ($0.15\ s^{-1}$). Hence, it can be confirmed that the rate-limiting step of the permeation assay was the permeation process and not the formation of the Tb^{3+} -ACA complex.

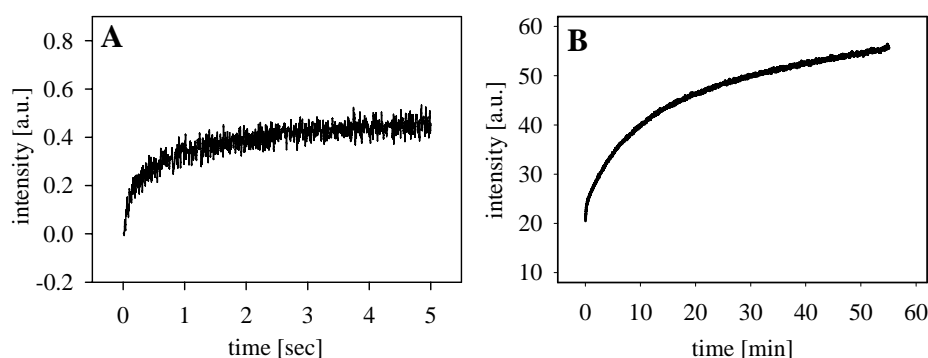


Figure 3.15: Kinetics of the complex formation between Tb^{3+} and SA (A) in comparison with permeation of SA into Tb^{3+} -containing liposomes (B). Tb^{3+} luminescence was recorded with λ_{ex} 318nm/ λ_{em} 545 nm at T 25 °C. (A) Solutions of 0.5 mM $TbCl_3$ and 0.5 mM SA in 20 mM MOPS, pH 7, were mixed in a volume ratio of 10:1 with a stopped-flow apparatus. (B) Tb^{3+} -loaded egg PhC liposomes were incubated in SUBS, pH 7.0, and 0.009 mM SA (final concentration) were added at time zero.

Kinetic analysis of membrane permeation

To investigate the permeation kinetics, Tb^{3+} -containing liposomes were incubated with the ACAs, excited at the appropriate wavelength (see Table 3.3) and the luminescence at 545 nm was recorded as described under section 2.8. The resulting luminescence/time curves were fitted with either a monoexponential (eq. 2.20) or a biexponential (eq. 2.21) function. Figure 3.16A shows data from a representative permeation assay with SA and egg PhC liposomes, together with the two fitted curves according to eqs. 2.20 and 2.21. The residuals of the fits are shown in Fig. 3.16B. The best fit with the lowest residuals was obtained with the biexponential function in all permeation assays. The maximum of the faster exponential term, I_{max_I} , was in all permeation experiments between 30 and 50 % of the total maximum, i.e. of the sum of I_{max_I} and $I_{max_{II}}$. The rate constant k_I of the faster exponential was used to calculate the apparent permeation coefficients $Perm_{app}$ according to eq. 2.22.

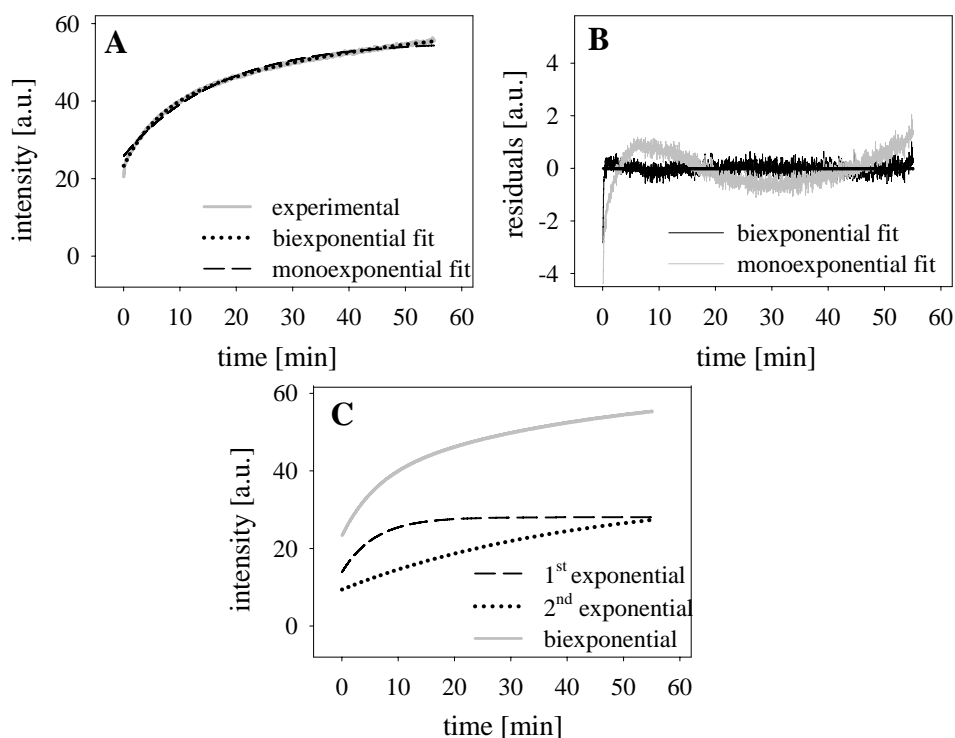


Figure 3.16: Kinetic analysis of the permeation curve. Tb^{3+} -loaded egg PhC liposomes were incubated in SUBS, pH 7.0, and 0.009 mM SA (final concentration) were added at time zero. Tb^{3+} luminescence was recorded with λ_{ex} 318nm/ λ_{em} 545 nm, T 25 °C. (A) Experimental luminescence/time curve and fits with a mono- and biexponential function, respectively. (B) Residuals of the fit functions. (C) Calculated 1st (fast) and 2nd (slow) exponential, respectively. The biexponential function is the sum of the two exponentials.

The pH at the membrane surface during permeation

In reply to our own publication [Thomae et al., 2005], the permeation of net neutral ACAs into the unbuffered liposomal lumen was suggested to induce the formation of a pH gradient between the outer and inner aqueous phase leading to artifacts in the measurements [Saparov et al., 2006]. To estimate the extent of a possible pH-gradient under our experimental conditions, we monitored the pH at the membrane surface using Tb^{3+} -loaded PhC, PhC/PhI 70/30 and PhC/StAm 85/15 liposomes containing the pH-sensitive fluorescent lipid fluorescein DHPE (0.5%, mol/mol). The pH-sensitive range as established with a calibration experiment was, depending on the lipid composition, between pH 4 and 7. For the permeation experiment liposomes with an unbuffered lumen were incubated with SA or without (control), respectively, in SUBS of different pH. Fig. 3.17 shows the DHPE fluorescence time course of a typical permeation experiment with the different liposome preparations. At time 0 liposomes were diluted with the buffer. Addition of SA is indicated by the arrow. For each lipid composition, the fluorescence increased with time in the presence and absence of SA. The maximal increase in pH as calculated from the calibration experiments was 0.5 within 40 min. The deviation of the membrane pH of the SA-containing sample from the control sample was maximally + 0.5 pH units. The observed

pH drift had no influence on the luminescence of ligated Tb^{3+} (data not shown). A permeation-induced pH-gradient as suggested by [Saparov et al., 2006] would lead to a decrease of the pH at the inner membrane surface instead of the observed increase. It has to be noted that it would be more precise to use a pH-sensitive dye which allows to estimate the pH from a fluorescence ratio between two different wavelengths instead of observing only changes at one fixed wavelength.

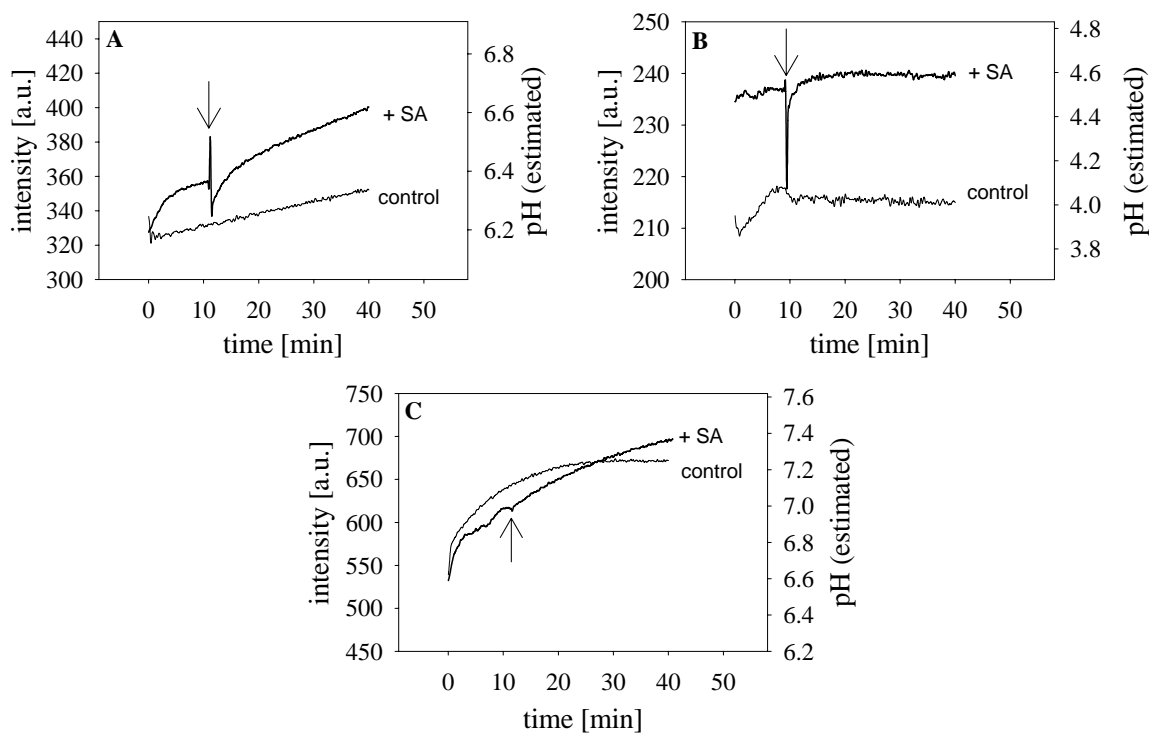


Figure 3.17: Monitoring the pH at the membrane surface using Tb^{3+} -liposomes containing the pH-sensitive fluorescent lipid probe DHPE; λ_{ex} 488 nm; λ_{em} 519 nm. Liposomes were diluted with SUBS (time 0) of the respective pH. Addition of SA is indicated by the arrow. (A) PhC (net neutral), SUBS pH 6.6; (B) PhC/PhI 70/30 (negatively charged), SUBS pH 5.5; (C) PhC/StAm (85/15) (positively charged), SUBS pH 6.6.

Influence of the intraliposomal buffer capacity on membrane permeation

In order to investigate, whether the observed kinetics are affected by a possible pH gradient resulting from the permeation of free acid into the unbuffered liposomal lumen, we prepared buffer-containing Tb^{3+} -liposomes by dissolving the lipid film in 200 mM MOPS buffer pH 6.5 or 200 mM HCl/KCl buffer pH 2.5, respectively. For the permeation assay liposomes were diluted with 200 mM MOPS pH 6.5, SUBS pH 6.5 or 200 mM HCl/KCl pH 2.5, respectively. At pH 6.5 SA is fully deprotonated while the ratio HA/A^- is 1.6 at pH 2.5. As shown in Table 3.4, the permeation coefficients were similar in preparations with different luminal buffer capacities. The Tb^{3+} -loading was, however, less efficient in the presence of buffer, leading to lower fluorescence signals (not shown). The differences in $\log Perm_{app}$ between SUBS- and MOPS-buffered samples were studied in more detail in section 3.4.1.

	$\log Perm_{app}$	
	pH 6.5	pH 2.5
Buffered lumen ^a	-8.16	-7.65
Buffer added after preparation ^b		
MOPS	-8.11	–
SUBS (unbuffered lumen)	-8.63	-7.34

Table 3.4: Influence of the intraliposomal buffer capacity on $\log Perm_{app}$ of SA at T 25°C.

^aLiposomes were prepared in the presence of 200 mM MOPS pH 6.5 or 200 mM HCl/KCl pH 2.5 and diluted with 200 mM MOPS pH 6.5 or SUBS pH 2.5 prior to the permeation experiment

^bLiposomes were prepared in the absence of buffer and diluted with the respective buffer prior to the permeation experiment

Influence of the complex association constant on membrane permeation

To elucidate the influence of the Tb(III)-complex association constant on the permeation coefficient, Tb³⁺ was incorporated into PhC liposomes as described in section 2.5.1 but in the presence of either 200 mM MOPS or 200 mM EDTA. The association constant of Tb³⁺ and the ACAs SA, OHNA and DPA is lowered by EDTA by several orders of magnitudes as compared to MOPS buffer (Table 3.5, Lombardi, D.; unpublished data). If the association constant would have a significant influence on the overall permeation rate the permeation coefficient would be considerably increased with EDTA-containing liposomes as compared to the reference system.¹ As shown in Table 3.5, the permeation coefficients obtained with MOPS- and EDTA-containing liposomes were similar. Since EDTA completely prevents the complex formation between Tb(III) and SA, no signal could be detected with SA and EDTA-containing liposomes serving at the same time as a control for the successful incorporation of EDTA into liposomes.

It can be concluded that the complex association constant does not influence the measured permeation rates of the ACAs used in the present study. Simulations as described in section 3.7 revealed indeed a range where the association constant does not affect the permeation coefficient. If the association constant is, however, exceeding a threshold it will change the apparent permeation rate.

Dependency of the membrane permeation on the solute and the lipid concentration

The dependency of the permeation coefficient on the ACA concentration was analyzed for three representative ACAs at different pH. The results are shown in Fig. 3.18. Varying the solute concentration in a range between c_{min} and c_{max} with $c_{max} \approx 10 \cdot c_{min}$ revealed no significant changes of $\log Perm_{app}$. c_{min} and c_{max} designate the smallest and highest tested solute concentration, respectively.

Together with the control experiments described above in this section these findings provide further evidence that within the ACA concentration range used no pH gradient is built up during

¹The influence of the complex association constant on the overall permeation rate was estimated by numerical simulations of the integrated rate laws as described in section 3.7.

ACA	$K_a [M^{-1}]^a$		$\log Perm_{app}$	
	MOPS	EDTA	MOPS ^b	EDTA ^c
SA	$2 \cdot 10^2$	– ^d	–8.16	no signal
OHNA	$1 \cdot 10^5$	$\leq 10^{-1}$	-8.02 ± 0.10	-8.18 ± 0.18
DPA	$8 \cdot 10^8$	$1 \cdot 10^3$	-8.19 ± 0.15	-8.21 ± 0.36

Table 3.5: Influence of the buffer type on the complex association constant K_a and on the permeation coefficient $\log Perm_{app}$ of SA, OHNA and DPA. All parameters were determined at pH 6.5 and T 25°C. $\log Perm_{app}$ were determined with PhC liposomes containing MOPS or EDTA in SUBS.

^aLombardi, D.; unpublished data

^bliposomes with MOPS-containing lumen

^cliposomes with EDTA-containing lumen

^dtoo low to be determined

the time course of the permeation experiments. Otherwise, this gradient would increase with increasing ACA concentrations leading to significantly different values of $\log Perm_{app}$.

Fig. 3.19 shows the influence of the lipid concentration on the membrane permeation of SA at pH 6.8 and pH 2.5. Increasing the lipid concentration 10fold, i.e. 10 mg/ml in comparison to

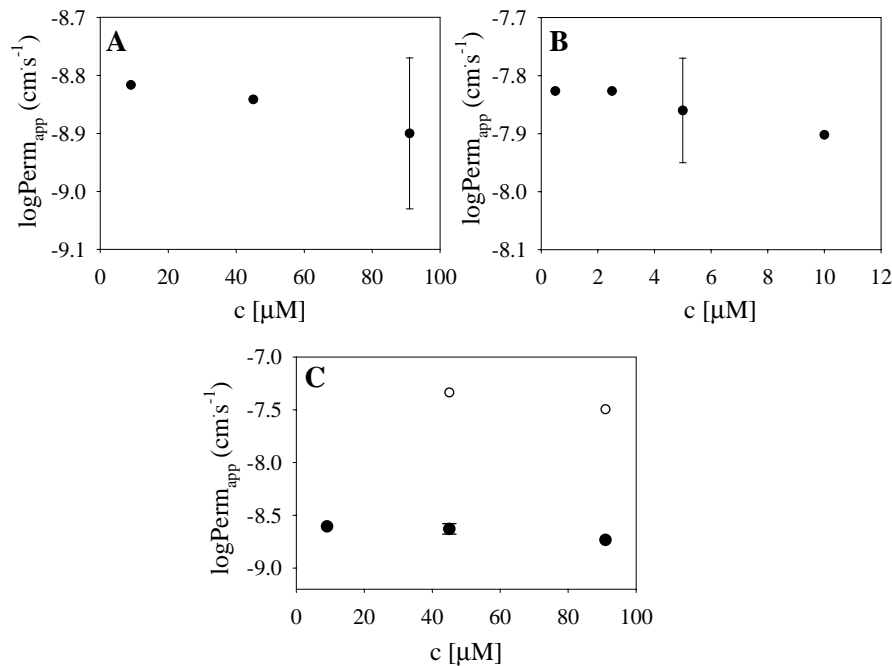


Figure 3.18: Influence of the solute concentration on $\log Perm_{app}$ of (A) DPA; (B) OHNA; and (C) SA at pH 6.8 (●) and pH 2.5 (○). PhC liposomes were used, the lipid concentration was 2 mg/ml, T 25°C. Data are from 1 or 3 (error bars, standard deviation) experiments, respectively.

3 Results

1 mg/ml, leads to an increase of $Perm_{app}$ by a factor ~ 2 . This is due to the changed volume ratios between the outer and inner aqueous phase and the lipid phase (see also section 3.7) leading to higher apparent rate constants for the association of the solute to the outer lipid leaflet, which results in a higher overall permeation rate. For all further permeation experiments a lipid concentration of ~ 2 mg/ml was used.

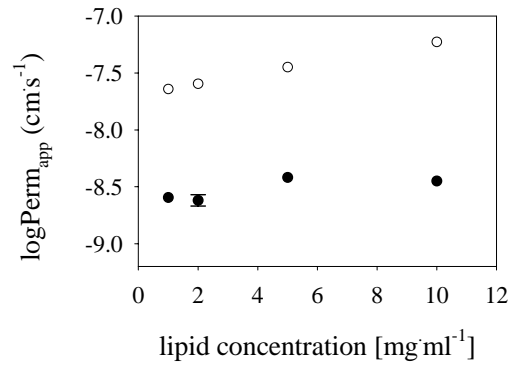


Figure 3.19: Influence of the lipid concentration on $\log Perm_{app}$ of SA at pH 6.8 (●) and pH 2.5 (○). PhC liposomes were used, the SA concentration was 0.05 mM, T 25°C . Data are from 1 or 3 (error bars, standard deviation) experiments, respectively.

3.4 Membrane permeation

3.4.1 Influence of the solute ionization state on membrane permeation

pH-Dependent permeation across egg phosphatidylcholine bilayers

The pH-dependent permeation of the three ACAs SA, OHNA and DPA (Fig. 3.1 and 3.4) across egg PhC bilayers was determined between pH \sim 3 and pH \sim 7. Permeation was not studied at pH values outside this pH range as the protonation of the PhC phosphate group below pH 3 affects drug-membrane interactions [Krämer et al., 1997] and precipitation occurred during the assay above pH 7.0, probably due to the hydroxylation of Tb³⁺. The permeation profiles are shown in Fig. 3.20. The three tested acids permeated slower at pH $\geq pK_a^{AH/A^-}$ than below or close to it, reaching a plateau one to two pH units above it. The $\log Perm_{app}/pH$ profiles were fitted with a Henderson-Hasselbalch function considering all ionization species with their intrinsic permeability coefficients $\log Perm^{AH}$ for the protonated compound, $\log Perm^{A^-}$ for the deprotonated acid and $\log Perm^{A^{2-}}$ for the di-deprotonated DPA (eq. 2.23). The fit parameters are shown in Table 3.6. The difference between the intrinsic $\log Perm$ values of two compound species differing by one proton, i.e. $\Delta \log Perm$ (Table 3.6), was highest for the pair of net neutral and deprotonated DPA, i.e. 2.2. The respective values for OHNA and SA were 1.1 and 1.7, i.e. the anions of the three tested acids permeated between 12 and 160 times slower than the respective neutral species. The complete deprotonation of DPA did not reduce permeation as compared to the mono-anion. The direct comparison of the fitted permeation/pH profiles of the tested acids is shown in Fig.3.20D.

	DPA	OHNA	SA
<i>logPerm</i> ^{AH}	-6.71 \pm 0.19	-6.78 \pm 0.06	-6.94 \pm 0.04
<i>logPerm</i> ^{A⁻}	-8.90 \pm 0.55	-7.87 \pm 0.07	-8.62 \pm 0.05
PhC <i>logPerm</i> ^{A²⁻}	-8.90 \pm 0.13	–	–
$\Delta \log Perm^{AH/A^-}$	2.2	1.1	1.7
$\Delta \log Perm^{A^-/A^{2-}}$	0.0	–	–
DPPC <i>logPerm</i> ^{AH}	n.d.	-7.90 \pm 0.17	n.d.
<i>logPerm</i> ^{A⁻}	n.d.	-8.32 \pm 0.18	n.d.
$\Delta \log Perm^{AH/A^-}$	n.d.	0.4	n.d.

Table 3.6: Membrane permeation parameters \pm estimated standard errors at T 25°C as determined with egg PhC liposomes in SUBS.

Beside the fits considering the permeation of all ionization species, $\log Perm_{app}/pH$ profiles were calculated from the fitted $\log Perm^{AH}$ values shown in Table 3.6 with eq. 2.24, neglecting the intrinsic permeation of the ionized species according to the pH-partition hypothesis. The calculated $\log Perm_{app}/pH$ profiles are shown in Fig.3.20A to C as broken lines. Additionally, $\log Perm^{AH*}$ values calculated from the experimental $\log Perm_{app}$ values with eq. 2.24 are shown

3 Results

as open triangles in the same graphs. If the pH-partition hypothesis would apply to PhC bilayer permeation, these values would be constant, i.e. pH-independent, and the broken lines would follow the experimental data.

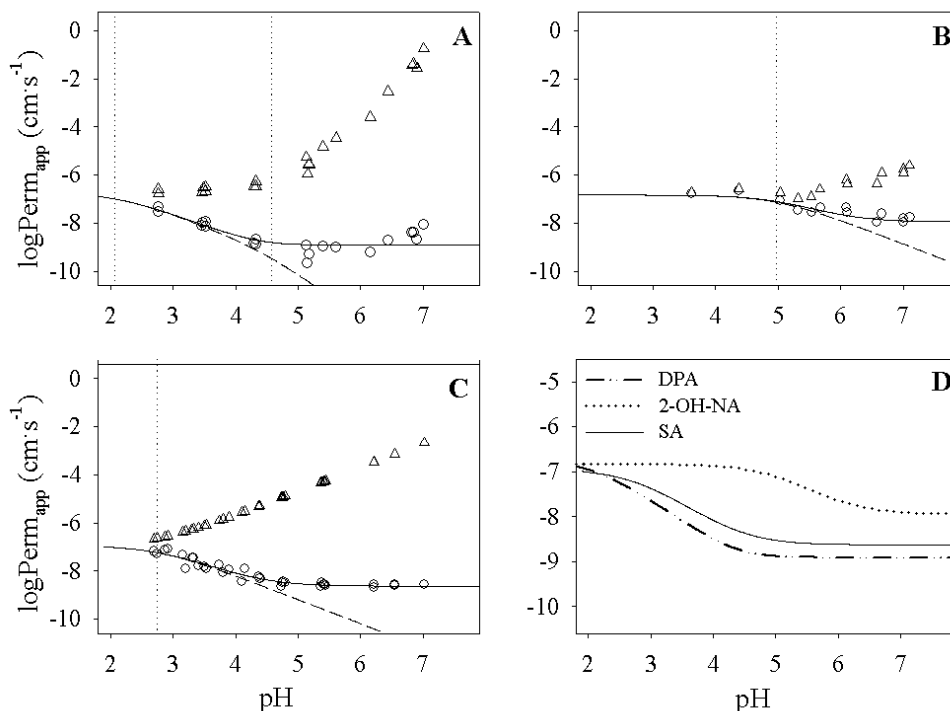


Figure 3.20: pH-Dependent permeation of DPA, OHNA, and SA across egg PhC bilayers at T 25°C in SUBS. The $\log Perm_{app}$ values (\circ) of (A) DPA, (B) OHNA, and (C) SA were calculated from the fast exponential term k_I of the biexponential kinetics of liposome entry. (A-C) (solid line) $\log Perm_{app}/pH$ profiles were fitted with a function based on the Henderson-Hasselbalch equation with the titrated pK_a of the respective acid (dotted line) and considering intrinsic permeation coefficients for each ionization species. The fitted intrinsic permeation coefficients are shown in Table 3.6. (D) Comparison of the fitted $\log Perm_{app}/pH$ profiles of the three acids. (A-C) (dashed line) Hypothetical $\log Perm_{app}/pH$ profile calculated from the fitted $\log Perm^{AH}$, neglecting permeation of the anionic species (see text for details). (Δ) $\log Perm^{AH*}$ values calculated for each experimental $\log Perm_{app}$ assuming that only the net neutral acid contributes to permeation (see text for details). Data of each profile are from ≥ 3 independent experiments.

Influence of counterions on permeation

To investigate the influence of counterions on the permeation of the neutral and deprotonated ACAs, permeation experiments with PhC bilayers were performed at pH 3.0 and pH 7.0 in either of the following buffer conditions: (i) SUBS, which contained about 0.2 M Na^+ , (ii) 0.2 M TRIS/HCl (only pH 7.0), (iii) SUBS containing 0.2 M TRIS/HCl, and (iv) 0.2 M TRIS containing 0.2 M NaCl (only pH 7.0). The $Perm_{app}$ values are shown in Fig. 3.21. At pH 7.0, where all three ACAs are $\geq 99\%$ deprotonated (DPA di-anionic), TRIS/HCl led to a 2.7fold

increase of the permeation coefficient of DPA and 4fold of SA as compared to SUBS, but had no influence on OHNA permeation at this pH. The effects of TRIS were independent of the presence of SUBS or NaCl in the experiments. At pH 3.0, the addition of TRIS to the SUBS increased the permeation of OHNA by a factor of about 1.4. The percentage of net neutral OHNA is 98.9 at this pH. No significant effect was observed on the permeation of the other two ACAs at pH 3.0. The weak increase of SA permeation at pH 3.0 in the presence of TRIS could be related to the 64% anionic SA present at pH 3.0.

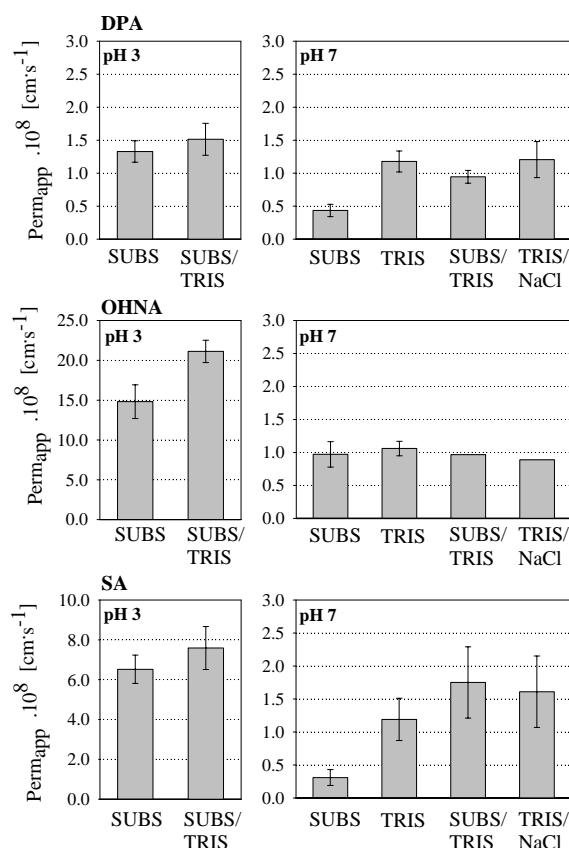


Figure 3.21: Influence of counterions on egg PhC bilayer permeation of DPA, OHNA and SA at T 25°C. $Perm_{app}$ were determined at pH 7.0 and pH 3.0 with Na^+ or protonated TRIS or both as possible counterions for permeation. (*SUBS/TRIS*) SUBS containing 0.2 M TRIS; (*TRIS*) 0.2 M TRIS/HCl; (*TRIS/NaCl*) 0.2 M TRIS containing 0.2 M NaCl. Shown are mean values and standard deviations of ≥ 3 independent experiments or values from a single experiment (no error bars).

Influence of the bilayer state on permeation

To test whether anion permeation also occurs in the gel state of the membrane, the pH-dependent permeation of OHNA was studied with DPPC liposomes at 25°C. The transition temperature from the liquid crystal to the gel state of DPPC is T_m 41°C [Marsh, 1990]. The parameters $\log Perm^{AH}$ and $\log Perm^{A^-}$ of this compound are well defined in the experimental permeation profile as the pK_a value of 4.97 is ideally located between the experimental pH limits (see

3 Results

Fig. 3.20). OHNA is therefore ideal for the comparison of the pH-dependent permeation in different systems. As shown in Fig. 3.22 and Table 3.6, the anion permeation was only ~ 3 times slower than the permeation of the net neutral compound in the DPPC liposome system. In comparison with the egg PhC system, $Perm^{AH}$ was ~ 13 times lower in the DPPC system whereas $Perm^{A^-}$ was ~ 3 times slower.

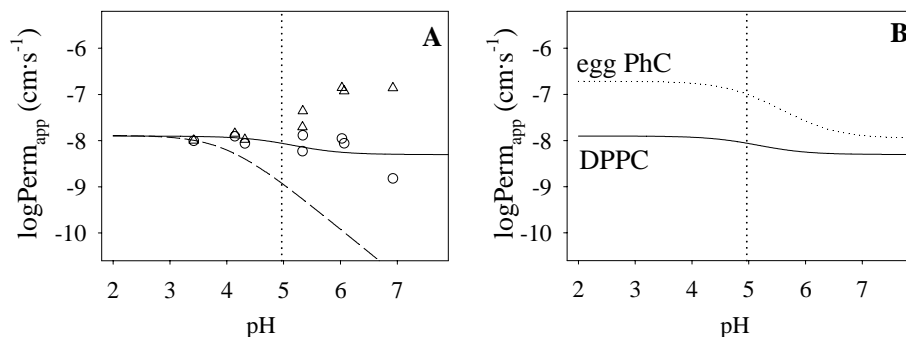


Figure 3.22: Influence of the bilayer state on OHNA permeation. (A) $\log Perm_{app}/pH$ profile of OHNA in DPPC liposomes (SUBS) at 25°C, i.e. $\leq T_c$. Symbols and lines as in Fig. 3.20. The fitted intrinsic permeation coefficients are shown in Table 3.6. (B) Comparison of the fitted $\log Perm_{app}/pH$ profiles of OHNA in egg PhC liposomes (liquid crystal state, dotted line) and in DPPC liposomes (gel state, solid line).

3.4.2 Influence of the lipid bilayer composition on membrane permeation

Study design

To investigate the influence of the lipids Chol, PhI and StAm on lipid bilayer permeation, $\log Perm_{app}$ of SA, AA and OHNA were determined with liposomes containing PhC and various amounts of the respective lipid. These result, as shown in Table 3.7 and Fig. 3.23 –3.25, were compared to the ones obtained with PhC liposomes.

		PhC	PhC/Chol 60/40	PhC/PhI 70/30	PhC/StAm 85/15
SA	$\log Perm^{AH}$	-6.94 ± 0.04	-7.01 ± 0.08	-7.01 ± 0.12	-7.10 ± 0.30
	$\log Perm^{A^-}$	-8.62 ± 0.05	-8.54 ± 0.08	-7.05 ± 0.04	-8.26 ± 0.09
AA	$\log Perm^{AH_2^+}$	-6.22 ± 0.05	-6.99 ± 0.17	-7.72 ± 1.63	n.d.
	$\log Perm^{AH}$	-8.73 ± 0.17	-7.61 ± 0.04	-7.03 ± 0.08	≥ -7.4
	$\log Perm^{A^-}$	-8.94 ± 0.05	-8.65 ± 0.05	-7.91 ± 0.14	-8.63 ± 0.14
OHNA	$\log Perm^{AH}$	-6.78 ± 0.06	-7.32 ± 0.04	-7.41 ± 0.10	-7.33 ± 0.11
	$\log Perm^{A^-}$	-7.87 ± 0.07	-8.35 ± 0.07	-7.59 ± 0.10	-7.68 ± 0.07

Table 3.7: Membrane permeation parameters in SUBS at T 25°C. Fitted values \pm standard errors are shown.

Membrane permeation of Salicylic acid

The influence of the lipid composition on the permeation behaviour of SA is shown in Fig. 3.23. As compared to PhC membranes, the permeation coefficients of net neutral and anionic SA were not affected by 40% Chol (mol/mol) present in the bilayer (Fig. 3.23 A,B). The same was found for 25% Chol (Fig. 3.23 B). The permeation coefficients of both ionization species were, however, increased 2fold with PhC/Chol 90/10 (mol/mol) liposomes (Fig. 3.23 B).

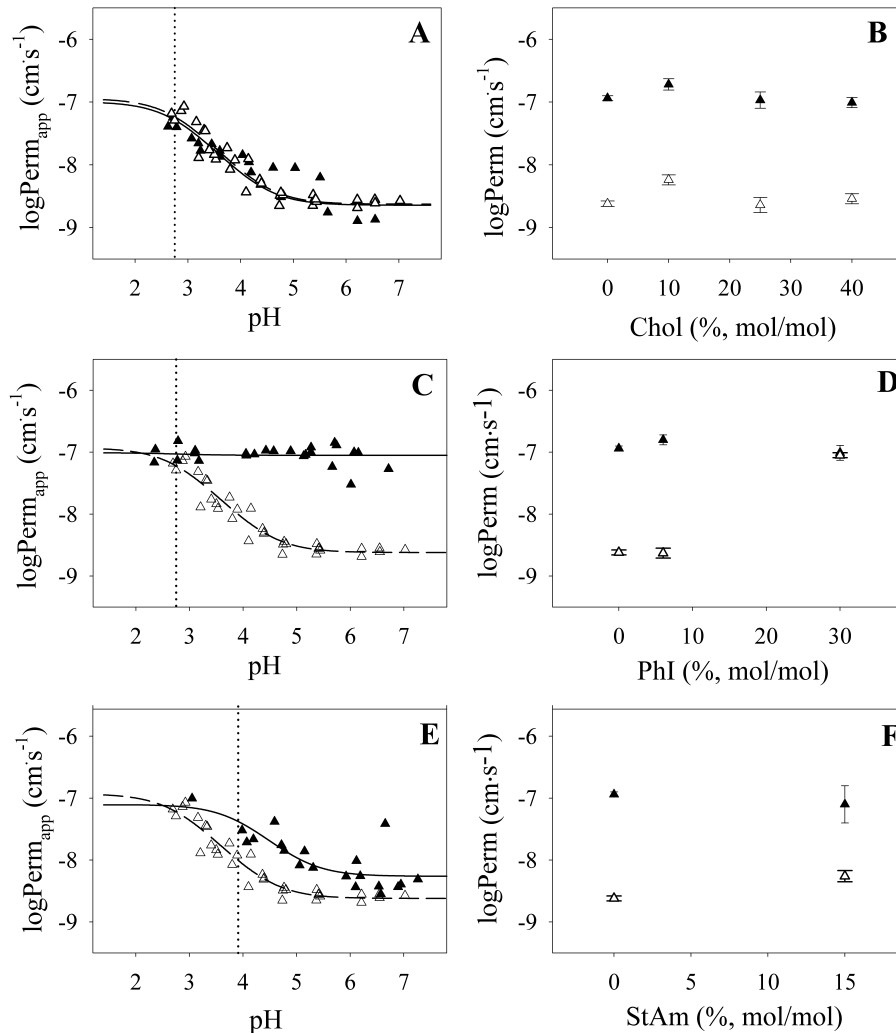


Figure 3.23: Influence of the lipid composition on the membrane permeation of SA across (A,B) PhC/Chol, (C,D) PhC/PhI and (E,F) PhC/StAm bilayers at T 25°C (SUBS). (left panel) Membrane permeation profiles Δ , (A,C,E) PhC; and \blacktriangle , (A) PhC/Chol 60/40, (C) PhC/PhI 70/30, (E) PhC/StAm 85/15. $\log Perm_{app}/pH$ profiles were fitted based on the Henderson-Hasselbalch equation with the titrated pK_a of SA (dotted lines) and considering the permeation of all ionization species (solid and dashed lines). (right panel) Fitted $\log Perm$ values (error bars, estimated standard errors) of the different ionization species (\blacktriangle , $\log Perm^{AH}$; Δ , $\log Perm^{A^-}$) for all tested concentrations of (B) Chol, (D) PhI and (F) StAm. Data are from 3 independent experiments.

3 Results

Neither the negatively charged PhI nor the positively charged StAm had a considerable effect on the permeation coefficient of the net neutral SA. The permeation coefficient of the anionic SA was, however, considerably increased in the presence of 30% PhI (Fig. 3.23 C,D) and 15% StAm (Fig. 3.23 E,F), respectively. Interestingly, with 30% PhI the anionic species of SA permeated with a similar rate as the net neutral species, while 6% PhI had no effect on $\log Perm^{A^-}$, as compared to PhC bilayers (Fig. 3.23 D). The permeation data with 15% StAm could only be fitted allowing a deviation of the inflection point by ~ 1 pH unit.

Membrane permeation of Anthranilic acid

As compared to PhC bilayers, the permeation of the net neutral species of AA was increased by a factor of 20 with 40% Chol, while $Perm^{A^-}$ was increased to a lower extent (Fig. 3.24 A,B). This led to an altered shape of the permeation profile from the one observed with PhC liposomes. In a similar way as with 40% Chol, the permeation profile of AA was affected by 10% and 33% Chol (Fig. 3.24 B). Interestingly, the permeation profile of AA was not changed in PhC/Chol 75/25 liposomes as compared to PhC bilayers.

Incorporation of 30% PhI resulted in a differently shaped permeation profile of AA in a similar way as observed with Chol, which is due to a higher increase of $Perm^{AH}$ as compared to $Perm^{A^-}$ (Fig. 3.24 C,D). Likewise, 6% PhI increased the $Perm^{AH}$ and $Perm^{A^-}$ of AA by the factor 10 and 3, respectively (Fig. 3.24 D). In the presence of StAm, no luminescence of the AA-Tb(III) complex was detectable below pH 4. The $Perm^{AH}$ of AA was therefore fitted with the data \geq pH 4 (Fig. 3.24 E,F). The estimated $Perm^{AH}$ was ≥ 20 times higher than in PhC liposomes.

As shown in Table 3.7 and Fig. 3.24, the net neutral AA permeated PhC bilayers 60 – 90 times slower than net neutral SA and OHNA, respectively, and with a similar permeation rate as its corresponding anionic species.

Membrane permeation of 2-Hydroxynicotinic acid

Figure 3.25 summarizes the effects of Chol (A,B), PhI (C,D) and StAm (E,F) on the permeation profile of OHNA. An increase of the Chol concentration led to a decrease of $\log Perm^{AH}$ and $\log Perm^{A^-}$. At 40% Chol the permeation coefficients of OHNA were reduced by a factor of 2–3 (Fig. 3.25 A,B). Lower concentrations of Chol reduced the permeation coefficients to a lower extent (Fig. 3.25 B). As already observed for SA and AA, the effect of 10% Chol deviated from the general trend. While $Perm^{AH}$ was 2fold decreased, $Perm^{A^-}$ of OHNA was increased by the factor of 1.5 – 2 in PhC/Chol 90/10 liposomes.

Concerning the negatively charged lipid PhI, the $Perm^{AH}$ of OHNA was 4fold reduced by 30% PhI, while $Perm^{A^-}$ was increased by a factor of 2 (Fig. 3.25 C,D). The same was found for 6% PhI (Fig. 3.25 D). The permeation coefficients of net neutral and anionic OHNA were affected by 15% of StAm in a similar way as described for PhI (Fig. 3.25 E,F). With both tested PhI concentrations and 15% StAm the net neutral OHNA permeated with a similar rate as its corresponding anion.

The net neutral species of OHNA permeated across PhC bilayers with a similar rate as SA (Table 3.7).

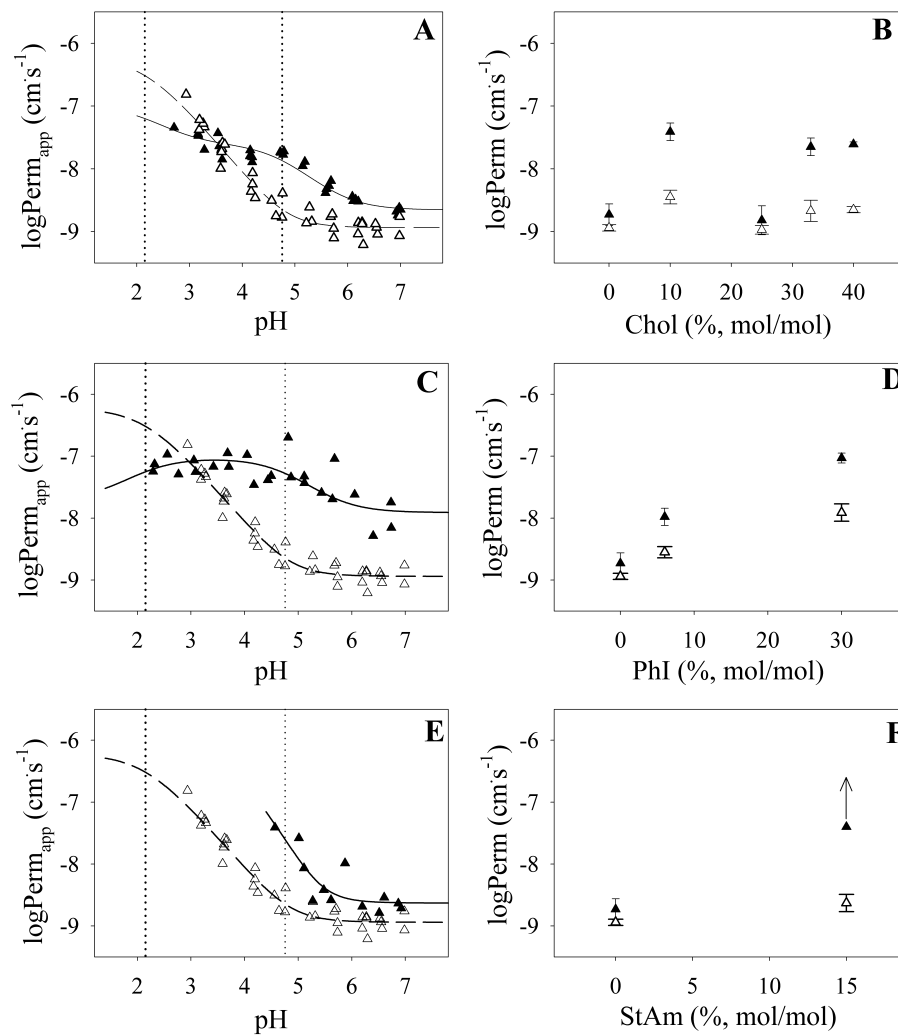


Figure 3.24: Influence of the lipid composition on the membrane permeation of AA across (A,B) PhC/Chol, (C,D) PhC/PhI and (E,F) PhC/StAm bilayers at T 25°C (SUBS). (left panel) Membrane permeation profiles Δ , (A,C,E) PhC; and \blacktriangle , (A) PhC/Chol 60/40, (C) PhC/PhI 70/30, (E) PhC/StAm 85/15. $\log Perm_{app}/pH$ profiles were fitted as described in Fig. 3.23 (dashed and solid lines). (right panel) Fitted $\log Perm$ values (error bars, estimated standard errors) of the different ionization species (\blacktriangle , $\log Perm^{AH}$; Δ , $\log Perm^{A^-}$) for the tested concentrations of (B) Chol, (D) PhI and (F) StAm. Data are from 3 independent experiments. (F) The arrow indicates that the value of $\log Perm^{AH}$ may be higher, but cannot be fitted (see text for details).

Relationship between the affinity and permeation profiles

Assuming a direct relationship between membrane affinity and membrane permeation and considering eq. 1.1, which is derived from Fick's First Law, a decrease in the membrane affinity is expected to result in a decreased permeation rate and vice versa. Comparing the results presented above with the findings shown in section 3.2, such a direct relationship could not be observed. The effects of the single lipids on the membrane affinities of the tested compounds followed predictable rules considering the bilayer rigidity and electrostatic interactions between the charged

3 Results

solutes and headgroup. The influence of the lipids on the permeation profiles appeared, however, more complex.

Membrane permeation was positively, negatively or not at all correlated to the membrane affinities. For instance, high concentrations of Chol (40 %) reduced the membrane affinities of the test compounds, but the corresponding permeation rates were not affected (SA), increased (AA) or decreased (OHNA). As expected from electrostatic interactions, the repelling net charges of PhI and StAm had opposite effects on the membrane affinities of the anionic species of the test compounds. Their effect on the permeation of the anionic species was, however, similar for all tested compounds increasing the anion permeation. These discrepancies will be further investigated based on a theoretical simulation in section 3.7.

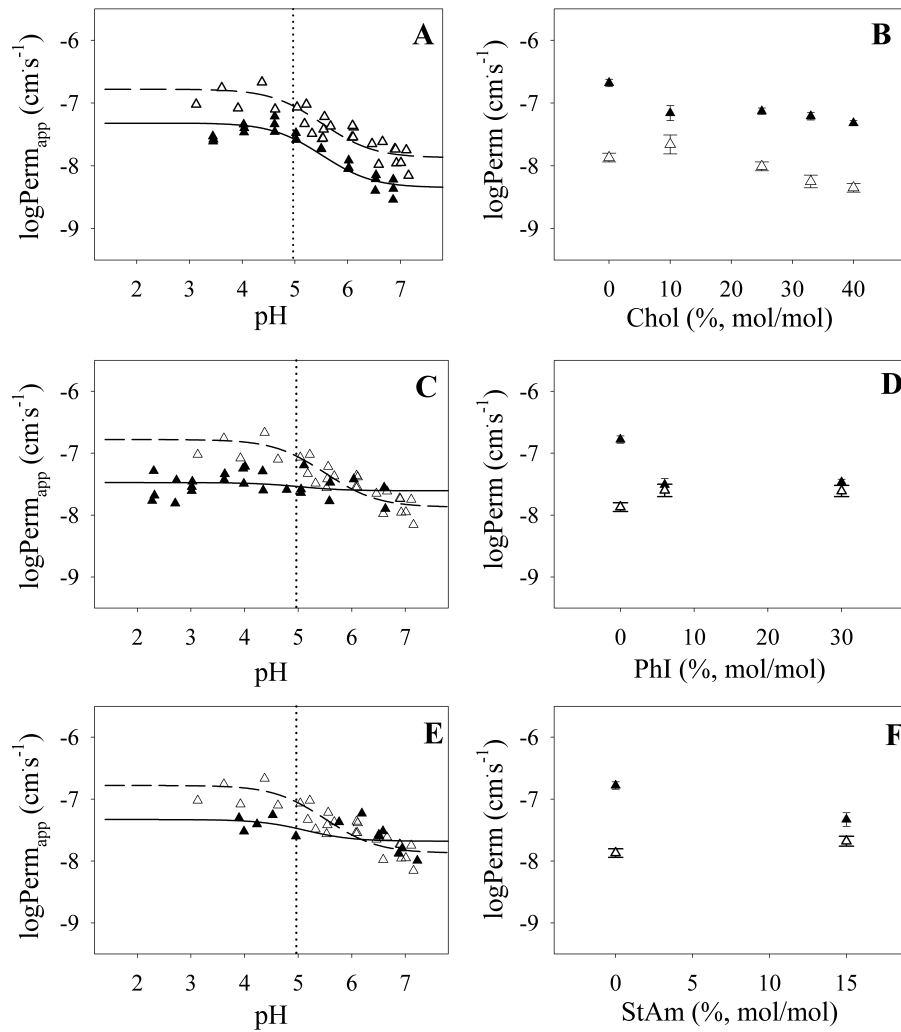


Figure 3.25: Influence of the lipid composition on the membrane permeation of OHNA across (A,B) PhC/Chol, (C,D) PhC/PhI and (E,F) PhC/StAm bilayers at T 25°C (SUBS). (left panel) Membrane permeation profiles Δ , (A,C,E) PhC; and \blacktriangle , (A) PhC/Chol 60/40, (C) PhC/PhI 70/30, (E) PhC/StAm 85/15. $\log Perm_{app}/pH$ profiles were fitted as described in Fig. 3.23 (dashed and solid lines). (right panel) Fitted $\log Perm$ values (error bars, estimated standard errors) of the different ionization species (\blacktriangle , $\log Perm^{AH}$; Δ , $\log Perm^{A^-}$) for the tested concentrations of (B) Chol, (D) PhI and (F) StAm. Data are from 3 independent experiments.

3.5 Structure-permeation relationships

3.5.1 „Biomix” lipid composition and verification thereof

Taking into account the variety of different lipids included in biological membranes the lipid composition of the liposomes was chosen according to Table 3.8. These so-called „biomix liposomes” (BM) aim to represent the major components of the rat liver plasma membrane [Daum, 1985]. Due to the incompatibility of sphingomyeline (SM) and Tb^{3+} leading to precipitation, the amount of SM usually present in the plasma membrane was replaced by PhC. Table 3.8 shows the composition of biomix liposomes.

The incorporation of the single lipids into the liposomes was verified by TLC as described in section 2.2.1. Figure 3.26 shows for a representative example the comparison of the lipid contents in the organic stock solution used to prepare the liposomes and in the resulting biomix liposomes. The good agreement of the spot intensity indicates that the single lipids were incorporated in the biomix liposomes to the same extent as present in the organic lipid solution. Additional density scanning of the spots revealed comparable amounts of the single lipids in both solutions (not shown).

lipid		plasma membrane ^a	biomix liposomes
Phosphatidylcholine	PhC	28	45
Sphingomyelin	SM	12	–
Cholesterol	Chol	28	25
Phosphatidylethanolamine	PhE	17	17
Phosphatidylserine	PhS	7	7
Phosphatidylinositol	PhI	6	6
Phosphatidic acid	PhA	≤ 1	–
Cardiolipin	CL	≤ 1	–
Lysophosphoglycerides	LG	≤ 1	–

Table 3.8: Composition of rat liver plasma membranes and biomix liposomes in % of total lipid (mol/mol). SM and minor lipids were replaced by PhC for the design of biomix liposomes.

^adata from Daum [1985]

3.5.2 Permeation profiles with egg phosphatidylcholine and biomix liposomes

The pH/permeation profiles of all compounds shown in Fig. 3.1 - 3.5 were determined with PhC and biomix liposomes. The fitted permeation parameters according to eq. 2.23 are shown in Table 3.9. The obtained pH/permeation profiles for the different ACA classes are shown in Fig. 3.27 - 3.31.

In both systems, the pH/permeation profile of all compounds except of CF and CFDA followed Henderson-Hasselbalch functions reaching two plateaus ~ 2 pH units above and below their respective pK_a values, indicating that permeation was controlled by the anionic species at pH 7.

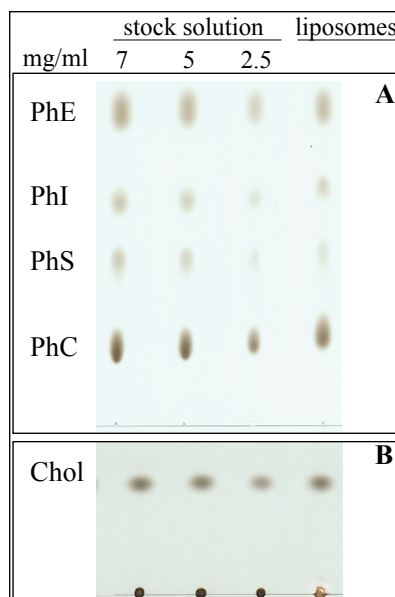


Figure 3.26: Comparison of the amount of lipids in the organic stock solution used for the preparation of biomix liposomes (stock solution) in different concentration and the resulting biomix liposomes (liposomes) as determined by TLC. The concentrations of the stock solution indicate the total mg lipid/ml. (A) TLC of the phospholipids. (B) TLC of Chol.

Increasing the lipophilicity of SA by methylation did not change the permeation behaviour as compared to the unmethylated SA. But, hydroxylation of SA (and thus increase of the molecule's hydrophilicity) led to higher permeation values of the net neutral species in the BM system (Fig. 3.27). Halogenation of SA (CSA) led to increased $\log Perm^{AH}$ and decreased $\log Perm^{A^-}$ values as compared to the dehalogenated SA (Fig. 3.28). A further increase in lipophilicity by halogenation and dehydroxylation (DCBA) reversed this effect. Exchanging the hydroxy group (SA, MSA) with the amine group (AA, MAA) changed significantly the permeation behaviour. The $\log Perm^{AH}$ values of the amino benzoic acid derivatives AA and MAA are extraordinarily low in the PhC and biomix system despite their average lipophilicity values (Fig. 3.29). The heteroaromatic analogon of SA, OHNA, showed a similar permeation behaviour of the net neutral species as SA, while the anionic species of OHNA permeated significantly faster in the PhC and biomix system (Fig. 3.30). Increasing the aromaticity of the system of the ACA led to an increase of the $\log Perm$ values of all ionization species as compared to the ACAs with a lower molecular weight ($MW \leq 200$). The net neutral species of the large ACAs AC, CF and CFDA were the fastest compounds among all tested ACAs (Fig. 3.31).

Comparing the permeation profiles of each ACA obtained with PhC and biomix liposomes, respectively, the permeation coefficients of all ionization species were equal or lower in the biomix system than in the PhC system. However, the extent of this effect was different among the solutes. As for the same solute, the permeation coefficients of the different ionization species could be affected to different extents.

	PhC					Biomix				
	$\log Perm^{AH_2^+}$	$\log Perm^{AH}$	$\log Perm^{A^-}$	$\log Perm^{A^{2-}}$		$\log Perm^{AH_2^+}$	$\log Perm^{AH}$	$\log Perm^{A^-}$	$\log Perm^{A^{2-}}$	
ACA										
SA	-	-6.94 ± 0.04	-8.62 ± 0.05	-	-	-7.36 ± 0.07	-8.95 ± 0.06	-	-	-
DHB	-	-6.97 ± 0.08	-8.17 ± 0.04	-	-	-6.99 ± 0.10	-8.84 ± 0.13	-	-	-
MSA	-	-6.85 ± 0.06	8.68 ± 0.07	-	-	-7.41 ± 0.08	-9.18 ± 0.09	-	-	-
CSA	-	-6.13 ± 0.09	-8.91 ± 0.11	-	-	-7.14 ± 0.08	-9.49 ± 0.10	-	-	-
DCBA	-	-7.17 ± 0.06	-8.45 ± 0.05	-	-	-7.58 ± 0.07	-8.65 ± 0.07	-	-	-
AA	-6.22 ± 0.05	-8.73 ± 0.17	-8.94 ± 0.05	-	-7.14 ± 0.11	-9.5 ± 0.36	-9.42 ± 0.09	-	-	-
MAA	-6.54 ± 0.11	-8.58 ± 0.20	-8.82 ± 0.11	-	-6.86 ± 0.08	-9.04 ± 0.14	-9.30 ± 0.07	-	-	-
OHNA	-	-6.78 ± 0.06	-7.87 ± 0.07	-	-	-7.39 ± 0.07	-8.42 ± 0.12	-	-	-
PCA	-	-6.98 ± 0.07	-8.50 ± 0.06	-	-	-7.43 ± 0.09	-9.11 ± 0.09	-	-	-
DPA	-	-6.71 ± 0.19	-8.90 ± 0.55	-8.90 ± 0.13	-	-7.97 ± 0.10	-9.03 ± 0.12	-9.03 ± 0.07	-	-
AC	-	-6.34 ± 0.11	-7.69 ± 0.21	-	-	-6.89 ± 0.08	-8.30 ± 0.57	-	-	-
CF	-	-6.64 ± 0.10	-7.99 ± 0.33	n.d.	-	-7.28 ± 0.10	-8.78 ± 1.48	n.d.	-	-
CFDA	-	-6.52 ± 0.09	-7.37 ± 0.20	n.d.	-	-6.94 ± 0.11	-8.20 ± 0.93	n.d.	-	-

Table 3.9: Fitted permeation parameters ± standard errors in the PhC and biomix system at T 25°C in SUBS. Data are from three independent experiments each.

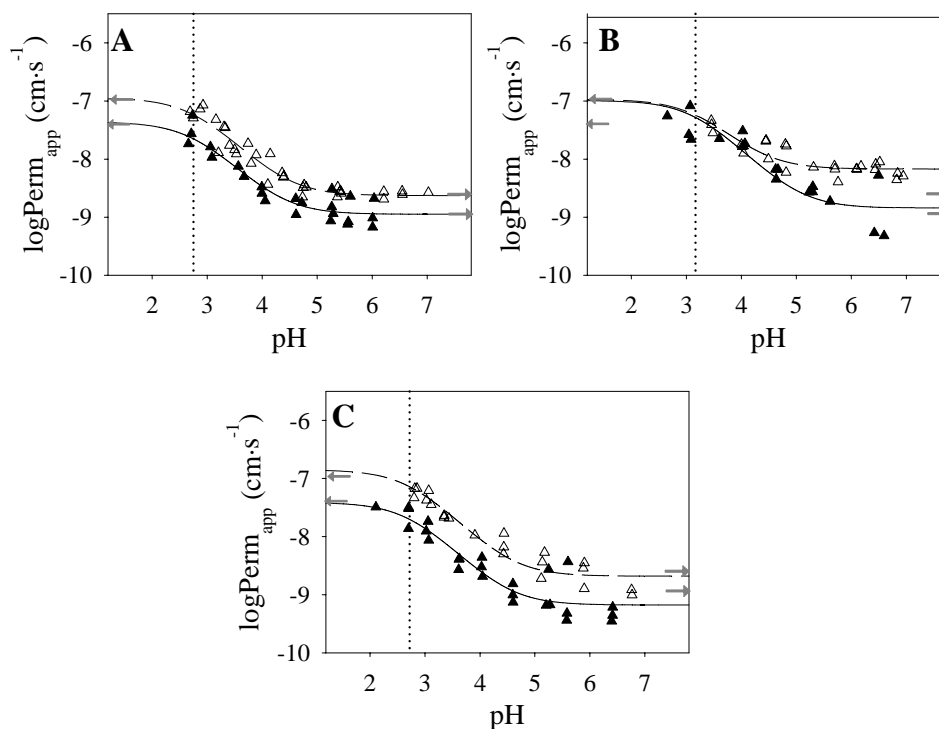


Figure 3.27: Salicylic acid derivatives: Apparent permeation coefficients at T 25°C (SUBS) of (A) SA, (B) DHB and (C) MSA obtained with PhC bilayers (Δ) and with biomix bilayers (\blacktriangle), $n=3$. The lines represent the fitted pH/permeation profiles according to a Henderson-Hasselbalch function (dashed line, PhC; full line, biomix). The pK_a values of the respective acids are indicated by the dotted line. For better comparison, the grey arrows indicate in all figures the intrinsic permeation coefficients of SA as reference values.

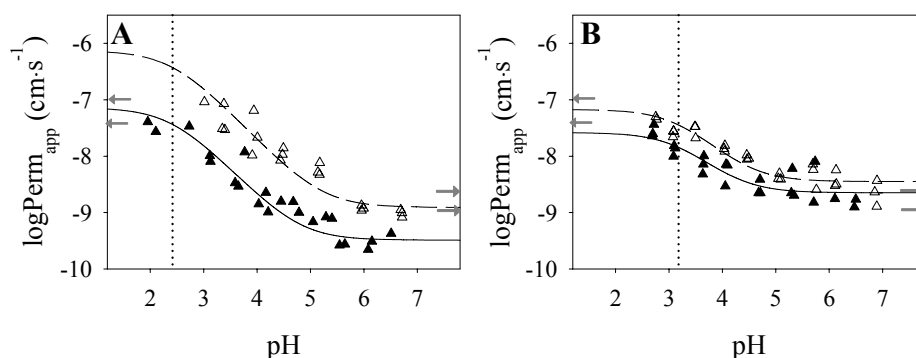


Figure 3.28: Halogenated benzoic acid derivatives: Apparent permeation coefficients at T 25°C (SUBS) of (A) CSA and (B) DCBA obtained with PhC bilayers (Δ) and with biomix bilayers (\blacktriangle), $n=3$. All symbols and lines as in Fig. 3.27.

3 Results

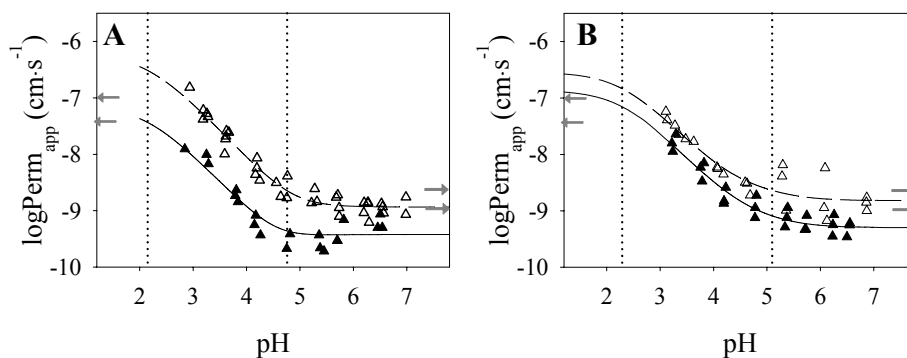


Figure 3.29: Aminobenzoic acid derivatives: Apparent permeation coefficients at T 25°C (SUBS) of (A) AA and (B) MAA obtained with PhC bilayers (Δ) and with biomix bilayers (\blacktriangle), $n=3$. All symbols and lines as in Fig. 3.27.

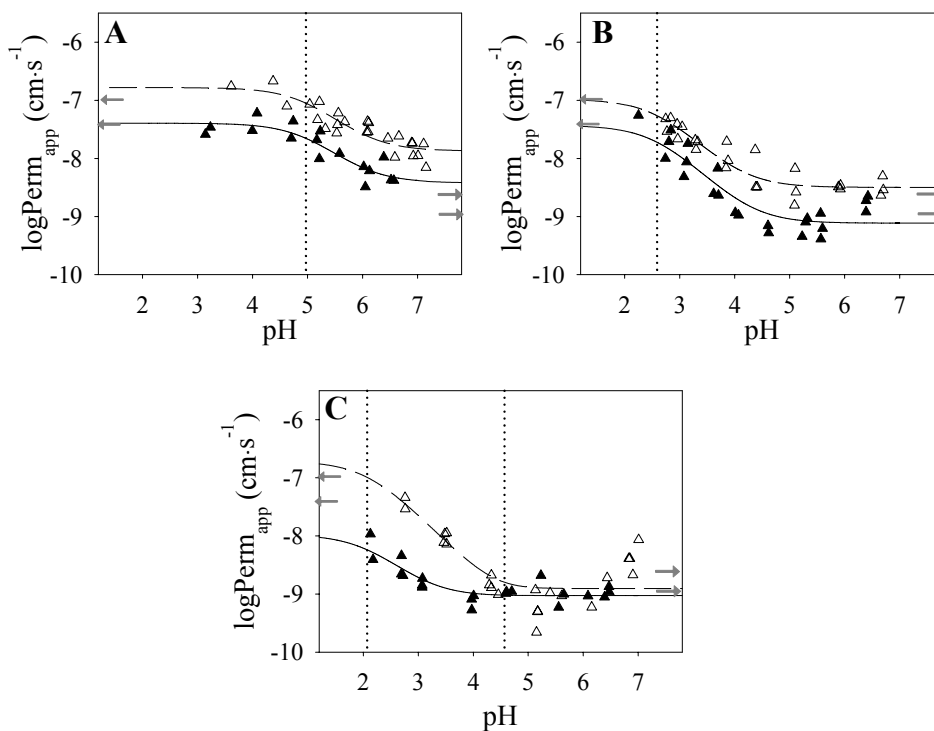


Figure 3.30: Heteroaromatic benzoic acid derivatives: Apparent permeation coefficients at T 25°C (SUBS) of (A) OHNA, (B) PCA and (C) DPA obtained with PhC bilayers (Δ) and with biomix bilayers (\blacktriangle), $n=3$. All symbols and lines as in Fig. 3.27.

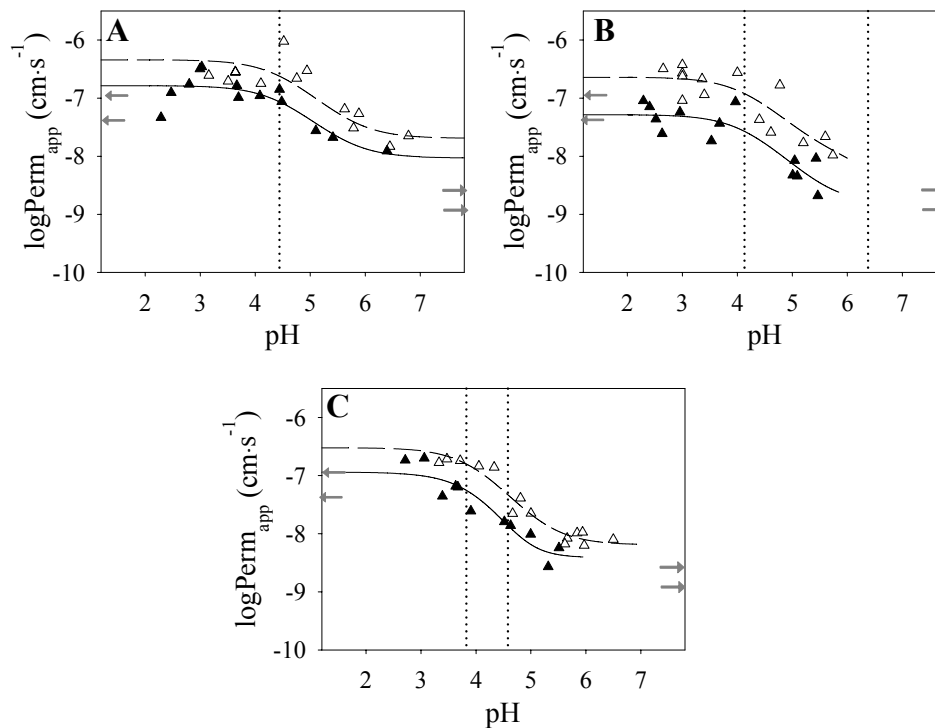


Figure 3.31: Large benzoic acid derivatives: Apparent permeation coefficients at T 25°C (SUBS) of (A) AC, (B) CF and (C) CFDA obtained with PhC bilayers (Δ) and with biomix bilayers (\blacktriangle), $n=3$. All symbols and lines as in Fig. 3.27.

3.5.3 Multivariate analysis of permeation data

Analysis strategy

To analyze the relationship between physicochemical compound properties (variables v) and the measured permeation values (responses) the following strategy was applied: (i) For each test compound (observations o) a set of physicochemical descriptors was obtained from different sources. The objective of these descriptors was the possibility to be measured or computed in an easy and fast way, i.e. either by automatized experiments or by computation algorithms. (ii) Each obtained descriptor was characterized regarding its distribution range for all observations. Ideally, the covered distribution would follow a standard distribution profile. (iii) To identify correlated parameters, the variables were analyzed by principal component analysis (PCA). To identify correlations in the responses, also the response matrix was analyzed by PCA. PCA also allows to identify observations with similar properties. (iv) To identify observations with similar properties in an independent approach data were analyzed by cluster analysis (CA). (v) The relationship between the molecular descriptors and the permeation values was analyzed by Partial Least Square Analysis (PLS). In each step, the models were evaluated regarding the number of variables and observations.

Organization and characterization of the data

The data were divided in an X-matrix and a Y-matrix. The number of matrix rows equaled the number of observations, i.e. the number of compounds. For each observation, the X-matrix contained experimentally derived or calculated molecular descriptors (variables), while the Y-matrix contained the $\log Perm$ values for each ionization species in the PhC and biomix system as shown in Table 3.9 (responses) and the differences between the single ionization species ($\Delta \log Perm$) calculated thereof. Table 3.10 shows the chosen molecular descriptors.

As descriptors of the molecule lipophilicity the experimentally determined $\log P_{Octanol}$ (EXPP) and several $\log P_{Octanol}$ values predicted by various algorithms (MILOGP, ALOGP, IALOGP, KOWWIN, XLOGP) were used. Two parameters were chosen to describe the polar surface area of the molecule (MIPSA, TPSA), i.e. the surface belonging to polar atoms. In a similar way, the hydrophilicity index (HI) is a measure for the hydrophilic groups. The H-bond capacities of the molecules are represented by the Abraham H-bond acidity (A) and basicity (B) as well as the number of hydrogen bond donors and acceptors (NHD, NHA). Ideally, NHD should be correlated with A and NHA with B. The molecular size is described by parameters as the Molecular weight (MW) and volume (MV) and the Abraham McGowan characteristic volume V_x (VX). The molecular flexibility is indicated by the number of rotatable bonds (NROTB), and the unsaturation of the molecule is measured as Unsaturation index (USI). Several electronic descriptors were added to the dataset, such as the E-state topological parameter (TIE) and the polarizability of a molecule (POL, ABRPOL). The molar refractivity is taken into account by two parameters (MRI, R2).

For each x-variable, the distribution of the data was analyzed using boxplots as shown in Fig. 3.32. The median of the data as a measure of the center of distribution is indicated by the bold line, while the box indicates the upper and lower quartile of the data. The whiskers (standard errors) indicate the upper and lower adjacent value, values higher or lower than this range are indicated by circles (outliers). A standard distribution is easily identified as symmetric boxplots with no outliers [Cleveland, 1993].

There is a good standard distribution for the experimental and calculated $\log P$ values and for the HI, the distribution is, however, considerably skewed for the NROTB, MV, POL, USI, R2 and VX. This is due to few observations with very large values as compared to the other observations. The removal of the three large ACAs AC, CF and CFDA from the observation set increased the distribution quality of these parameters except of NROTB and USI. The two latter were excluded from the data analysis by PLS.

The responses were divided into groups. From all response values the median for one y-parameter, e.g. $\log Perm^{AH}$ in PhC liposomes, was calculated, response values above the median were classified as *fast* and values below the median were classified as *slow* compounds.

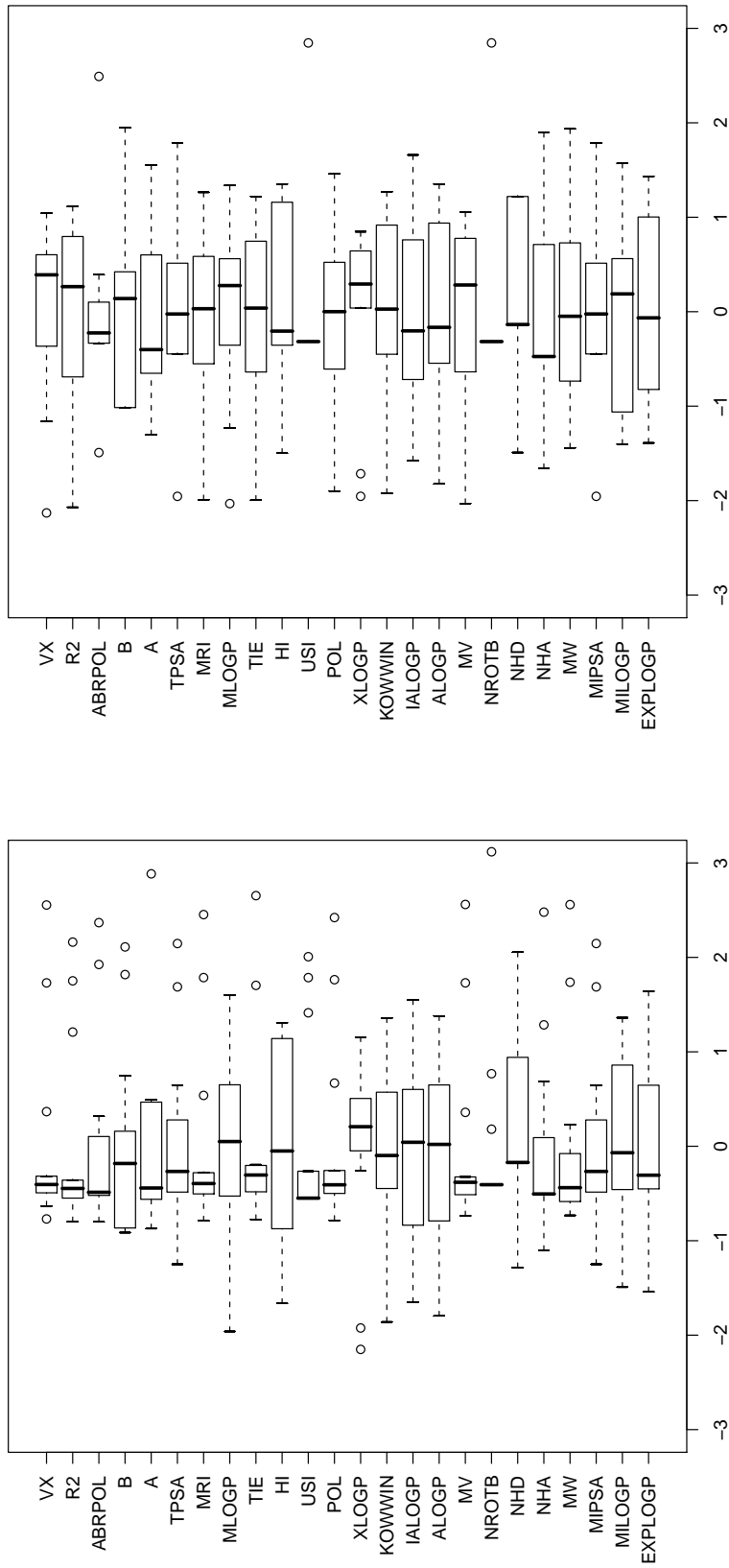


Figure 3.32: Distribution range of variable values by boxplot analysis after mean-centering and scaling to unite variance. Bold line, median; box, upper and lower quartile; dashed lines, upper and lower adjacent value; \circ , outliers. (left panel) All ACAs ($\sigma = 13$). (right panel) Small ACAs ($\sigma = 10$).

name	abb.	description
experimental $\log P_{Oct}$	EXPP	determined by potentiometric titration
molinspiration $\log P$	MLOGP	predicted $\log P$ based on group contributions
AlogP	ALOGP	predicted $\log P$ based on neural networks
IA logP	IALOGP	predicted $\log P$ based on neural networks
KowWin	KOWWIN	predicted $\log P$ based on fragment contributions
XlogP	XLOGP	predicted $\log P$ based on atom contributions
Moriguchi $\log P_{Oct}$	MLOGP	predicted $\log P$ based on group contributions
Topological polar surface area	MIPSA	calculated polar surface area based on tabulated surface contributions
Molecular weight	MW	sum of the atom weights
number of hydrogen bond acceptors	NHA	number of O and N atoms
number of hydrogen bond donors	NHD	number of OH and NH groups
number of rotatable bonds	NROTB	any single non-ring bond, bounded to a nonterminal non-hydrogen atom
Molecular volume	MV	calculated based on group contributions
Polarizability	POL	ease of distortion of the electron cloud of a molecular entity by an electric field
Unsaturation index	USI	multiple bond descriptor
Hydrophilicity index	HI	based on count descriptors of hydrophilic groups
E-state topological parameter TIE	TIE	indication of electronic accessibility of a molecule
Ghose-Crippen molar refractivity	MRI	calculated by group-contribution methods
Topological polar surface area	TPSA	see MIPSA
Hydrogen bond acidity α	A	ability to donate hydrogen bonds
Hydrogen bond basicity β	B	ability to accept hydrogen bonds
Polarity / polarizability	ABRPOL	see POL
Excess molar refraction R^2	R2	refractive index related to the molecule polarizability and size
McGowan characteristic volume V_x	VX	sum of atomic volume parameters for all molecule atoms

Table 3.10: Molecular descriptors used for the Multivariate Analysis. See section 2.10 for the calculation sources.

Correlation between experimentally derived and calculated $\log P$ values

The correlation between the $\log P_{Oct}$ values as determined by potentiometric titration and the calculated values is shown in Fig. 3.33. The experimental $\log P_{Oct}$ values corresponded best to the calculated values MILOGP, ALOGP and IALOGP. The agreement for the $\log P$ values calculated by the KOWWIN and XLOGP algorithms was significantly lower than for the other algorithms. These findings cannot be generalized but might be due to similarities/dissimilarities between the compounds tested here and the training sets used for the calculation algorithms. With another set of test compounds, the quality of the prediction algorithms could be different. All algorithms overestimated the lipophilicity of CFDA, AC and OHNA. The experimentally determined partition coefficient of AC, however, was unexpectedly low (as discussed in section 3.1)

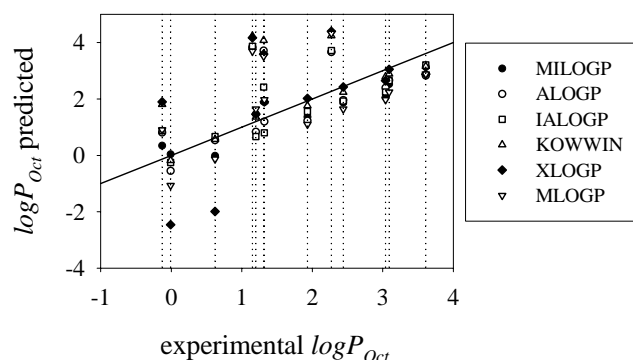


Figure 3.33: Correlation between experimental $\log P_{Oct}$ and predicted $\log P_{Oct}$ by various algorithms.

Principal Component Analysis of the X-matrix and Y-matrix

A Principal Component Analysis of all observations ($n=13$) with all X-variables ($v=24$) revealed a model with 5 significant principal components (PC), R^2 0.995 and Q^2 0.932. The first two PC describe however already 84% of the variability in the data set. The loading and scores for the first and second PC of this analysis are shown in Fig. 3.34. Regarding the scores, i.e. the observations, there are clearly two groups of compounds separated on the first PC. The separation is mainly due to differences in size-related descriptors, such as MW, MV, MRI, VX, POL and ABRPOL. Indeed the observations with positive scores on the first PC are the larger compounds (CF, CFDA, AC). The size-related descriptors are closely correlated with each other. On the second PC the group of small compounds is separated in two more groups which is mainly due to polarity-related parameters (NHD, NHA, A, B, MIPSAs, TPSA) and the lipophilicity parameters EXPP and all calculated $\log P$ parameters. Positive scores on the second PC indicate high values of the polar characteristics and low lipophilicity values and vice versa. The lipophilicity parameters are inversely correlated with the polarity-related parameters as obvious from the loading plot. There is no clear separation between *fast* and *slow* permeating compounds. This model provides good values for the explained and predicted variance but explains mainly differences and similarities due to size-related descriptors. The model fails to explain the different permeation values of the test compounds. Additionally, the number of PCs is too high for the relatively small observation set, the model might be overfitted.

3 Results

In the subsequent analysis, the large compounds (AC, CF, CFDA) were removed from the observation set to avoid an overestimation of the size influence and new models were built and evaluated with smaller numbers of variables. However, no model was obtained showing a reasonable clustering of *fast* and *slow* permeating compounds.

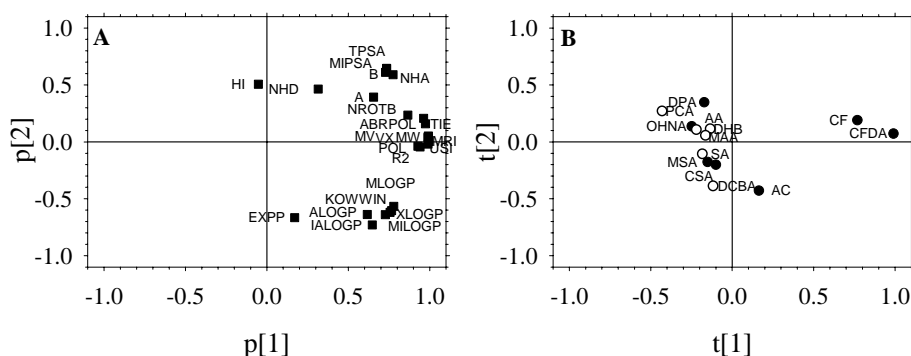


Figure 3.34: PCA of X-matrix: $v = 24$, $o = 13$, $PC=5$, R^2 0.995, Q^2 0.932. (A) Loadings on PC 1 and PC 2. (B) Scores on PC 1 and PC 2. Observations were classified as *fast* (●) and *slow* (○) according to their $\log Perm_{PhC}^{AH}$.

PCA of the response matrix omitting the large compounds revealed a 2 PC model with R^2 equals 0.945 and Q^2 0.793. The score and loading plots are shown in Fig. 3.35. There is a strong correlation between $\log Perm_{PhC}^{AH}$ and $\log Perm_{BM}^{AH}$; $\log Perm_{PhC}^{A-}$ and $\log Perm_{BM}^{A-}$; and the difference of the intrinsic permeation coefficients of the different ionization species in either of the tested systems (ΔPhC and ΔBM). This indicates that fast compounds (neutral or ionized species) in the PC system have also high $\log Perm$ values in the biomix system. Observations with high Δ values in the PhC system have also large Δ values in the biomix system. Additionally, the Δ values are closely correlated with the permeation coefficients of the net neutral compounds, indicating that observation with high values for $\log Perm^{AH}$ have also high differences between $\log Perm^{AH}$ and $\log Perm^{A-}$.

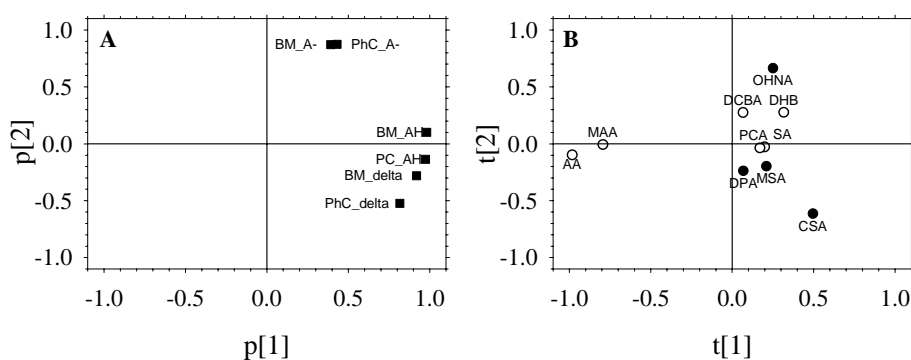


Figure 3.35: PCA of Y-matrix: $v=6$, $o=10$, $PC=2$, R^2 0.945, Q^2 0.793. (A) Loadings on PC 1 and PC 2. (B) Scores on PC 1 and PC 2. Observations were classified as *fast* (●) and *slow* (○) according to their $\log Perm_{PhC}^{AH}$.

The scores reflect a similar permeation behaviour of the amino benzoic acid derivatives MAA and AA, which form a cluster clearly separated from the other observations. This means that AA and MAA are highly different from the permeation values of all other ACAs. As described above, the permeation of their net neutral species is extraordinary slow. The $\log Perm^{AH}$ values of AA and MAA are ≥ 10 fold lower than of the other compounds, leading to a $\log Perm$ „gap” between -7.17 and -8.58. It is possible that permeation-reducing effect of the amine group hides any other structure-permeation relationship. It is also obvious that the classification into *fast* and *slow* compounds based on the median is biased with such a $\log Perm$ „gap”. PCA of the response matrix omitting AA and MAA revealed similar correlations for the response variables $\log Perm_{PhC}^{A-}$ and $\log Perm_{BM}^{A-}$; and ΔPhC and ΔBM as including them (data not shown). No correlation could be obtained for $\log Perm_{PhC}^{AH}$ and $\log Perm_{BM}^{AH}$, however this analysis is not reasonable due to the small variable range.

Cluster analysis of the X-matrix

To identify observations with similar properties by an independent approach, the X-matrix omitting the large ACAs AC, CF and CFDA was analyzed by CA. Figure 3.36 shows the Euclidian distances of the observations from each other in the multidimensional space. The more similar two observations are, the lower is their distance. The observations are separated in two clusters. The heteroaromatic ACAs (OHNA, DPA, PCA) form one cluster with DPA separated from the other two. Within the second cluster, MSA and CSA as well as SA show very similar properties. Additionally, AA and MAA are very similar. DCBA is separated from the other ACAs, suggesting a different permeation behaviour based on the molecular properties.

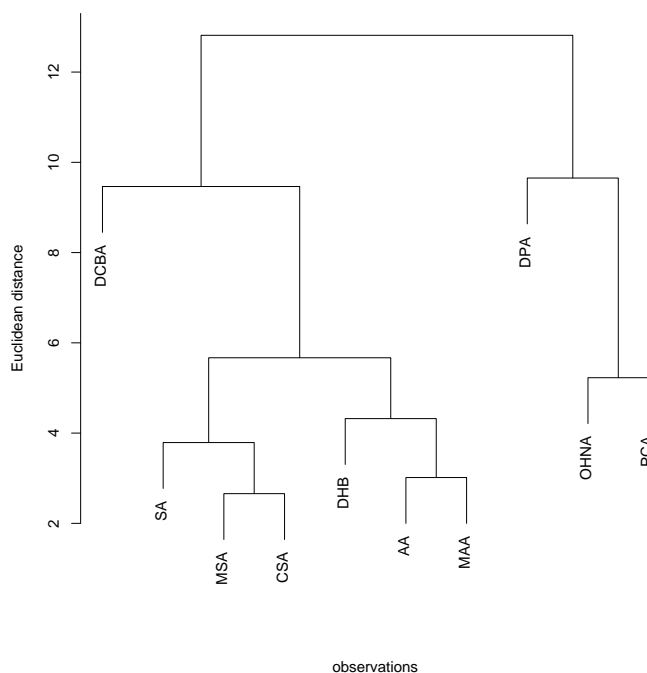


Figure 3.36: Cluster analysis of the X-matrix ($\sigma=10$). The dendrogram shows the Euclidian distance between two data points in a multidimensional space plotted on the y-axis. Observations with similar properties appear at small heights and as part of the same subtree.

Partial Least Square Analysis

To understand the relationship between the individual descriptors and the responses and to detect variables of higher importance, the linear correlation coefficients between each variable and each response were calculated individually using the 10 smaller compounds. The obtained correlation coefficients are shown in Table 3.11. In general, the R^2 and Q^2 values for the single variables were low. The highest correlations were obtained between $\log Perm^{AH}$ and NHD, HI, IALOGP, MRI and TIE for both systems, PhC and Biomix. This analysis suggests that the permeation coefficients are influenced not by single factors, but that permeation is a multifactorial process.

Variable	PhC				Biomix			
	$\log Perm^{AH}$		$\log Perm^{A^-}$		$\log Perm^{AH}$		$\log Perm^{A^-}$	
	R^2	Q^2	R^2	Q^2	R^2	Q^2	R^2	Q^2
EXPP	0.04	-0.08	0.07	-0.23	0.06	-0.02	0.03	-0.34
MILOGP	0.00	-0.07	0.06	-0.24	0.00	-0.06	0.04	-0.31
MIPSA	0.00	-0.03	0.00	-0.28	0.00	-0.05	0.00	-0.35
MW	0.07	-0.10	0.03	-0.17	0.03	-0.10	0.01	-0.35
NHA	0.08	0.01	0.03	-0.40	0.02	-0.10	0.02	-0.27
NHD	0.29	-0.10	0.03	-0.18	0.25	-0.10	0.12	-0.25
MV	0.01	-0.10	0.16	-0.03	0.03	-0.07	0.04	-0.24
ALOGP	0.06	-0.10	0.02	-0.08	0.06	-0.10	0.00	-0.21
IALOGP	0.13	-0.08	0.00	-0.11	0.16	-0.03	0.01	-0.24
KOWWIN	0.02	-0.10	0.00	-0.11	0.04	-0.10	0.00	-0.14
XLOGP	0.00	-0.07	0.01	-0.08	0.01	-0.06	0.00	-0.09
POL	0.06	-0.06	0.15	-0.04	0.07	-0.03	0.04	-0.31
HI	0.33	-0.05	0.02	-0.19	0.26	-0.10	0.10	-0.20
TIE	0.10	-0.10	0.02	-0.43	0.06	-0.10	0.00	-0.28
MLOGP	0.03	-0.04	0.02	-0.08	0.01	-0.07	0.01	-0.17
MRI	0.09	-0.06	0.17	0.01	0.10	0.00	0.06	-0.26
TPSA	0.01	-0.03	0.00	-0.28	0.00	-0.05	0.00	-0.35
A	0.10	-0.03	0.02	-0.33	0.05	-0.06	0.00	-0.21
B	0.05	-0.10	0.01	-0.15	0.14	0.04	0.00	-0.13
ABRPOL	0.00	-0.06	0.02	-0.96	0.02	-0.09	0.01	-0.17
R2	0.15	-0.10	0.05	-0.53	0.11	-0.10	0.05	-0.62
VX	0.01	-0.09	0.19	-0.06	0.02	-0.07	0.03	-0.25

Table 3.11: R^2 and Q^2 values obtained from correlations between fitted $\log Perm$ values and each individual variable. $R^2 \geq 0.1$ and positive Q^2 values are indicated in **bold**.

To analyze the relationship between all variables and the responses, a number of PLS models were built leaving out different variables. The most reasonable models obtained are discussed

below.

Analyzing the relationship to $\log Perm_{PhC}^{AH}$ a 2 PC model was found ($o=10, v=10; R^2$ 0.881, Q^2 0.472). Figure 3.37 shows the score and loading plot of this model. $\log Perm_{PhC}^{AH}$ is positively correlated with EXPP on PC 1 and 2. Descriptors of the molecule polarity (HI, MIPSA, B, POL, NHD) are inversely correlated to $\log Perm_{PhC}^{AH}$ on PC 1, but positively correlated to the response value on PC 2. The observations cluster well into two groups, which correspond to the groups found by PCA of the response matrix. The amino benzoic acid derivatives are slow in relation to the other observations. In comparison with the other ACAs, the HI of AA and MAA is strikingly different and the B values are relatively high. The HI and B are negatively correlated with $\log Perm^{AH}$, which could explain the slow permeation behaviour. However, it is also possible that the high HI values of AA and MAA bias the analysis, but do not influence $\log Perm_{PhC}^{AH}$. This should be investigated by choosing further compounds (see section 3.5.5). Figure 3.37 shows also the variable importance for the projection (VIP) for each parameter on both PC. Values above 1 indicate a high importance of the variable, values below 0.5 indicate that a variable is without relevance for the model. The most important variables used for the model are HI, NHD and TIE. The first two account for the hydrophilicity and hydrogen bond capacity of a molecule, while the latter describes the electronic accessibility of a compound.

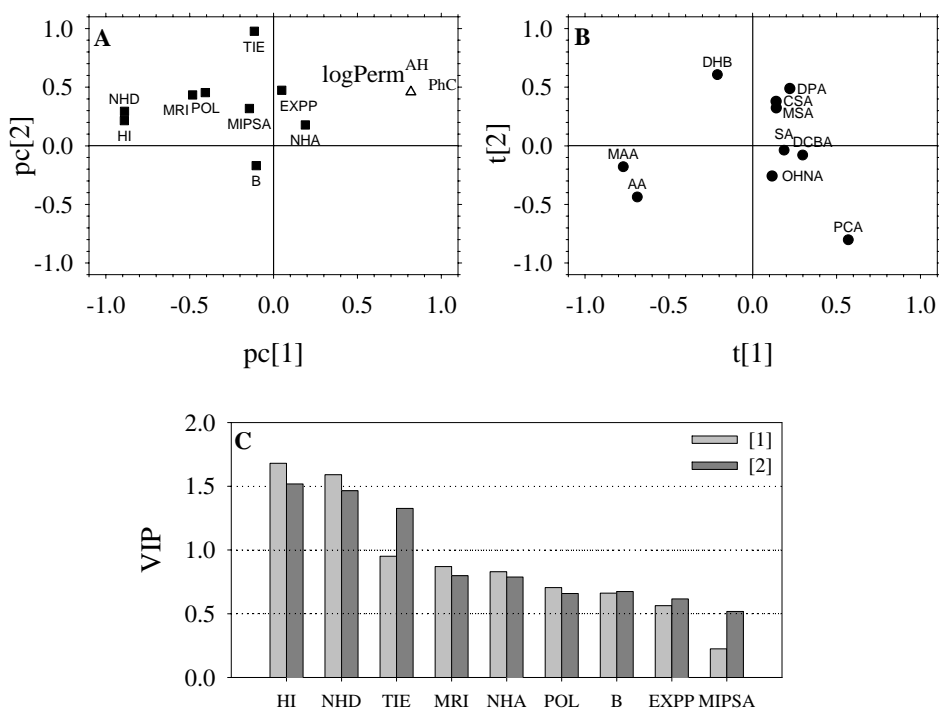


Figure 3.37: PLS $\log Perm_{PhC}^{AH}$: $v = 10$ ($x = 9, y = 1$), $o = 10$, PC=2, R^2 0.881, Q^2 0.472. (A) Loadings of the x-(■) and y-(△) variables. (B) Scores (●) of observations. (C) Importance of the variables for the projection (VIP) for PC 1 (light grey) and PC 2 (dark grey).

With the permeation coefficient of the net neutral species in the biomix system, $\log Perm_{BM}^{AH}$, the best model obtained revealed similar results as compared to the same response in the PhC systems. This is not surprising, since these two response parameters are closely correlated as found

3 Results

by PCA (compare Figure 3.35). The results of this model are shown in Figure 3.38 ($\sigma=10$, $\nu=10$; 1 PC, R^2 0.580, Q^2 0.313). Again, the observations cluster in two groups (positive scores/negative scores). The VIP plot in Figure 3.38 reflects a very similar importance of descriptors for the compound polarity (HI, NHD, B) as observed in the PhC system.

Analyzing the relationship of the molecular descriptors to the differences in the permeation coefficients between net neutral and ionized species, respectively revealed no satisfying model in both lipid systems. Alternatively, the close correlation between $\log Perm^{AH}$ and the Δ values could be used to predict the difference in the permeation coefficients of net neutral and ionized species.

No reasonable model was obtained to predict $\log Perm^{A^-}$ in the PhC and the BM system. This is not surprising since the calculated molecular descriptors account for the neutral species. The difference in the $\log Perm^{AH}$ values between the PhC and the BM system could neither be modeled by the chosen molecular descriptors.

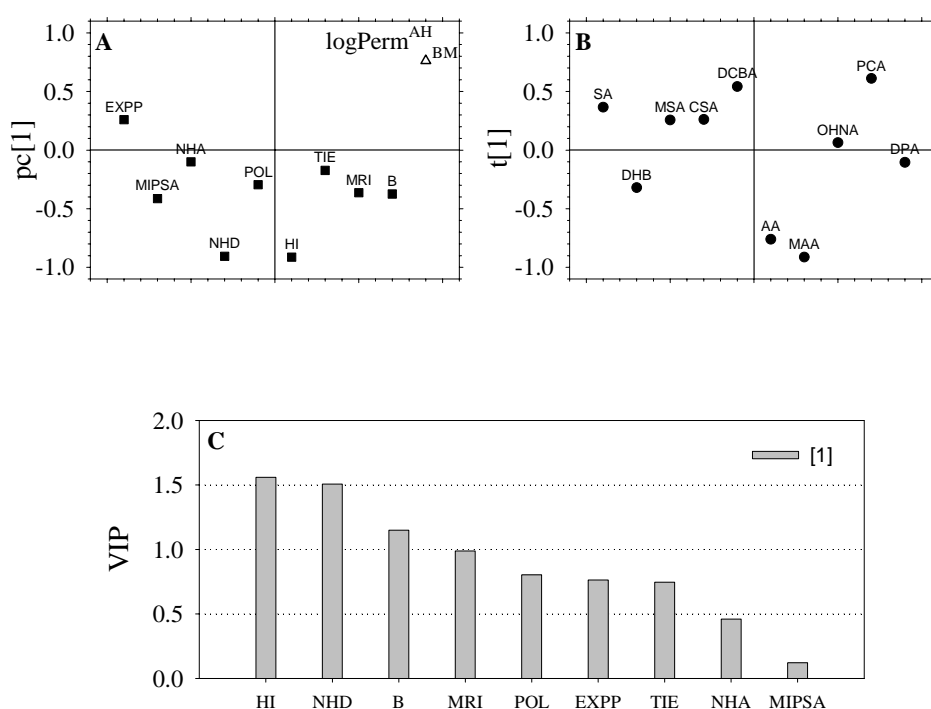


Figure 3.38: PLS $\log Perm_{BM}^{AH}$: $\nu = 10$ ($x = 9$, $y = 1 \triangle$), $\sigma = 10$, PC=1, R^2 0.580, Q^2 0.313. (A) Loadings of the x- and y-variables. (B) Scores (\bullet) of observations. (C) Importance of the variables for the projection (VIP) for PC 1 (light grey).

3.5.4 Structure-permeation relationships: Conclusions

A test set of thirteen structurally similar ACAs was used to investigate the relationship between physicochemical properties of the compounds and their permeation behaviour. Due to the limitations of the test set and the uneven distribution of some of the molecular descriptors no clear relationship could be obtained. It became, however, evident, that differences in the permeation behaviour cannot be explained with only one parameter, e.g. lipophilicity. A set of multivariate

analysis techniques was applied to analyze the permeation behaviour as a multifactorial process.

This analysis disclosed the importance of the lipophilicity descriptor EXPP and parameters describing the size, polar surface area, hydrogen bond properties and electronic accessibility of the molecules for the permeation behaviour of a compound. The lipophilicity is favourable for the permeation of a compound, whereas the polar characteristics can influence the permeation negatively and positively, indicating an optimum for these parameters. Increase in size of the test compounds led to an increase in lipophilicity which in turn increased the permeation coefficients.

The quality of the obtained models was in general poor ($Q^2 \leq 0.5$), which is probably due to the low number of observations. It has also to be noted, that the large difference between AA and MAA in comparison to the other ACAs might hide other structure-permeation relationships.

3.5.5 Study design for further investigations

To obtain a significant structure-permeation relationship this study should be extended in a systematic manner. A set of suggestions is depicted in Fig. 3.39.

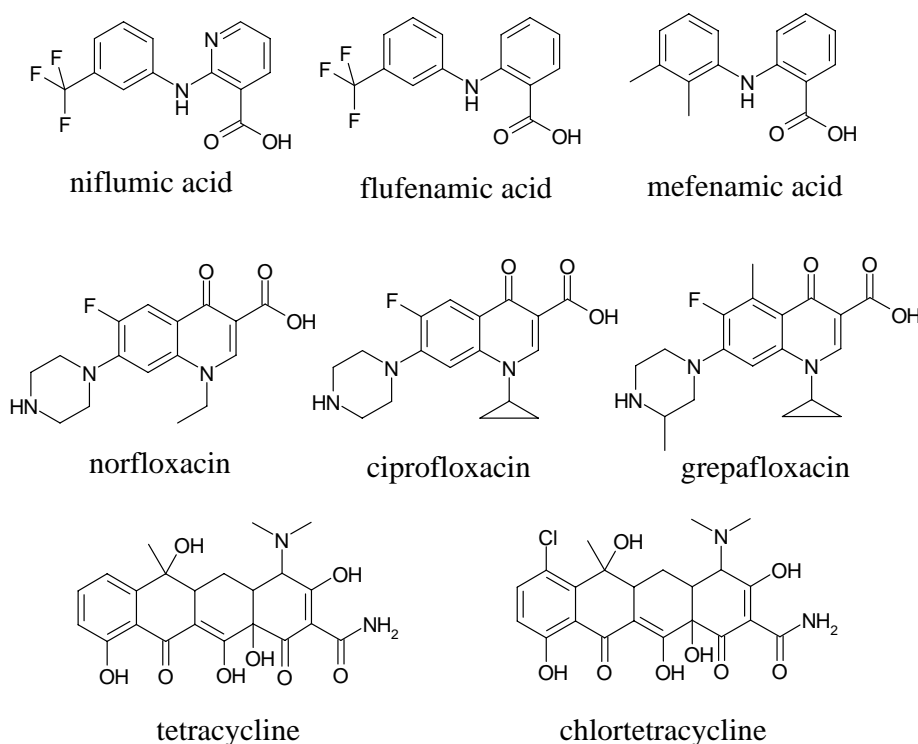


Figure 3.39: Study design for further investigations: Structures of suggested ACAs.

The test series should include a larger number of possible zwitterions. This would facilitate to understand whether the extraordinary behaviour of AA and MAA is due to their amine group or due to their zwitterionic character. Possible ACAs could be niflumic acid and its derivatives flufenamic acid and mefenamic acid or gyrase inhibitors such as norfloxacin, grepafloxacin and ciprofloxacin. The interaction of these two ACA classes with Tb^{3+} has been shown by Arnaud and Georges [2003] and by Ocana et al. [2001]. These compounds would also extend the number of large ACAs, increasing at the same time the compounds with a high flexibility (niflumic acid

3 Results

and derivatives) and high H-bond capacities (gyrase inhibitors). Choosing several compounds from the same class would allow to study the direct effect of substituents.

Furthermore, tetracycline and chlortetracycline should be included in the study, which have been shown to interact with Tb^{3+} by Arnaud and Georges [2003]. Due to their large polar surface area and high number of hydrogen bond donors they would significantly change the distribution shape for these parameters, which would otherwise be considerably skewed. Figure 3.40 shows a comparison of the boxplots of selected parameters with and without the tetracyclines. Even though the tetracyclines are outliers, the resulting distributions are less skewed than if they are omitted. Another approach to obtain better distributions would be the reduction of small compounds.

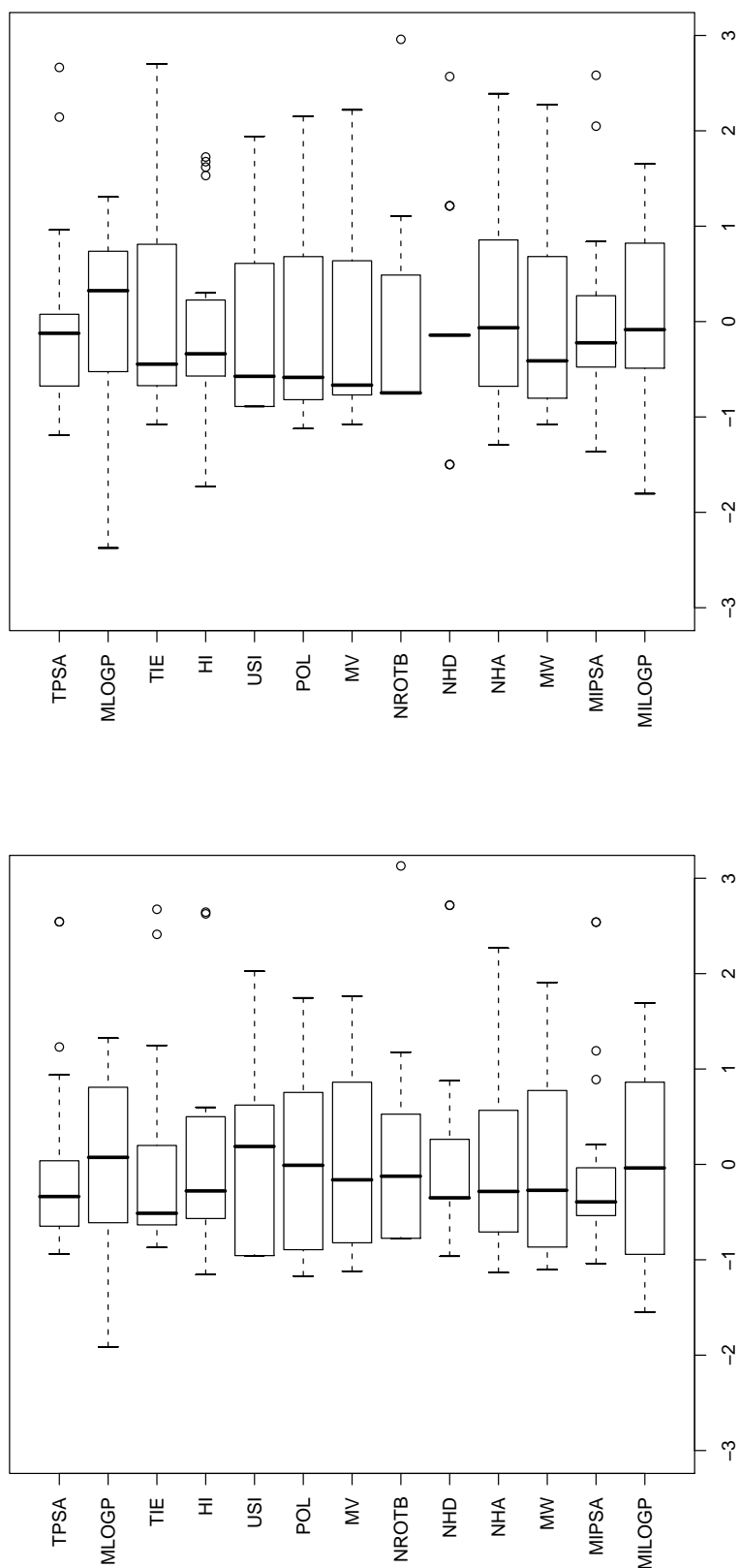


Figure 3.40: Distribution range of selected parameters for the design of an extended study with the compounds shown in Fig. 3.39: (left panel), including tetracycline and chlortetracycline; (right panel), without tetracycline and chlortetracycline. In comparison with the distribution of the original study (compare Fig. 3.32) the quality of the distribution is considerably increased for MW, MV, NROTB. Even though tetracycline and chlortetracycline are outliers, the distributions including them are less skewed than the corresponding distributions without these two compounds (e.g. NHD, HI). A better distribution for TPSA and MIPSAs could be obtained omitting some of the small ACAs.

3.6 Permeation of peptides across lipid bilayers

3.6.1 Peptide characterization

In order to compare the lipid bilayer permeation properties of α - and β -peptides and to study the influence of the molecular weight on the permeation process, a series of α - and β -peptides conjugated to dipicolinic acid (DPA) was prepared by solid-phase peptide synthesis as described in section 2.1.4. Conjugation of the peptides to DPA through its monobenzyl ester provides a free aromatic carboxylic acid moiety for detection in the Tb(III)-assay and allows for the direct comparison of the permeation behaviour of the α - and β -peptidic analogs.

The synthesized peptide conjugates **1-12** (Table 3.12) contain residues with the hydrophobic sidechains of valine (Val), alanine (Ala) and leucine (Leu), with the exception of the arginine (Arg) derivatives **11** (H-2,6-PyDA-Arg-OH) and **12** (H-2,6-(β^3 hArg)₈-NH₂) that possess cationic side chains.

The RP HPLC retention times of the DPA-peptide conjugates are shown in Table 3.12 [Gardiner et al., 2006]. As observed before [Seebach et al., 1996] the β -peptides showed longer retention times t_R on a reversed phase HPLC column than the corresponding α -peptides. The differences in t_R increase with increasing chain length. These findings suggest that β -peptides are less polar than their α -counterparts due to the additional methyl group per amino acid residue.

The peptides were also characterized by circular dichroism spectroscopy. The CD spectra suggested a lack of secondary structure in water and methanol for all α -peptides and all short-chain β -peptides. The β -hexapeptides **8** (H-2,6-PyDA- β^3 hVal- β^3 hAla- β^3 hVal- β^3 hAla- β^3 hVal-OH) and **10** (H-2,6-PyDA- β^3 hVal- β^3 hAla- β^3 hLeu- β^3 hVal- β^3 hAla- β^3 hLeu-OH) as well as the β -octapeptide **12** exhibited in methanol weak but characteristic cotton effects at 215 nm which could be considered characteristic of a 14-helical secondary structure. The CD spectra are discussed in more detail in Gardiner et al. [2006].

3.6.2 Interaction of DPA-labeled peptides with Tb³⁺

DPA was coupled to the N-terminus of the peptides to ligate Tb³⁺ entrapped in the aqueous lumen of the liposomes and thus, to monitor the peptide permeation across the bilayer. The excitation of the DPA-Tb(III)-complex leads to an increase in the Tb³⁺ luminescence. The excitation maximum of the complex between Tb³⁺ and the DPA-coupled peptides was observed at 275 nm. In Fig. 3.41, the emission spectra with the three characteristic Tb³⁺ peaks at λ_{em} 490, 545 and 585 nm are shown for the representative example **5** (H-2,6-PyDA- β^3 hVal- β^3 hAla- β^3 hVal- β^3 hVal-OH). For all peptides the signal at 545 nm was always the most prominent peak. The signal height was dependent on the ligand concentration within the chosen concentration range. No luminescence was detected in the absence of Tb³⁺.

3.6 Permeation of peptides across lipid bilayers

#	structure	MW	t_R^a [min]
1		365.4	18.0
2		393.4	18.1
3		492.6	19.4
4		535.6	18.6
5		591.7	21.9
6		606.7	18.3
7		705.8	19.6
8		790.0	26.4
9		756.4	22.3
10		840.5	28.7
11		323.3	8.4
12		1550.0	34.3 ^b

Table 3.12: Characterization of the peptides investigated. Peptide number #, structure, molecular weight MW , and RP C18 HPLC retention times t_R (see section 2.1.4 and Gardiner et al. [2006] for details).

^a10% Acetonitrile in water (0.1% TFA) for 5 min, then 10 – 95% in 30 min.

^b3% Acetonitrile in water (0.1% TFA) for 5 min, then 3 – 20% in 40 min.

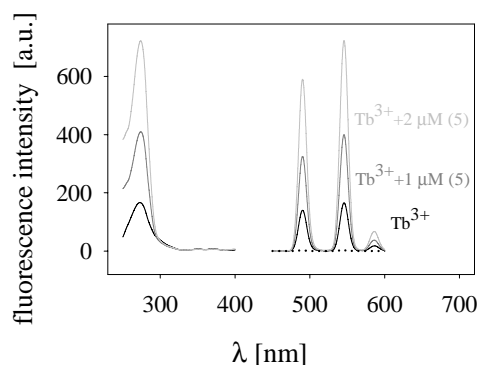


Figure 3.41: Excitation and emission spectra of 0.5 mM Tb^{3+} alone and in combination with various concentrations of peptide **5**. Emission spectra were recorded with λ_{ex} 275 nm, excitation spectra were recorded with λ_{em} 545 nm. The peptide increases the luminescence of the complex in a concentration-dependent manner. 2 μM **5** alone showed only the background signal (dotted line). Peptide **5** was chosen here as representative example, spectra of the other peptides are similar.

3.6.3 Permeation of peptides across egg phosphatidylcholine bilayers

Representative permeation curves of the DPA-labeled peptides obtained using the Tb(III)-permeation assay are shown in Fig. 3.42. DPA and a blank (vehicle containing neither peptide nor DPA) were run as controls in each permeation experiment. No permeation was observed for the polycationic **12** which is in agreement with previous findings [Seebach et al., 2004], and thus **12** served as a negative control.

To elucidate whether DPA can carry an amino-acid cargo into a liposome or whether on the other hand one attached amino acid can significantly change the permeation behaviour of DPA itself, we chose the DPA-derivative **11** of arginine. Arginine has the highest hydrophilicity among the natural amino acids [Black and Mould, 1991], and hydrophilicity is described to unfavourably influence membrane permeation [Ano et al., 2004; Chakrabarti et al., 1994]. Thus, arginine is expected to permeate very slowly on its own and should therefore reduce the permeation coefficient of DPA. Indeed, at pH 6.8 **11** permeated with $\log\text{Perm}_{app} \leq 8.38$ and in some experiments permeation was not detectable at all. Thus, the attachment of arginine decreases the permeation of DPA by at least a factor of three ($\log\text{Perm}_{app} \sim -8.0$ at pH 6.8 in TRIS).

3.6.4 pH-Dependent permeation behaviour of DPA- $\beta^3\text{hVal}$ - $\beta^3\text{hAla}$ - $\beta^3\text{hLeu}$ -OH

To investigate further the influence of the attached DPA on the permeation of a peptide derivative, the pH-dependent permeation of **3** (DPA- $\beta^3\text{hVal}$ - $\beta^3\text{hAla}$ - $\beta^3\text{hLeu}$ -OH) was measured. In Fig. 3.43 we show the permeation/pH profiles of **3** and of DPA alone. While the permeation of DPA was pH-dependent in the tested pH range (pH 2 - 7, pK_a 2.07 and 4.57) (see section 3.4.1), the permeation of its tripeptide derivative **3** was not. This provides evidence that DPA is not the major contributor to the permeation of the tested peptides. This also means that the ionization state of the terminal carboxylic acid groups of the peptide had no influence on the permeation of the constructs.

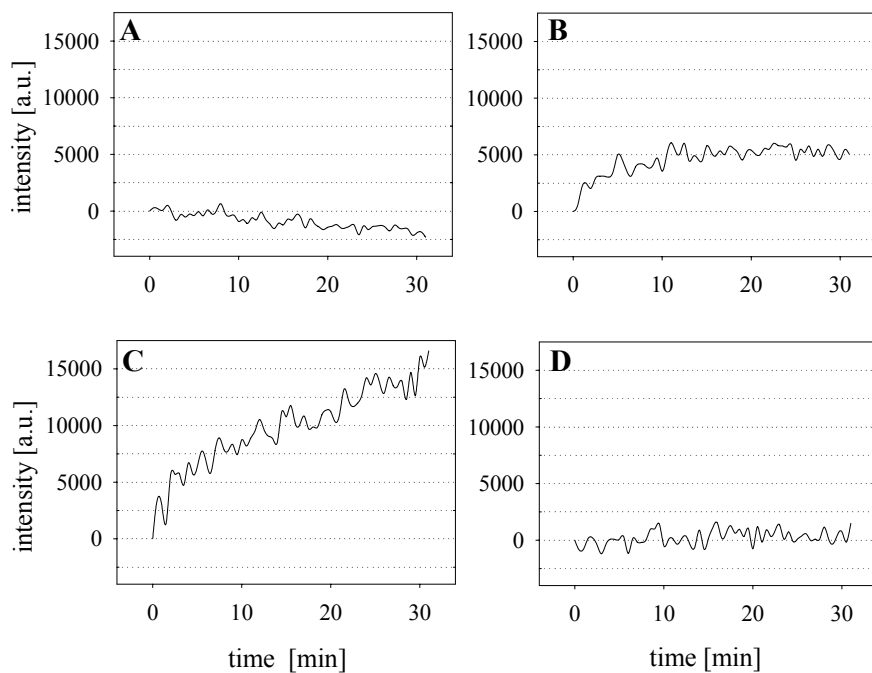


Figure 3.42: Permeation of peptides across egg PhC bilayers, T 25°C, pH 6.8 (adjusted with 200 mM TRIS). Representative luminescence/time curves of (A) blank, (B) peptide **5**, (C) DPA (positive control) and (D) peptide **12** (negative control).

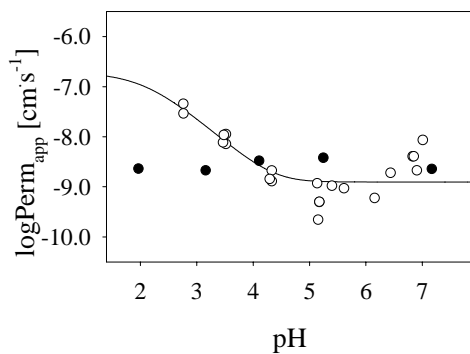


Figure 3.43: Influence of pH on the permeation of peptide **3** and DPA across egg PhC bilayers, T 25°C. ○, DPA (control); ●, peptide **3**; (line), fit of the DPA pH/permeation profile according to a Henderson-Hasselbalch function. The pH of the solutions was adjusted with SUBS.

3.6.5 Comparison of the lipid-bilayer permeation of the α - and β -peptides and influence of the molecular weight

All tested DPA- α -peptides permeated, if at all, with a $\log Perm_{app} \leq 8.1$. The β -peptide conjugates permeated better than their α -peptidic analogs. Significant permeation of the β -peptides could be observed in all experiments. As shown in Fig. 3.44, the average permeation coefficient of the β -peptides decreased with increasing molecular weight, the difference was, however, not significant. It has been shown before that an increase in molecular weight decreases the permeation of peptides [Malkia et al., 2004; Chakrabarti et al., 1994]. The largest tested β -peptide **10** ($\log Perm_{app} = -8.74 \pm 0.39$) permeated approximately five times slower than the smallest β -peptide **2** ($\log Perm_{app} = -8.06 \pm 0.24$). The average permeation coefficients of all DPA-coupled peptides were lower than the one of DPA alone. It has to be noted that the choice of the buffer influenced the overall permeation coefficient.

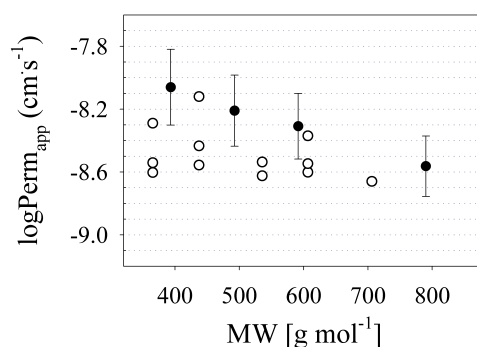


Figure 3.44: Influence of the molecular weight on the permeation of α -(\circ) and β -peptides (\bullet) across egg PhC bilayers. α -Peptides, single experiments with detectable permeation coefficients are shown. β -Peptides, shown are the average values of $n \geq 3$ experiments with the standard deviations (error bars) at T 25°C, pH 6.8 (adjusted with 200 mM TRIS).

3.7 Simulations of lipid bilayer permeation

3.7.1 Simulation of the influence of P and the translocation rate constants

The permeation process across a lipid bilayer was simulated according to eq. 2.25 taking into account the partitioning and translocation rate constants which were adjusted to our experimental conditions. The ratios of the apparent partitioning rate constants (k'_1/k'_{-1} and k'_{-3}/k'_3 , with $k'_{-1} = k'_3$ and $k'_{-3} = 100 \cdot k'_1$) are given by the distribution of the compounds between the aqueous and the bilayer phases and can be calculated from the partition coefficients and the volume ratios of the aqueous and lipid phases. To vary the partition coefficient P in the simulations we changed either k'_{-1} at a constant k'_1 or alternatively kept k'_{-1} constant and varied k'_1 .

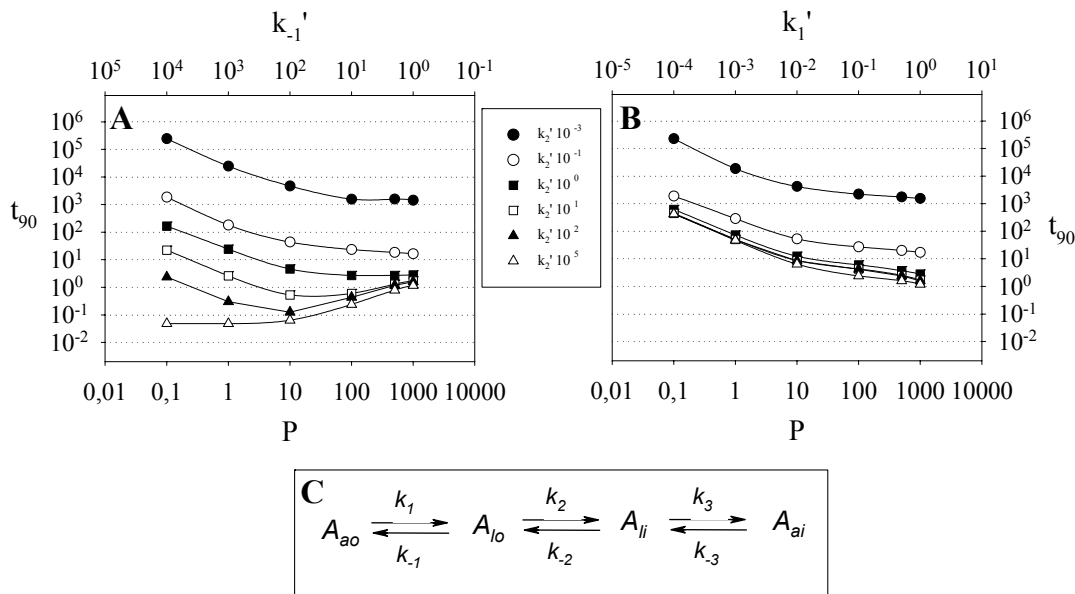


Figure 3.45: Simulation of membrane permeation. (A) $k'_1 = 1$, (B) $k'_{-1} = 1$, (C) model

Fig. 3.45 A shows the simulation results with the settings $k'_1 = 1$ and k'_2 between 0.001 and 100000. The partition coefficient P was set to values between 0.1 and 1000. The remaining apparent rate constants were calculated from these parameters as described in section 2.9.4. The value t_{90} designates the time point when 90% of the maximal luminal permeant concentration A_{ai} is reached. It is negatively correlated with the overall permeation rate. With $k'_1 = 1$, the simulation revealed the following results. (i) If $k'_2 \leq k'_{-1}$ the permeation rate increases with increasing k'_2 . At a constant k'_2 ($= k'_{-2}$), an increase in P , i.e. a decrease in k'_{-1} , results in an increase of the permeation rate. Under these conditions low P values are unfavourable for the permeation rate. Interestingly, above a certain threshold of P , under the chosen conditions if $P \geq 100$ ($k'_{-1} \leq 10$), any further increase in P , i.e. decrease in k'_{-1} , is without influence on the permeation rate. This is an important finding regarding the interpretation of our experimental data. (ii) If $k'_2 \geq k'_{-1}$, t_{90} is independent of k'_2 . Under these conditions and at a constant k'_1 , the permeation rate is determined by k'_{-1} and k'_3 , and thus, by P . Surprisingly and in contrast to the findings with $k'_2 \leq k'_{-1}$, high P values result in a lower permeation rate, while low membrane affinity leads to faster permeation. In this range k'_3 is rate-limiting. At $P = 10$ (and $k'_2 \geq k'_{-1}$), a further decrease in P has no influence on the permeation rate.

3 Results

The above simulations were performed with a constant k'_1 and variations in P were achieved by altering k'_{-1} . Fig. 3.45 B shows the results with the settings $k'_{-1} = 1$, k'_2 between 0.001 and 10, and P between 0.1 and 1000. In this case alterations in P were accomplished by varying k'_1 . For (i) $k'_2 \leq k'_{-1}$ the simulations revealed a similar picture as in Fig. 3.45 A. The permeation rate is determined by k'_2 and P and is positively correlated with the two. In parallel to the findings described above with $k'_1 = 1$, the influence of P on the permeation rate is more pronounced if $P \leq 100$. (ii) In contrast to the findings described for a constant $k'_1 = 1$, the simulations with the settings used in Fig. 3.45 B revealed a direct relationship between P and the permeation rate also in the case $k'_2 \geq k'_{-1}$. To conclude, an increase in the membrane affinity may lead to an increase or a decrease in the permeation rate constant or may have no effect at all, depending on the ratios between the single rate constants of the partitioning and flip-flop processes as well as on the volume ratios of the membrane and the aqueous phases.

3.7.2 Simulation of the influence of the lipid concentration

The influence of the lipid concentration on the overall permeation rate was simulated by estimating the volume ratios between the outer and inner aqueous phases and the lipid phase as described in section 2.9.3 for lipid concentrations between 1 and 20 mg/ml. The results shown in Fig. 3.46 indicate that with increasing lipid concentration the overall permeation rate increases. Increasing the lipid concentration 20fold, i.e. from 1 mg/ml to 20 mg/ml, decreased t_{90} by a factor of ~ 1.5 . These simulation results are in good agreement with our experimental findings described in section 3.3.2. Increase of the lipid concentration led to higher $\log Perm$ values, i.e. to an increase of the overall permeation rate.

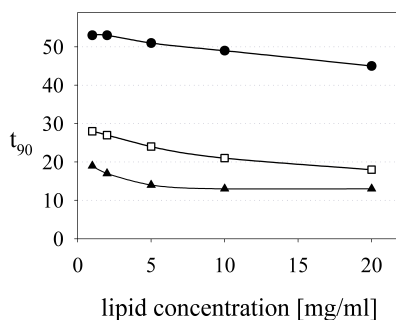


Figure 3.46: Simulation of the influence of the lipid concentration on the permeation rate.

●, P 10; □ P 100; ▲, P 1000. In all simulations $k'_{-1} = k'_3 = 1$ and $k'_2 = k'_{-2} = 0.1$.

3.7.3 Simulation of the influence of the Tb(III) complex association constant

The differential equation system as described in section 2.9.1 describes the process of lipid bilayer permeation as a 3-step-model. The permeation into Tb(III)-containing liposomes, however, should rather be described as a 4-step-model, with the complex formation between A_{ai} and Tb^{3+} as last step and k_4' and k_{-4}' as the complex association and dissociation rate constants. The

rate laws described by eq. 2.28 have thus to be extended in the following way with $[A_{Tb}]$, the solute concentration in complex with Tb(III):

$$\begin{aligned}
 d[A_{ao}]/dt &= -k'_1 \cdot [A_{ao}] + k'_{-1} \cdot [A_{lo}] \\
 d[A_{lo}]/dt &= k'_1 \cdot [A_{ao}] - (k'_{-1} + k'_2) \cdot [A_{lo}] + k'_{-2} \cdot [A_{li}] \\
 d[A_{li}]/dt &= k'_2 \cdot [A_{lo}] - (k'_{-2} + k'_3) \cdot [A_{li}] + k'_{-3} \cdot [A_{ai}] \\
 d[A_{ai}]/dt &= k'_3 \cdot [A_{li}] - (k'_{-3} + k'_4) \cdot [A_{ai}] + k'_{-4} \cdot [A_{Tb}] \\
 d[A_{Tb}]/dt &= k'_4 \cdot [A_{ai}] - k'_{-4} \cdot [A_{Tb}]
 \end{aligned} \tag{3.1}$$

The influence of the complex association constant was simulated by varying k'_4 and k'_{-4} , and the results are shown as a function of the complex association constant in Fig. 3.47. The complex formation decreases the overall permeation rate if the association constant is above a threshold, which is dependent on the ratios of all rate constants. Below this threshold, the permeation rate is independent of the complex association constant. Our experiments shown in section 3.3.2 revealed no influence of the complex association constant on the overall permeation rate.

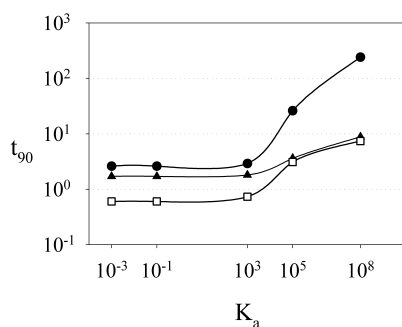


Figure 3.47: Simulation of the influence of the complex association constant K_a on the permeation rate. ●, P 1; □ P 100; ▲, P 1000. In all simulations $k'_1 = 1$ and $k'_2 = k'_{-2} = 10$.

4 Discussion

The present thesis is focused on the investigation of lipid bilayer permeation of drug-like molecules. On one hand it was of interest to investigate the influence of the solute structure and ionization state while on the other hand the impact of the barrier structure on the permeation process was explored. Furthermore, the relationship between membrane affinity and membrane permeation was of special concern.

The experimental part of this work is based on the measurement of membrane affinities to and membrane permeation across liposomal membranes. Equilibrium dialysis presents a well-characterized system to study membrane affinities [Pauletti and Wunderli-Allenspach, 1994]. The Tb(III)-permeation assay as introduced by Krämer and Wunderli-Allenspach [2003] was modified which increased the signal sensitivity and allowed thus to test a broader range of compounds. Additionally, the pH-dependency of the excitation spectra as found in the present work led to the possibility to measure the permeation rates at different pH values. In the work of Krämer and Wunderli-Allenspach [2003] it has been demonstrated that the luminescence signal was specific for the intraliposomal formation of the Tb(III)-ACA-complex. Since the permeation experiments in the present work were usually conducted in SUBS, which extinguishes the luminescence of the complex, Tb(III) eventually remaining in the outer aqueous phase could not cause a luminescence signal. As shown in Krämer and Wunderli-Allenspach [2003], the leakage of Tb^{3+} was negligible during the time course of the experiments, which is at the same time an indication for the stability of the liposomes. The same conclusion was drawn by Sigler et al. [2000] who calculated an apparent permeation coefficient of $7.5 \cdot 10^{-12} \text{ cm} \cdot \text{s}^{-1}$ for Tb^{3+} at pH 7 from phosphatidylethanolamine/phosphatidylglycerol liposomes.

The luminescence of the Tb(III)-ACA-complex is very sensitive which is of advantage for a high lipid/solute ratio to avoid any membrane saturation or unspecific effects of the solute on the membrane. Under the standard assay conditions, i.e. a lipid concentration of $\sim 2 \text{ mg/ml}$ and ACA concentrations of about $5 - 100 \text{ } \mu\text{M}$, the sample lipid/solute ratio was $\sim 20-500$. Even if the intraliposomal Tb^{3+} concentration is high ($5-7 \text{ mM}$, [Krämer and Wunderli-Allenspach, 2003]), its adsorption to the lipid bilayer can be excluded, since zetapotential measurements showed no difference between Tb^{3+} -containing and Tb^{3+} -free liposomes.

Furthermore, it was ensured that Tb(III) functions as probe only, but does not affect the permeation process. On one hand, it was concluded from stopped-flow experiments that the permeation kinetics of the ACAs across the liposomal membrane are slower than the kinetic of the complex formation of the ACAs with Tb^{3+} . On the other hand, it was important to determine to which extent the complex association constant K_a affects the permeation coefficient. For this purpose, K_a was modified by entrapping EDTA together with Tb(III) into liposomes. As revealed by thermodynamic studies (Lombardi, D.; unpublished data) the association constant is lowered in the presence of EDTA by several magnitudes. The permeation coefficients for two representative ACAs were, however, in a similar range as with EDTA-free liposomes, indicating that the complex formation constant does not affect the permeation coefficient. The kinetic simulations showed, that an increase of the Tb(III)-ACA-complex association constant K_a might decrease the

4 Discussion

permeation rate, but does indeed not affect the permeation coefficient if K_a is below a particular threshold.

These control experiments showed, that Tb^{3+} is a suitable probe for the liposomal permeation assay. It allows the measurement of a wide range of solutes. Due to its hydrophilicity and high charge density it is localized in the liposomal lumen and neither accumulates in the lipid bilayer nor leaks out of the liposomes. The complex formation has no influence on the permeation rate of the ACAs tested.

Interestingly, the luminescence/time curve were best fitted by biexponential functions. The biexponential shape was independent of the pH, the lipid bilayer composition and state as well as the buffer system. As the faster exponential reached 30-50% of the maximal luminescence intensity and was determinant for the initial slope of the kinetics, it was used for the calculation of $Perm_{app}$ in all experiments. It is most likely that the biexponential function is due to the single steps underlying the overall permeation process, since the simulation of the permeation process based on a 3-step model revealed triexponential functions.

Additionally, a theoretical calculation was performed, to analyze, whether the fast phase is due to translocation without desorption from the inner leaflet and the slow phase to the desorption step. In this case the ratio of the luminescence maxima of the two exponentials would be pH-dependent as, e.g. the ratio of membrane located to aqueous SA is ~ 30 times higher at pH 3 than at pH 7. However, this was not the case in our study.

The permeation profiles of all tested ACAs except of CF and CFDA followed in all liposome systems Henderson-Hasselbalch functions with two plateaus determined by the intrinsic permeation coefficient of the net neutral and the anionic species. The permeation coefficients of the net neutral species were generally higher than or equal to the permeation coefficients of the anionic species, except for the permeation of AA. For all ACAs except of CF and CFDA, the ratio between the permeation coefficients of the different ionization species was 12 – 600. This is a significant discrepancy with the pH-partition hypothesis, according to which only the net neutral species contributes to the apparent permeation coefficient while the permeation of the charged species is negligible [Brodie and Hogben, 1957; Shore et al., 1957].

As illustrated in Fig. 4.1, the overall permeation rate is determined to equal extents by the neutral and anionic species, if the product of $Perm^{AH}$ and α^{AH} equals the product of $Perm^{A^-}$ and α^{A^-} , or in other words, if the ratio of $Perm^{AH}/Perm^{A^-}$ equals the ratio α^{A^-}/α^{AH} . If the pH is lower or higher than this particular point, the permeation is controlled either by the neutral or the anionic species. Considering the small ratios $\log Perm^{AH}/\log Perm^{A^-}$ found in this work, it can be concluded that at physiological pH 7.4 the permeation of all tested ACAs except of CF and CFDA is controlled by the anionic species, whereas the permeation of the neutral species is negligible. The calculation of the $\log Perm^{AH*}$ values at each experimental pH assuming no permeation of the anionic species, illustrated how this assumption can lead to erroneous estimates of $\log Perm^{AH}$.

The relatively high permeation coefficients of the anionic species as compared to the net neutral acid could be related to the membrane fluidity and to the formation of dynamic pores in the liquid crystal bilayer [Jansen and Blume, 1995]. At 25°C, DPPC bilayers are in the gel state, resulting in a more rigid membrane and a significantly lower occurrence of dynamic pores as compared to the crystal state [Lawaczeck, 1988]. The permeation coefficients of OHNA with DPPC were about 10 times slower than across liquid crystal egg PhC bilayers at the same temperature, which is probably due to higher motion restrictions as a result of the decreased

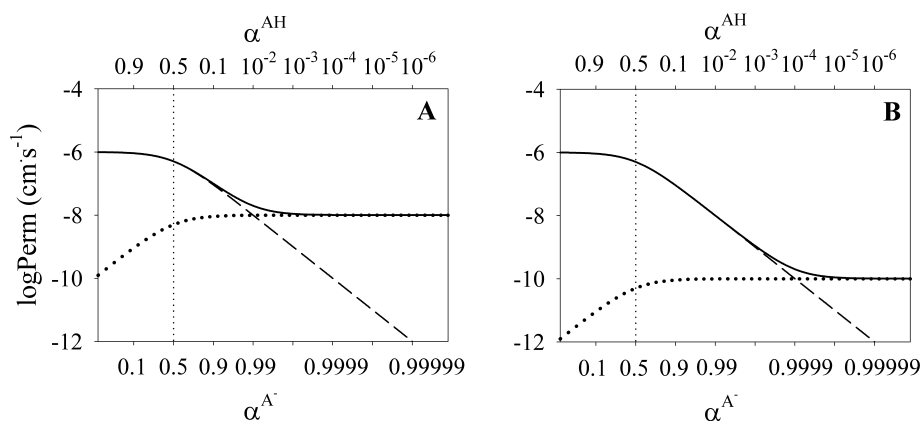


Figure 4.1: Simulation of the permeation profiles of an acidic compound. Full line, overall permeation coefficient; dashed line, contribution of neutral species; thick dotted line, contribution of anionic species; thin dotted line, pK_a . The overall permeation rate is determined by the anionic species, if $\text{Perm}^{\text{AH}} \cdot \alpha^{\text{AH}} \leq \text{Perm}^{\text{A}^-} \cdot \alpha^{\text{A}^-}$. (A) $\text{Perm}^{\text{AH}} 10^{-6}$; $\text{Perm}^{\text{A}^-} 10^{-8}$. The permeation is controlled by the anionic species at $\text{pH} \geq \text{pK}_a + 2$. (B) $\text{Perm}^{\text{AH}} 10^{-6}$; $\text{Perm}^{\text{A}^-} 10^{-10}$. The permeation is controlled by the anionic species at $\text{pH} \geq \text{pK}_a + 4$.

membrane fluidity. The sigmoidal shape of the pH/permeation profile was, however, retained also in the gel state, the anionic species was only 3 times slower than the net neutral species. If anion permeation would be dependent on the presence of dynamic pores in the membrane, we would expect a much higher ratio of neutral/anion permeation. Thus, it can be concluded that the unexpected high permeation of the ionic species is not related to the fluidity of the membrane or due to the formation of pores. In addition, pores allowing ACA anion exchange as observed in our case would also possibly result in a higher Tb^{3+} leakage than observed by Krämer and Wunderli-Allenspach [2003] and Wilschut et al. [1980].

We can rule out charge delocalization within the ACA due to intramolecular hydrogen bonds formation as reason for the the low ratio between neutral/anion permeation, since some of the tested ACAs, e.g. DPA and DCBA have no potential to form intramolecular hydrogen bonds.

Another possible explanation for the high permeation of the anionic species could be the enhanced permeation of ionic solutes by lipophilic counterions as described by Neubert [1989]. To investigate the influence of counterions in this study, SUBS was replaced with TRIS and the permeation of SA, OHNA and DPA at pH 3 and pH 7, respectively, were determined. The TRIS cation, i.e. the protonated base, is more lipophilic than Na^+ and would therefore be more effective as counterion for ion-pair permeation of the tested ACAs. In accordance with this hypothesis, TRIS enhanced the permeation of anionic SA and DPA, but did not affect the permeation of net neutral SA and DPA. The permeation-enhancing effect of TRIS on the net neutral OHNA but not on deprotonated OHNA was unexpected and suggests that TRIS might increase the permeation rate not only by acting as lipophilic counterion. However, it should be noticed that net neutral OHNA is rather considered as zwitterionic species, which might be affected in its permeation behaviour by counterions. An influence of the buffer and thus, of the counterions, was also found for the permeation of small peptides. The effects of counterions on the permeation rates could, however, also be due to their influence on the physicochemical properties of the lipid bilayer.

Our findings deviate significantly from the pH-partition hypothesis and from the pioneering permeation studies by Gutknecht and Tosteson [1973], who investigated the permeation of neutral and anionic SA with planar lipid bilayers. The permeation coefficient of salicylic acid was $0.7 \text{ cm} \cdot \text{s}^{-1}$ while the permeation of the salicylate was negligible. However, this large difference in the permeation rate of the single ionization species is not directly reflected in the experimental data of Gutknecht and Tosteson [1973], but rather due to the data correction for the unstirred water layer. Plotting the permeation data (experimental flux / concentration) of Gutknecht and coworkers against the pH, the shapes of the permeation profiles are notably similar to the profiles in the present work, with the exception that the inflection point of the profile by Gutknecht and Tosteson is around pH 6 instead of 2.75, i.e. the pK_a of SA. This significant shift of the dissociation constant was explained with the presence of the UWL. Including diffusion coefficients of HA and A^- across the UWL led to a correction of the permeation coefficients of the net neutral SA by the factor 10^5 . However, the authors did not consider that the pH at the membrane surface is shifted to lower pH values than in the bulk solution caused by the high amount of salicylate anions in the bilayer [Krämer et al., 1997]. This surface-charge induced pH drop could explain part of the observed shift of the inflection point in the redrawn permeation/pH profile and would result in a significantly lower correction factor for the UWL, if taken into account. It should, in addition, be kept in mind that the planar lipid bilayers of Gutknecht and Tosteson contained decane. The solvent could have a similar effect on the partitioning of salicylic acid and salicylate as n-octanol; the ratio between the two partition coefficients of net neutral and anionic species is higher in the n-octanol/buffer system than in the egg PhC liposomes. Finally, it should be taken into account that in the experiments by Gutknecht and Tosteson measurements at \geq pH 5 were done at a total SA concentration of 0.1 M. Considering the partition coefficient of the anionic species in our liposomal system, i.e. 7, and a molar local lipid concentration of about 1 M within the bilayer, this leads to permeant/lipid ratios in the range of 1/1, which certainly affects the membrane properties and thus, the permeation of the solute.

Several studies have been published observing deviations from the pH-partition hypothesis. Nogami and Matsuzawa [1961] found the ratio of 6 for the permeation of the net neutral and anionic SA through segments of rat intestine. Investigating the pH-dependent transport of cationic drugs across Caco-2 cell monolayers, Palm et al. [1999] observed a significant contribution of the ionized species when the fraction of the neutral species was ≤ 0.1 . The permeation coefficient of the unionized form of alfentanil and cimetidine was 150 and 30 times higher than of the cationic species, respectively. Transport studies using porcine buccal mucosa in a Franz type diffusion cell revealed that the permeation rate of neutral ondansetron was only 7 times higher than the rate of its cationic species [Mashru et al., 2005]. Applying $^1\text{H-NMR}$ studies, Males and coworkers found a difference of 13 for the permeation coefficients of neutral and anionic glycolic acid, while the monomethylarsonic acid anion permeated at least 10^4 times slower than its corresponding neutral form [Males and Herring, 1999; Males et al., 1998].

Our findings were challenged and devaluated as artefacts by Saporov et al. [2006]. Their main criticism was the formation of a transmembranal pH gradient by the permeating net neutral species into the unbuffered liposomal lumen, leading to erroneous measurements. Our control experiments revealed, however, no significant difference if the permeation coefficients obtained with buffered and unbuffered liposomes were compared. Thus, unbuffered liposomes were used for the permeation experiments, if not indicated otherwise, since the Tb(III) loading was higher omitting buffer in the preparation step. In addition, no acidification of the inner leaflet was observed after adding pH-sensitive fluorescent lipid probes to the membrane. If the permeating acid would build up a significant pH gradient, this effect and thus the measured permeation

coefficients would be dependent on the ACA concentration. Our experiments showed, however, no significant effect of the permeant concentration on the permeation rate.

Considering all permeant ionization species and proton concentrations at the experimental pH values, the theoretical pH shift is minor. Another evidence for the absence of a transmembranal pH shift is the good agreement of the experimental inflection points of the pH/permeation profiles with the pK_a values as determined by potentiometric titration. If the pH which determines the permeation, i.e. the pH at the membrane surface, would be different than the bulk (measured) pH, the inflection point would deviate from the titrated pK_a by the same value as the difference between the bulk pH and the pH determining permeation [Winne, 1977]. This deviation of the inflection point from the pK_a has been described for the membrane affinity of the base propranolol to net negatively charged liposomes [Krämer et al., 1998a] and has also been observed in the present work for the affinity and permeation profiles with charged liposomes. The extent of the shift could, however, well be explained by the zeta potential of the charged liposomes for PhI, but not for StAm (see below). Equally, the inflection points of the pH/permeation profiles would not superimpose with the titrated pK_a values if the plateau at $pH \leq pK_a$ would be shifted to low values as suggested by Saparov et al. [2006].

We found no significant permeation of the di-anionic species for the two ACAs CF and CFDA in two different liposomal systems. CFDA, which is the esterified CF, is commonly used in viability assays [Morono et al., 2004; Breeuwer et al., 1995]. CFDA is able to diffuse through the cell membrane of intact cells into the cytoplasm where it is hydrolyzed by intracellular non-specific esterases, which are active in viable cells, but not in dead cells. The hydrolyzation results in the more hydrophilic impermeable CF, which shows a characteristic fluorescence different from CFDA and accumulates in the cells. The impermeability of CF across lipid bilayers is exploited by leakage assays. CF is entrapped into liposomes in self-quenching concentrations and the influence of e.g. leakage-inducing agents is investigated [Ambroggio et al., 2005; Weinstein et al., 1977]. In agreement with these studies, we found no permeation of the di-anionic CF, but, we neither observed permeation of di-anionic CFDA. Comparing the permeation of the net neutral species, $\log Perm^{AH}$ of CFDA is only marginally higher than $\log Perm^{AH}$ of CF, which is intriguing taking into account the 10fold higher affinity of CFDA to octanol as compared to its unesterified analog and the similarity of the other physicochemical properties. Certainly, the permeation of CFDA into cells could also be due to transport proteins, however, this was to our knowledge not described in the studies. The application of CFDA as viability marker for a wide range of different cells, even bacterial cells [Bunthof et al., 2001], does not indicate the existence of specific transport phenomena, either. It could be possible that the Tb(III)-permeation assay has a lower sensitivity than cells. It would be interesting, to investigate the effect of esterification further with smaller ACAs, such as salicylic acid in comparison with acetylsalicylic acid.

The possibility to have liposomal systems to measure both, membrane affinity and membrane permeation, provided the opportunity to compare directly the influence of the lipid composition on both processes and investigate the relationship between them. For this part of the study, the ACAs SA, AA and OHNA were chosen as representative examples. These three molecules are of interest since they differ in their structure and dissociation behaviour and cover a $\log P_{Octanol}$ range of ~ 2.5 . The membrane composition was systematically varied by adding cholesterol or the charged lipids phosphatidylinositol and stearylamine, respectively. Assuming a direct relationship between membrane affinity and membrane permeation, a decrease in the membrane affinity would result in a decreased permeation rate. However, kinetic simulations based on the 3-step model revealed that membrane permeation could be positively, negatively or not correlated

to changes of the membrane affinity, depending on the interplay of the single rate constants.

First evidences that membrane permeation cannot be simply predicted from membrane affinities were already obtained from the affinities of the test compounds to net neutral egg PhC bilayers. For instance, the affinity of neutral SA to PhC bilayers was ≥ 100 times higher than that of OHNA while the corresponding values for membrane permeation were in the same range. In contrast, $\log P^{AH}$ was similar for SA and AA, but $\log Perm^{AH}$ was significantly lower for AA.

Chol is found in biological membranes in variable amounts and leads to major changes in the structure and fluidity of the lipid bilayer [Mouritsen and Zuckermann, 2004; Urbina et al., 1995; Kusumi et al., 1986] which in turn influence the membrane affinity and permeation of solutes. Several studies [Henriksen et al., 2006; Kurad et al., 2004; Lagerquist et al., 2001; Urbina et al., 1995] revealed a significant decrease of the membrane affinity of a variety of acidic, basic and neutral drugs when Chol was present in phospholipid bilayers. This was assigned to motion restrictions of the fatty acyl chain regions close to the lipid head groups and to the higher rigidity of the membrane induced by Chol in general, leading to an impeded integration of the drug molecules into the lipid bilayer. De Gier et al. [1968] observed decreased permeation coefficients of glycerol and erythritol with 10 to 50% Chol in egg PhC bilayers. Frezard and Garnier-Suillerot [1998] described decreased permeability coefficients of anthracyclines with increasing amounts of Chol between 20 and 45% in egg PhC/egg phosphatidic acid membranes at pH 6.

In this study, we found a significant decrease in the membrane affinity of the net neutral and anionic species of SA and AA in the presence of 25% and 40% Chol as compared to PhC liposomes. The membrane affinities of the neutral and ionized species were affected in a similar manner, i.e. the effect of Chol was independent of the ionization state of the compound. This supports the hypothesis that the reduction of the membrane affinity is rather due to the lower flexibility of the lipid bilayer than to an influence in the head group region. The latter would probably affect electrostatic interactions and therefore have divergent effects on the affinity of neutral and ionized species. The influence of Chol on the permeation of the tested compounds did, however, not correspond to its influence on their membrane affinity. The membrane permeation of SA was not influenced by 25% and 40% Chol, despite the significant decrease in membrane affinity at these Chol contents. Except at 10% Chol, we observed a decrease in the permeation coefficients of OHNA with all tested Chol concentrations. This effect was independent of the ionization state of the solute and thus probably due to a general influence of Chol on the rigidity of the membrane. The different behaviours of SA and OHNA are coherent with the simulation results. Under the condition that the apparent translocation rate constant is slower than the apparent membrane dissociation rate constant ($k'_2 \leq k'_{-1}$), changes of P above a certain threshold, which depends on the single apparent rate constants, have no influence on the permeation rate. A decrease of P values below this threshold leads instead to a decrease of the permeation rate.

In general, the membrane affinity is dependent on the ionization state of the solute and on the net charges of the membrane lipids. Positively charged propranolol and desipramine had a higher affinity to negatively charged than to net neutral membranes due to electrostatic attraction forces [Marenchino et al., 2004; Krämer et al., 1998a]. In the presence of the negatively charged PhI, we found a major decrease in the membrane affinity of the negatively charged species of SA and AA, the affinity of the neutral species was less affected. These effects could be assigned to the electrostatic repulsion between the anionic species and the negatively charged membrane. In contrast, $\log P^{A^-}$ of SA and AA were considerably increased in the presence of 15% StAm while $\log P^{AH}$ remained unchanged or was slightly decreased. The increase in $\log P^{A^-}$ is probably due to the electrostatic attractions between the positively charged membrane and the negatively

charged solute. As for Chol, the influence of the charged lipids PhI and StAm on the membrane affinity was consistent for SA and AA. Surprisingly, the permeation of the anions was increased in the presence of both PhI and StAm, respectively. The permeation-enhancing effect of PhI would certainly not be expected from the membrane affinity measurements. The experimental results can, however, be simulated by varying the rate constants of partitioning and translocation. If the apparent translocation rate constant is higher than the apparent dissociation rate constant ($k'_2 \geq k'_{-1}$), a decrease of a solute's membrane affinity is favorable for its permeation. Another possible explanation would be changes in the translocation rate constants, which are not reflected by the affinity measurements, but considerably affect the permeation rate.

From the results presented here and the cited partition studies it can be concluded that the influence of particular lipids on the membrane affinity of acids and bases is predictable in a qualitative manner considering the rigidity of the bilayer and the electrostatic interactions between the charged solutes and the lipid headgroups. In contrast to the findings in the partition experiments, changes in the lipid composition had unpredictable effects on membrane permeation. There was no clear correlation between membrane affinity and permeation. Kinetic simulations showed, however, that these discrepancies are due to the interplay of the single rate constants.

The net neutral AA shows a striking permeation behaviour. In PhC and in the presence of 25% Chol it permeated less than two times faster than the anion and about 300 times slower than the cation. This might be due to strong electrostatic attraction forces between the zwitterionic AA and the lipid headgroups lowering the chance for a flip-flop event. The addition of other lipids (except 25% Chol) beside PhC led to an increase of the permeation coefficient of the net neutral AA. This permeation enhancing effect of Chol, PhI or StAm could either be related to an interruption of the electrostatic attractions between phosphatidylcholine head groups and net neutral AA [Yeagle et al., 1977] or a shifted equilibrium between zwitterionic and net neutral species at the membrane surface.

Investigating the influence of Chol on membrane permeation, we found a discontinuous behavior at 10% with all tested compounds. This is in line with the exceptional membrane behaviour at low Chol concentrations observed before [Parasassi et al., 1995; Mouritsen and Jorgensen, 1994; Corvera et al., 1992] and could be related to the peculiarities in the phase diagrams of PhC/Chol mixtures as suggested by Mouritsen and Zuckermann [2004]. These authors described increased binding of ethanol to dimyristoylphosphatidylcholine bilayers with 4% Chol while 35% Chol had the opposite effect. Additionally they observed that low levels (5%) of Chol increased the Na^+ flux across dipalmitoylphosphatidylcholine bilayers, while the effect was inverse with 40% Chol. The exceptional behaviour found for the permeation profiles of SA and AA at 10% Chol is likely to be due to the structural characteristics of the Chol-containing membrane. The membrane is affected in a different manner by low Chol concentrations than by high Chol concentrations. Interestingly, 10% Chol had no significant effect on the membrane affinity of SA and AA.

The addition of StAm to the bilayer led to significant deviations of the inflection points of the $\log D/pH$ profiles (SA, AA) and of the $\log Perm_{app}/pH$ profile (AA) from the titrated pK_a values. Since the dissociation constant of StAm in our liposomal systems was estimated by zeta potential measurement of the liposomes revealing an apparent pK_a of ~ 9.7 , it can be excluded that the dissociation equilibrium of the amine group interferes with the experimental data, the membrane is positively charged within the investigated pH range. The shift of the inflection point to higher values could be due to the formation of micelles by StAm and the permeant in the aqueous phase. Size distribution measurements, however, did not reveal the presence of micelles.

A series of 13 structurally related ACAs was chosen to investigate the influence of the solute's structure on the permeation process with two different lipid compositions. The permeation across egg PhC bilayers was compared to „biomix” liposomes based on the composition of rat liver plasma membranes [Daum, 1985]. In agreement with our above discussion, the correlation between the lipophilicity parameter $\log P_{Octanol}$ and the permeation coefficient in both systems was poor. No reasonable correlation to other physicochemical parameters was obtained, suggesting that membrane permeation is a multifactorial process. Hence, it was necessary to explore the influences on membrane permeation by means of multivariate analysis techniques.

The categorization of the test compounds according to their physicochemical properties revealed two groups mainly due to differences of their size and size-related properties. Even though the impact of the molecular size on membrane permeation has been shown by several studies [Kobayashi et al., 2004; Mitragotri et al., 1999] we omitted the larger molecules for the further analysis due to the skewed distribution of all size-related parameters.

The subsequent analysis of the relationship between the solute's physicochemical parameters and their permeation rates revealed that membrane permeation is favoured by the solute's lipophilicity, which is in agreement with the positive correlation between the $\log D_{Octanol}^{7.4}$ and the Caco-2 cell permeability as found by Yazdanian et al. [1998] as well as the positive sigmoidal correlation between the calculated $\log P_{Octanol}$ and the fraction absorbed in humans described by Zhao et al. [2002]. It is evident, that a certain membrane affinity of the permeant is necessary to intercalate into and traverse the lipid bilayer. These findings are also in line with our kinetic simulation results, which indicate a positive sigmoidal relationship between the partition coefficient and the permeation rate if $k'_2 \leq k'_1$. The hydrophilicity of the tested molecule was expressed by the polar surface area and the hydrogen bond donor and acceptor capacities, which have been shown to be closely correlated to each other [Abraham et al., 2002]. Previous studies showed that membrane permeation is in general negatively correlated to the polarity of the molecules [Zhao et al., 2002; Winiwarter et al., 1998; Palm et al., 1997] Our results are in agreement with these findings, but indicate the existence of an optimum range for the polarity of a molecule. A certain hydrophilicity is probably necessary for the insertion into the lipid leaflets, whereas too strong interactions with the lipid headgroups due to, e.g. a high number of hydrogen bond donors and acceptors might limit the transmembrane passage. A similar optimum was reported for a solute's lipophilicity [Kubinyi, 1979], which could not be shown in the present study. It is, however, probable, that the lipophilicity range covered by the tested compounds was too small to detect an optimal range. Additionally, the electronic accessibility of the molecules was revealed as favourable influence on lipid bilayer permeation which is in accordance with the PLS prediction studies of human intestinal drug absorption by Norinder et al. [1999].

Our study was limited by the extraordinary low permeation coefficients of the net neutral anthranilic acid derivatives. As discussed above, this might be due to the strong interaction of the lipid headgroups with the zwitterionic molecules. However, other zwitterionic molecules in this study (OHNA) did not show a particularly slow permeation behaviour. Unlike OHNA, the anthranilic acid derivatives are also strong hydrogen bond donors. A slow permeation of strong hydrogen bond donors across human skin has been reported by el Tayar et al. [1991a]. It is interesting to note, that in contrast to the findings with Chol, PhI and StAm the shape of the pH/permeation profile did not change with biomix liposomes as compared to PhC bilayers. The high difference in $\log Perm^{AH}$ of the anthranilic acid derivatives as compared to the other test compounds could hide further structure-permeation relationships. Care should be taken in the evaluation of variables such as the hydrophilicity index, which is high for AA and MAA. They might be indeed of significance in the determination of $\log Perm^{AH}$, but their importance could

on the other hand be overestimated due to the low $\log Perm^{AH}$ of AA and MAA.

To avoid these problems, the study should be extended systematically by choosing, e.g. other zwitterionic molecules, larger and highly flexible molecules as well as molecules of high polarity. A first indication for a less problematic analysis is given by a regular distribution of the physicochemical properties with a minimal number of outliers.

For each tested ACA, the permeation coefficients obtained with biomix liposomes were equal or lower than the corresponding permeation coefficients obtained with PhC liposomes. The extent of this effect was distinct for different solutes and for the single ionization species. As already found for the influence of single lipids on the permeation process, the changes of the permeation profile between PhC and biomix liposomes were unpredictable. Also taking into account a variety of physicochemical descriptors no reasonable model was obtained to explain the differences between PhC and biomix permeation coefficients. This is another indication for the complex interplay between the single rate constants affecting the overall permeation rate as revealed by the kinetic simulations.

The differences in the permeation coefficients between net neutral and anionic species could also not be modeled. This could be due to the lack of suitable descriptors of the ionized molecules. However, the close correlation between $\log Perm^{AH}$ and ΔPhC or ΔBM , respectively, indicates that compounds with a high permeation rate of the net neutral species have a low permeation rate of the corresponding anionic species and vice versa. Again, this correlation could be biased by the extraordinary low $\log Perm^{AH}$ and the small ΔPhC and ΔBM values of the anthranilic acid derivatives. The repetition of the analysis omitting AA and MAA is difficult to interpret, because the $\log Perm$ values cover only a small range then.

In summary, the present results have to be considered as pilot study for the investigations of quantitative structure-permeation relationships. Sophisticated analysis methods were applied to extract informations from large data matrices. The analysis was limited by the uneven distribution of the physicochemical parameters as well as the permeation coefficients. Size and size-related descriptors as well as lipophilicity were favorable for permeation. The polarity of a molecule has to be in an optimal range.

The interpretation of lipid bilayer permeation as 3-step model according to Lauger et al. [1981] and the kinetic simulation based on the rate laws derived from the model prove as valuable tool to understand the time course of a permeating solute as function of the single rate constants and thus, helped to analyze the interplay of the rate constants. A representative screenshot of the interactive Java applet is shown in Fig. 4.2. As mentioned in the above discussion, the kinetic simulations showed in agreement with the experimental data, that membrane permeation can be positively, negatively or not correlated to the membrane affinity.

It is important to note, that the overall permeation rate is dependent on the dimensions of the system, i.e. the volume ratios between the single aqueous and lipid compartments. This was taken into account by the transformation of the rate constants k into apparent rate constants k' . With increasing volume of the compartment where the rate constant originates from, the apparent rate constant will decrease. Thus, the rate-limiting step might change by changing the system dimensions. Another important consequence is, that experimental permeation rates obtained with different experimental set-ups cannot be compared due to the differences in the system dimensions. This was reflected by the control experiments investigating the influence of the liposome concentration on the permeation rate. An increase of the liposome concentration, i.e. a decrease of the volume ratio between the outer aqueous compartment and the other compartments, would e.g. result in an increase of k'_1 . This would lead to an increased permeation rate, if k'_1 is rate-

determining, which is in accordance with our experimental data.

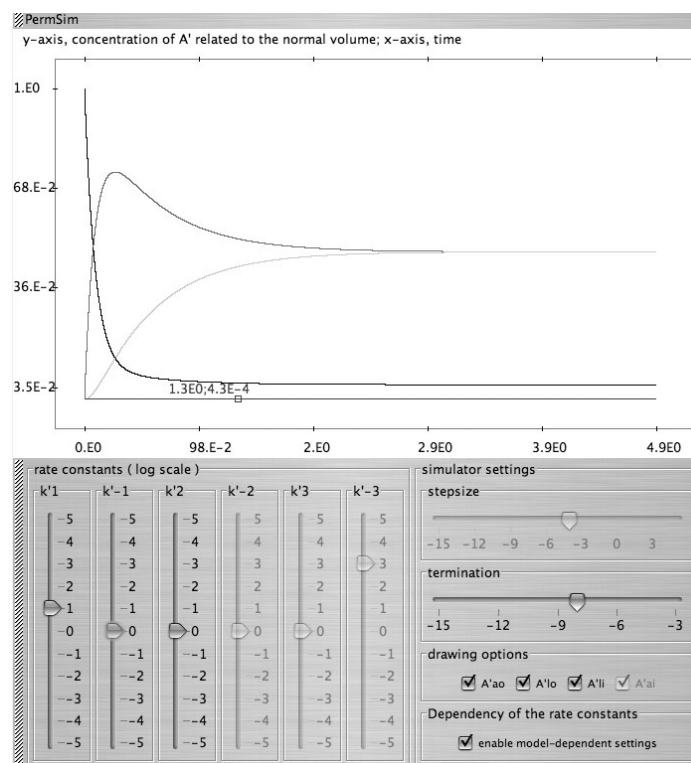


Figure 4.2: PermSim - interactive simulation of membrane permeation. Screenshot of the freely available Java applet. The single rate constants can be chosen according to the liposomal model or model-independently. The solute concentrations displayed in the plot are selected by the user. The permeation rate will be automatically calculated and displayed as t_{90} . See <http://n.ethz.ch/student/athomae/permsim/> for more information.

Apart from small drug-like molecules, the permeation of a series of small α - and β -peptides was investigated. For this purpose, the peptides were linked to DPA, which functioned as probe for the Tb(III)-permeation assay. The DPA-coupled peptide with the highest permeation coefficient was DPA- β -Val- β -Val-OH (**2**), which permeated at a similar rate as DPA alone. In contrast, the DPA- α -dipeptide (**1**) permeated at least 3 times slower than its β -analog. The difference between β - and α -peptides was less pronounced for the longer peptides but was still obvious for the tetrapeptides **4** and **5**.

From these different permeation rate constants of the tested DPA-peptides it can be concluded, though DPA must have an influence on the permeation of the tested conjugates, it is neither the driving force nor the rate-determining component. Differences in permeation must be due to the attached peptides. The permeation/pH profile of DPA- β^3 hVal- β^3 hAla- β^3 hLeu-OH (**3**) provides further evidence that DPA has only a minor influence on the permeation of the DPA-coupled peptides. While the permeation of DPA alone is strongly dependent on its ionization state, the permeation of **3** is not pH-dependent in the range between pH 2 and 7, where the pK_a of the carboxylic group of the coupled DPA would be expected. If attached DPA would be the driving force for permeation, its ionization state would have a similar influence as observed for DPA

alone. The data also show that the ionization state of the carboxylic acid at the peptide C-terminus has no influence on the permeation coefficient. This is not completely unexpected as the ionization state of a carboxylic acid may have a lower influence on permeation than expected from the pH-partition hypothesis as observed before in this work for smaller acids.

The observed difference between the permeation rates of analogous α - and β -peptide derivatives is difficult to rationalize. Several explanations are possible. (i) The permeation rate may depend upon a primary interaction between the peptide and the polar surface of the bilayer. The fundamental difference between a linear conformation of an α - and a β -peptide is that the latter is polar, in the sense that all NH bonds point in the same direction and all C=O bonds in the opposite direction, while there is an alternation of these bonds in the extended form of an α -peptide. Also, hydrophobic R groups are covering both faces of a linear α -peptidic conformation, while they are all on the same face of a linear β -peptidic arrangement. The distribution of the polar and hydrophobic groups along the peptides could influence their behaviour and arrangement in contact with the bilayer and eventually determine the permeation rate. (ii) We expected, that the additional methylene groups in each amino acid of the β -peptides increase their lipophilicity as compared to the α -analogs. This is supported by the RP-HPLC retention times with a C18 column and water/acetonitrile as the mobile phase: β -peptide derivatives have generally longer retention times than the α -analogs. From the general positive influence of lipophilicity on membrane permeation, it could be concluded that the gain in lipophilicity leads to a higher partitioning into the lipid bilayer and therefore to a faster permeation of the β -peptides [Malkia et al., 2004; Camenisch et al., 1998; Testa et al., 1996]. (iii) β -Peptides form secondary structures, such as helices and turns, with much shorter chain lengths than α -peptides. In these folded conformations intramolecular hydrogen bonding takes place, reducing or preventing the intermolecular interactions with other molecules or with polar surfaces, and rendering the structure altogether less polar or more lipophilic. In agreement with our investigations on structure-permeation relationships, an increased lipophilicity as well as a reduced polarity of the molecule might be favorable for its permeation rate. Although the CD and NMR investigations of the DPA-derivatives provide evidence for secondary structure formation only of the longer-chain peptides **8** and **10** [Gardiner et al., 2006], the lipophilic interior of the liposome bilayer may induce intramolecular hydrogen bonding and thus accommodate the permeating β -peptides better than the corresponding α -peptides.

In conclusion, we showed that DPA- β -peptidic conjugates permeate lipid bilayers at an increased rate as compared to their α -analogs. We suggest that the differing distribution of polar and hydrophobic groups along the backbone of β -peptides, the increased lipophilicity, and the greater tendency of β -peptides to form intramolecular hydrogen bonds, are contributing factors towards this effect. The increased permeation of β -peptides across lipid bilayers, together with their enhanced proteolytic and metabolic stability, is a favourable finding towards the possible use of β -peptides as therapeutic agents.

5 Conclusions and Outlook

In the present work, lipid bilayer permeation of small drug-like molecules and peptides was investigated using a liposomal assay. In addition to the experimental data, lipid bilayer permeation was modeled as a 3-step-process, from which a system of differential equations were derived and solved numerically.

The most surprising finding was the significant contribution of the anionic species to the overall permeation rate for all ACAs tested with the exception of CF and CFDA. In contrast to the expectations of the pH-partition hypothesis, permeation can be controlled by the anionic species already at 1 – 3 pH units above their pK_a .

No direct relationship was found between the membrane affinity of three representative compounds and their permeation behaviour. Changes of the membrane affinities induced by changes in the lipid compositions followed plausible rules considering bilayer rigidity and electrostatic interactions and are therefore predictable. Bilayer permeation instead appeared more complex. A certain lipid composition can even have opposite effects on a compound's partitioning and permeation. Theoretical simulations, however, disclosed that permeation may indeed positively, negatively or not be correlated with membrane affinity, which is in agreement with the experimental data.

The analysis of a series of thirteen structurally diverse ACAs did not reveal a quantitative structure-permeation relationship, but confirmed the interplay of several factors determining permeation. It is not sufficient, to predict permeation from only one parameter. Lipophilicity of the molecule as expressed by the octanol/water partition coefficient as well as the hydrogen bond descriptors have a major influence on lipid bilayer permeation.

The permeation assay was also applied to investigate the permeation of peptides. β -peptides were found to permeate better than their α -analogs. In line with our structure-permeation findings, the increased lipophilicity and decreased hydrogen bond capacity of the β -peptides as compared to the α -peptides could be the reason for the obtained differences in their permeation behaviour.

The present study can be extended to explore further details of lipid bilayer permeation. As already described above, the set of compounds used to model the structure-permeation relationships should be enlarged. Even though the biomix liposomes aim to mimic the biological membrane composition, they present a symmetrical bilayer, which is not physiological. It would be highly interesting to follow the permeation process across asymmetric bilayers. On the other hand, it would also be useful, to establish a permeation assay for a larger range of compounds, e.g. bases. Ideally, the permeation data presented here could be confirmed by an independent method. Certainly, insight into the single rate constants would contribute to the understanding of the permeation process. To contribute to the intriguing findings of the permeation of the ionized species it would be helpful, to use sophisticated molecular modeling methods to model the energy barrier present in the membrane.

Bibliography

- M. H. Abraham. Hydrogen bond and other descriptors for thalidomide and its N-alkyl analogs; prediction of physicochemical and biological properties. *European Journal of Pharmaceutical Sciences*, 21:465–469, 2004.
- M. H. Abraham and H. S. Chadha. Applications of a solvation equation to drug transport properties. In V. Pliska, B. Testa, and H van de Waterbeemd, editors, *Lipophilicity in Drug Action and Toxicology*, volume 4 of *Methods and Principles in Medicinal Chemistry*, pages 311–337. VCH Verlagsgesellschaft mbH, Weinheim, 1996.
- M. H. Abraham, A. Ibrahim, A. M. Zissimos, Y. H. Zhao, J. Comer, and D. P. Reynolds. Application of hydrogen bonding calculations in property based drug design. *Drug Discovery Today*, 7:1056–1063, 2002.
- Q. Al-Awqati. One hundred years of membrane permeability: Does Overton still rule? *Nature Cell Biology*, 1:E201–2, 1999.
- B. Alberts, A. Johnson, J. Lewis, M. Raff, K. Roberts, and P. Walter. *The Cell*. Garland Science, New York, 2005.
- R. J. Alger and J. H. Prestegard. Nuclear magnetic resonance study of acetic acid permeation of large unilamellar membranes. *Biophysical Journal*, 28:1–14, 1979.
- J. E. Allan. Ionization constants and ionization profiles. In B. Testa and H. van de Waterbeemd, editors, *ADME-Tox: The Fate of Drugs in the Body*, volume 5 of *Comprehensive Medicinal Chemistry*. 2006.
- E. E. Ambroggio, F. Separovic, J. H. Bowie, G. D. Fidelio, and L. A. Bagatolli. Direct visualization of membrane leakage induced by the antibiotic peptides: maculatin, citropin, and aurein. *Biophysical Journal*, 89:1874–1881, 2005.
- S. Ambudkar. Purification and reconstitution of functional human P-glycoprotein. *Journal of Bioenergetics and Biomembranes*, 27:23–29, 1995.
- R. Ano, Y. Kimura, M. Shima, R. Matsuno, T. Ueno, and M. Akamatsu. Relationships between structure and high-throughput screening permeability of peptide derivatives and related compounds with artificial membranes: Application to prediction of Caco-2 cell permeability. *Bioorganic and Medicinal Chemistry*, 12:257–264, 2004.
- N. Arnaud and J. Georges. Comprehensive study of the luminescent properties and lifetimes of Eu³⁺ and Tb³⁺ chelated with various ligands in aqueous solutions: Influence of the synergic agent, the surfactant and the energy level of the ligand triplet. *Spectrochimica Acta. Part A, Molecular and Biomolecular Spectroscopy*, 59:1829–1840, 2003.

Bibliography

- P. Artursson, K. Palm, and K. Luthman. Caco-2 monolayers in experimental and theoretical predictions of drug transport. *Advanced Drug Delivery Reviews*, 46:27–43, 2001.
- A. Avdeef. Refinement of partition coefficients and ionization constants of multiprotic substances. *Journal of Pharmaceutical Sciences*, 82:183–190, 1993.
- A. Avdeef and B. Testa. Physicochemical profiling in drug research: A brief survey of the state-of-the-art of experimental techniques. *Cellular and Molecular Life Sciences*, 59:1681–1689, 2002.
- A. D. Bangham, M. M. Standish, and J. C. Watkins. Diffusion of univalent ions across the lamellae of swollen phospholipids. *Journal of Molecular Biology*, 13:238–252, 1965.
- Y. Barenholz and G. Cevc. Structure and properties of membranes. In A. Baszkin and W. Norde, editors, *Physical Chemistry of Biological Interfaces*. Dekker, New York, USA, 2000.
- D. Bemporad, C. Luttmann, and J. W. Essex. Behaviour of small solutes and large drugs in a lipid bilayer from computer simulations. *Biochimica et Biophysica Acta*, 1718:1–21, 2005.
- M. P. Bemquerer, Jr. Bloch, C., H. F. Brito, E. E. Teotonio, and M. T. Miranda. Steady-state luminescence investigation of the binding of Eu(III) and Tb(III) ions with synthetic peptides derived from plant thionins. *Journal of Inorganic Biochemistry*, 91:363–370, 2002.
- S. D. Black and D. R. Mould. Development of hydrophobicity parameters to analyze proteins which bear post- or cotranslational modifications. *Analytical Biochemistry*, 193:72–82, 1991.
- K. Blomberg, P. Hurskainen, and I. Hemmila. Terbium and rhodamine as labels in a homogeneous time-resolved fluorometric energy transfer assay of the beta subunit of human chorionic gonadotropin in serum. *Clinical Chemistry*, 45:855–861, 1999.
- P. Breeuwer, J. L. Drocourt, N. Bunschoten, M. H. Zwietering, F. M. Rombouts, and T. Abee. Characterization of uptake and hydrolysis of fluorescein diacetate and carboxyfluorescein diacetate by intracellular esterases in *Saccharomyces cerevisiae*, which result in accumulation of fluorescent product. *Applied and Environmental Microbiology*, 61:1614–1619, 1995.
- H. Brockman. Dipole potential of lipid membranes. *Chemistry and Physics of Lipids*, 73:57–79, 1994.
- B. B. Brodie and C. A. Hogben. Some physico-chemical factors in drug action. *Journal of Pharmacy and Pharmacology*, 9:345–380, 1957.
- K. Bucher, S. Belli, H. Wunderli-Allenspach, and S. D. Krämer. P-glycoprotein in a detergent-free membrane environment: Influence of cholesterol on verapamil and progesterone binding and ATPase activation. manuscript submitted.
- C. J. Bunthof, K. Bloemen, P. Breeuwer, F. M. Rombouts, and T. Abee. Flow cytometric assessment of viability of lactic acid bacteria. *Applied and Environmental Microbiology*, 67: 2326–2335, 2001.
- G. Camenisch, G. Folkers, and H. van de Waterbeemd. Review of theoretical passive drug absorption models: Historical background, recent developments and limitations. *Pharmaceutica Acta Helveticae*, 71:309–327, 1996.

- G. Camenisch, J. Alsenz, H. van de Waterbeemd, and G. Folkers. Estimation of permeability by passive diffusion through Caco-2 cell monolayers using the drug's lipophilicity and molecular weight. *European Journal of Pharmaceutical Sciences*, 6:313–319, 1998.
- G. Cevc. Membrane electrostatics. *Biochimica Biophysica Acta*, 1031:311–382, 1990.
- A. C. Chakrabarti, I. Clark-Lewis, and P. R. Cullis. Influence of charge, charge distribution, and hydrophobicity on the transport of short model peptides into liposomes in response to transmembrane pH gradients. *Biochemistry*, 33:8479–8485, 1994.
- W. S. Cleveland. *Visualizing Data*. Hobart Press, Summit, New Jersey, 1993.
- J. Cordy, N. Hooper, and A. Turner. The involvement of lipid rafts in Alzheimer's disease. *Molecular Membrane Biology*, 23:111–122, 2006.
- E. Corvera, O. G. Mouritsen, M. A. Singer, and M. J. Zuckermann. The permeability and the effect of acyl-chain length for phospholipid bilayers containing cholesterol: theory and experiment. *Biochimica et Biophysica Acta*, 1107:261–270, 1992.
- G. Daum. Lipids of mitochondria. *Biochimica et Biophysica Acta*, 822:1–42, 1985.
- J. De Gier, J. G. Mandersloot, and L. L. M. Van Deenen. Lipid composition and permeability of liposomes. *Biochimica et Biophysica Acta*, 150:666–675, 1968.
- D. W. Deamer. The first living systems: A bioenergetic perspective. *Microbiology and Molecular Biology Reviews*, 61:239–261, 1997.
- E. Deconinck, D. Coomans, and Y. Vander Heyden. Exploration of linear modelling techniques and their combination with multivariate adaptive regression splines to predict gastro-intestinal absorption of drugs. *Journal of Pharmaceutical and Biomedical Analysis*, In Press, 2006.
- L. Di, E. H. Kerns, K. Fan, O. J. McConnell, and G. T. Carter. High throughput artificial membrane permeability assay for blood-brain barrier. *European Journal of Medicinal Chemistry*, 38:223–232, 2003.
- J. M. Diamond and Y. Katz. Interpretation of nonelectrolyte partition coefficients between dimyristoyl lecithin and water. *Journal of Membrane Biology*, 17:121–154, 1974.
- E. A. Disalvo and S. Simon, editors. *Permeability and stability of lipid bilayers*. CRC Press, Florida, U.S., 1995.
- C. Dordas and P. H. Brown. Permeability of boric acid across lipid bilayers and factors affecting it. *Journal of Membrane Biology*, 175:95–105, 2000.
- A. Egorova and S. Beltyukova. Sensitization of europium luminescence in complexes with thiaprophenic acid. *Journal of Fluorescence*, 9:245–249, 1999.
- A. Egorova, S. Beltyukova, O. Teslyuk, and V. Karpinchik. Application of f–f luminescence of terbium ion for determination of non-steroidal anti-inflammatory drug niflumic acid. *Journal of Pharmaceutical and Biomedical Analysis*, 24:1081–1085, 2001.

Bibliography

- N. el Tayar, R. S. Tsai, B. Testa, P. A. Carrupt, C. Hansch, and A. Leo. Percutaneous penetration of drugs: A quantitative structure-permeability relationship study. *Journal of Pharmaceutical Sciences*, 80:744–749, 1991a.
- N. el Tayar, R. S. Tsai, B. Testa, P. A. Carrupt, and A. Leo. Partitioning of solutes in different solvent systems: the contribution of hydrogen-bonding capacity and polarity. *Journal of Pharmaceutical Sciences*, 80:590–8, 1991b.
- M. Elbanowski and B. Makowska. The lanthanides as luminescent probes in investigations of biochemical systems. *Journal of Photochemistry and Photobiology*, 99:85–92, 1996.
- D. M. Engelman. Membranes are more mosaic than fluid. *Nature*, 438:578–580, 2005.
- L. Erikson, E. Johansson, N. Kettaneh-Wold, and S. Wold. *Multi- and Megavariate Data Analysis*. Umetrics AB, Umeå, Sweden, 2001.
- G. D. Eytan. Mechanism of multidrug resistance in relation to passive membrane permeation. *Biomedicine and Pharmacotherapy*, 59:90–97, 2005.
- G. D. Eytan and P. W. Kuchel. Mechanism of action of P-glycoprotein in relation to passive membrane permeation. *International Review of Cytology*, 190:175–250, 1999.
- G. D. Eytan, R. Regev, G. Oren, and Y. G. Assaraf. The role of passive transbilayer drug movement in multidrug resistance and its modulation. *Journal of Biological Chemistry*, 271: 12897–12902, 1996.
- M. Fix and D. L. Melchior. The fluorosomeTM technique for investigating membrane on- and off-loading of drugs by beta-CD and sonicated SUV. *FEBS Letters*, 516:109–112, 2002.
- G. E. Flaten, H. Bunjes, K. Luthman, and M. Brandl. Drug permeability across a phospholipid vesicle-based barrier 2. Characterization of barrier structure, storage stability and stability towards pH changes. *European Journal of Pharmaceutical Sciences*, 28:336–343, 2006a.
- G. E. Flaten, A. B. Dhanikula, K. Luthman, and M. Brandl. Drug permeability across a phospholipid vesicle based barrier: A novel approach for studying passive diffusion. *European Journal of Pharmaceutical Sciences*, 27:80–90, 2006b.
- Th. Förster. Zwischenmolekulare Energiewanderung und Fluoreszenz. *Annalen der Physik*, 2: 285–303, 1948.
- Free online Cheminformatics Services. Molinspiration, July 2006. URL <http://www.molinspiration.com>.
- F. Frezard and A. Garnier-Suillerot. DNA-containing liposomes as a model for the study of cell membrane permeation by anthracycline derivatives. *Biochemistry*, 30:5038–5043, 1991.
- F. Frezard and A. Garnier-Suillerot. Permeability of lipid bilayer to anthracycline derivatives. Role of the bilayer composition and of the temperature. *Biochimica et Biophysica Acta*, 1389: 13–22, 1998.

- M. Fujikawa, R. Ano, K. Nakao, R. Shimizu, and M. Akamatsu. Relationships between structure and high-throughput screening permeability of diverse drugs with artificial membranes: Application to prediction of Caco-2 cell permeability. *Bioorganic and Medicinal Chemistry*, 13:4721–4732, 2005.
- J. Gardiner, A. V. Thomae, R. I. Mathad, D. Seebach, and S. D. Krämer. Comparison of permeation through phosphatidylcholine bilayers of N-Dipicolinyl- α - and β -Oligopeptides. *Chemistry and Biodiversity*, 3:1181–1201, 2006.
- P. Geladi and B. R. Kowalski. Partial least-squares regression: A tutorial. *Analytica Chimica Acta*, 185:1–17, 1986.
- A. Gomez-Hens and M. P. Aguilar-Caballo. Terbium-sensitized luminescence: A selective and versatile analytical approach. *Trends in Analytical Chemistry*, 21:131–141, 2002.
- J. T. Goodwin, R. A. Conradi, N. F. Ho, and P. S. Burton. Physicochemical determinants of passive membrane permeability: Role of solute hydrogen-bonding potential and volume. *Journal of Medicinal Chemistry*, 44:3721–3729, 2001.
- J. Gutknecht and D. C. Tosteson. Diffusion of weak acids across lipid bilayer membranes: Effects of chemical reactions in the unstirred layers. *Science*, 182:1258–1261, 1973.
- J. Gutknecht and D. C. Tosteson. Diffusion of weak acids through lipid bilayer membranes. Role of chemical reactions in the unstirred layer. *Science*, 182:1258–1261, 1982.
- C. Hansch, A. Leo, S. B. Mekapati, and A. Kurup. QSAR and ADME. *Bioorganic and Medicinal Chemistry*, 12:3391–3400, 2004.
- K. Hashizaki, H. Taguchi, C. Itoh, H. Sakai, M. Abe, Y. Saito, and N. Ogawa. Effects of poly(ethylene glycol) (PEG) chain length of PEG-lipid on the permeability of liposomal bilayer membranes. *Chemical and Pharmaceutical Bulletin*, 51:815–820, 2003.
- K. Hashizaki, H. Taguchi, H. Sakai, M. Abe, Y. Saito, and N. Ogawa. Carboxyfluorescein leakage from poly(ethylene glycol)-grafted liposomes induced by the interaction with serum. *Chemical and Pharmaceutical Bulletin*, 54:80–84, 2006.
- J. Henriksen, A. C. Rowat, E. Brief, Y. W. Hsueh, J. L. Thewalt, M. J. Zuckermann, and J. H. Ipsen. Universal behavior of membranes with sterols. *Biophysical Journal*, 90:1639–49, 2006.
- C. A. Hogben, D. J. Tocco, B. B. Brodie, and L. S. Schanker. On the mechanism of intestinal absorption of drugs. *Journal of Pharmacology and Experimental Therapeutics*, 125:275–282, 1959.
- J. M. Holopainen, M. I. Angelova, and P. K. Kinnunen. Vectorial budding of vesicles by asymmetrical enzymatic formation of ceramide in giant liposomes. *Biophysical Journal*, 78:830–8, 2000.
- M. J. Hope, M. B. Bally, G. Webb, and P. R. Cullis. Production of large unilamellar vesicles by a rapid extrusion procedure. characterization of size distribution, trapped volume and ability to maintain a membrane potential. *Biochimica et Biophysica Acta*, 812:55–65, 1985.

Bibliography

- C. Huang and J. T. Mason. Geometric packing constraints in egg phosphatidylcholine vesicles. *Proceedings of the National Academy of Sciences of the United States of America*, 75:308–310, 1978.
- J. H. Ipsen, G. Karlstrom, O. G. Mouritsen, H. Wennerstrom, and M. J. Zuckermann. Phase equilibria in the phosphatidylcholine-cholesterol system. *Biochimica et Biophysica Acta*, 905:162–172, 1987.
- M. Jansen and A. Blume. A comparative study of diffusive and osmotic water permeation across bilayers composed of phospholipids with different head groups and fatty acyl chains. *Biophysical Journal*, 68:997–1008, 1995.
- N. Kahya, D. Scherfeld, K. Bacia, and P. Schwille. Lipid domain formation and dynamics in giant unilamellar vesicles explored by fluorescence correlation spectroscopy. *Journal of Structural Biology*, 147:77–89, 2004.
- M. Kansy, F. Senner, and K. Gubernator. Physicochemical high throughput screening: Parallel artificial membrane permeation assay in the description of passive absorption processes. *Journal of Medicinal Chemistry*, 41:1007–1010, 1998.
- E. H. Kerns. High throughput physicochemical profiling for drug discovery. *Journal of Pharmaceutical Sciences*, 90:1838–1858, 2001.
- Y. Kobayashi, T. Komatsu, M. Sumi, S. Numajiri, M. Miyamoto, D. Kobayashi, K. Sugibayashi, and Y. Morimoto. In vitro permeation of several drugs through the human nail plate: Relationship between physicochemical properties and nail permeability of drugs. *European Journal of Pharmaceutical Sciences*, 21:471–477, 2004.
- R. Kramer. *Chemometric techniques for quantitative analysis*. Marcel Dekker, New York, USA, 1998.
- S. D. Krämer. Liposome/water partitioning: Theory, techniques and applications. In B. Testa, H. van de Waterbeemd, G. Folkers, and R. Guy, editors, *Pharmacokinetic Optimization in Drug Research: Biological, Physicochemical and Computational Strategies*, pages 401–428. VCHA and Wiley-VCH, Zurich and Weinheim, 2001.
- S. D. Krämer. Lipid bilayers in ADME: Permeation barriers and distribution compartments. In B. Testa, S.D. Krämer, H. Wunderli-Allenspach, and G. Folkers, editors, *Pharmacokinetic Profiling in Drug Research: Biological, Physicochemical and Computational Strategies*. Wiley-VCH, Weinheim, 2006.
- S. D. Krämer. Absorption prediction from physicochemical parameters. *Pharmaceutical Science and Technology Today*, 2:373–380, 1999.
- S. D. Krämer and H. Wunderli-Allenspach. Physicochemical properties in pharmacokinetic lead optimization. *Il Farmaco*, 56:145–148, 2001.
- S. D. Krämer and H. Wunderli-Allenspach. No entry for TAT(44-57) into liposomes and intact MDCK cells: Novel approach to study membrane permeation of cell-penetrating peptides. *Biochimica et Biophysica Acta*, 1609:161–169, 2003.

- S. D. Krämer, C. Jakits-Deiser, and H. Wunderli-Allenspach. Free fatty acids cause pH-dependent changes in drug-lipid membrane interactions around physiological pH. *Pharmaceutical Research*, 14:827–832, 1997.
- S. D. Krämer, A. Braun, C. Jakits-Deiser, and H. Wunderli-Allenspach. Towards the predictability of drug-lipid membrane interactions: the pH-dependent affinity of propranolol to phosphatidylinositol containing liposomes. *Pharmaceutical Research*, 15:739–744, 1998a.
- S. D. Krämer, J.-C. Gautier, and P. Saudemon. Considerations on the potentiometric log P determination. *Pharmaceutical Research*, 15:1310–1313, 1998b.
- S. D. Krämer, J. A. Hurley, D. J. Begley, and N. J. Abbott. Lipids in blood-brain barrier models in vitro I: TLC and HPLC for the analysis of lipid classes and long polyunsaturated fatty acids. *In Vitro Cellular and Developmental Biology - Animal*, 38:557–565, 2002.
- A. V. Krylov, P. Pohl, M. L. Zeidel, and W. G. Hill. Water permeability of asymmetric planar lipid bilayers: leaflets of different composition offer independent and additive resistances to permeation. *Journal of General Physiology*, 118:333–340, 2001.
- H. Kubinyi. Lipophilicity and biological activity. Drug transport and drug distribution in model systems and in biological systems. *Arzneimittelforschung*, 29:1067–1080, 1979.
- D. Kurad, G. Jeschke, and D. Marsh. Lateral ordering of lipid chains in cholesterol-containing membranes: high-field spin-label EPR. *Biophysical Journal*, 86:264–271, 2004.
- A. Kusumi, W. K. Subczynski, M. Pasenkiewicz-Gierula, J. S. Hyde, and H. Merkle. Spin-label studies on phosphatidylcholine-cholesterol membranes: effects of alkyl chain length and unsaturation in the fluid phase. *Biochimica et Biophysica Acta*, 854:307–317, 1986.
- C. Lagerquist, F. Beigi, A. Karlen, H. Lennernas, and P. Lundahl. Effects of cholesterol and model transmembrane proteins on drug partitioning into lipid bilayers as analysed by immobilized-liposome chromatography. *Journal of Pharmacy and Pharmacology*, 53:1477–1487, 2001.
- P. Lauger, R. Benz, G. Stark, E. Bamberg, P. C. Jordan, A. Fahr, and W. Brock. Relaxation studies of ion transport systems in lipid bilayer membranes. *Quarterly Reviews of Biophysics*, 14:513–598, 1981.
- R. Lawaczeck. Defect structures in membranes: routes of the permeation of small molecules. *Berichte der Bunsen-Gesellschaft für Physikalische Chemie*, 92:961–963, 1988.
- H. Lennernas. Human intestinal permeability. *Journal of Pharmaceutical Sciences*, 87:403–410, 1998.
- C. A. Lipinski, F. Lombardo, B. W. Dominy, and P. J. Feeney. Experimental and computational approaches to estimate solubility and permeability in drug discovery and development settings. *Advanced Drug Delivery Reviews*, 46:3–26, 2001.
- T. Loftsson, F. Konradsdottir, and M. Masson. Development and evaluation of an artificial membrane for determination of drug availability. *International Journal of Pharmaceutics*, 326:60–68, 2006.

Bibliography

- R. E. London. Correlation of carboxyl carbon titration shifts and pK values. *Journal of Magnetic Resonance*, 38:173–177, 1980.
- S. Maji, K. Sundararajan, and K. S. Viswanathan. Effect of ligand structure on synergism in Tb³⁺-aromatic acid complexes: Fluorescence lifetime studies. *Spectrochimica Acta Part A: Molecular and Biomolecular Spectroscopy*, 59:455–461, 2003.
- R. G. Males and F. G. Herring. A ¹H-NMR study of the permeation of glycolic acid through phospholipid membranes. *Biochimica et Biophysica Acta*, 1416:333–338, 1999.
- R. G. Males, J. C. Nelson, P. S. Phillips, W. R. Cullen, and F. G. Herring. Vesicular membrane permeability of monomethylarsonic and dimethylarsinic acids. *Biophysical Chemistry*, 70: 75–85, 1998.
- A. Malkia, L. Murtomaki, A. Urtti, and K. Kontturi. Drug permeation in biomembranes: In vitro and in silico prediction and influence of physicochemical properties. *European Journal of Pharmaceutical Sciences*, 23:13–47, 2004.
- M. Marenchino, A. L. Alpstag-Wohrle, B. Christen, H. Wunderli-Allenspach, and S. D. Krämer. alpha-Tocopherol influences the lipid membrane affinity of desipramine in a pH-dependent manner. *European Journal of Pharmaceutical Sciences*, 21:313–321, 2004.
- S. J. Marrink and H. J. Berendsen. Permeation process of small molecules across lipid membranes studied by molecular dynamics simulations. *Journal of Physical Chemistry*, 100: 16729–16738, 1996.
- D. Marsh. *CRC Handbook of Lipid Bilayers*. CRC Press, Boca Raton, Florida, 1990.
- R. B. Martin and F. S. Richardson. Lanthanides as probes for calcium in biological systems. *Quarterly Reviews of Biophysics*, 12:181–209, 1979.
- R. C. Mashru, V. B. Sutariya, M. G. Sankalia, and J. M. Sankalia. Effect of pH on in vitro permeation of ondansetron hydrochloride across porcine buccal mucosa. *Pharmaceutical Development and Technology*, 10:241–247, 2005.
- S. McLaughlin. The electrostatic properties of membranes. *Annual Review of Biophysics and Biophysical Chemistry*, 18:113–136, 1989.
- L. A. Meijer, F. A. M. Leermakers, and J. Lyklema. Self-consistent-field modeling of complex molecules with united atom detail in inhomogeneous system. Cyclic and branched foreign molecules in dimyristoylphosphatidylcholine membranes. *Journal of Chemical Physics*, 110: 6560–6579, 1999.
- L. Miao, M. Nielsen, J. Thewalt, J. H. Ipsen, M. Bloom, M. J. Zuckermann, and O. G. Mouritsen. From lanosterol to cholesterol: Structural evolution and differential effects on lipid bilayers. *Biophysical Journal*, 82:1429–1444, 2002.
- E. Migliavacca. Applied introduction to multivariate methods used in drug discovery. *Mini Reviews in Medicinal Chemistry*, 3:831–848, 2003.

- S. Mitragotri, M. E. Johnson, D. Blankschtein, and R. Langer. An analysis of the size selectivity of solute partitioning, diffusion, and permeation across lipid bilayers. *Biophysical Journal*, 77:1268–1283, 1999.
- Y. Morono, S. Takano, K. Miyanaga, Y. Tanji, H. Unno, and K. Hori. Application of glutaraldehyde for the staining of esterase-active cells with carboxyfluorescein diacetate. *Biotechnology Letters*, 26:379–383, 2004.
- O. G. Mouritsen and K. Jorgensen. Dynamical order and disorder in lipid bilayers. *Chemistry and Physics of Lipids*, 73:3–25, 1994.
- O. G. Mouritsen and K. Jorgensen. Small-scale lipid-membrane structure: Simulation versus experiment. *Current Opinion in Structural Biology*, 7:518–527, 1997.
- O. G. Mouritsen and M. J. Zuckermann. What's so special about cholesterol? *Lipids*, 39:1101–1113, 2004.
- R. Neubert. Ion pair transport across membranes. *Pharmaceutical Research*, 6:743–747, 1989.
- H. Nogami and T. Matsuzawa. Studies on absorption and excretion of drugs. I. Kinetics of penetration of acidic drug, salicylic acid, through the intestinal barrier in vitro. *Chemical and Pharmaceutical Bulletin*, 9:532–540, 1961.
- U. Norinder, T. Osterberg, and P. Artursson. Theoretical calculation and prediction of intestinal absorption of drugs in humans using MolSurf parametrization and PLS statistics. *European Journal of Pharmaceutical Sciences*, 8:49–56, 1999.
- J. A. Ocana, M. Callejon, and F. J. Barragan. Application of terbium-sensitized luminescence for the determination of grepafloxacin in human urine and serum. *Journal of Pharmaceutical Sciences*, 90:1553–1557, 2001.
- E. Overton. Über die osmotischen Eigenschaften der lebenden Pflanzen- und Tierzelle. *Vierteljahresschrift der Naturforschenden Gesellschaft Zürich*, 44:88–135, 1899.
- A. Pagliara, P. A. Carrupt, G. Caron, P. Gaillard, and B. Testa. Lipophilicity profile of ampholytes. *Chemical Reviews*, 97:3385–3400, 1997.
- A. Pagliara, M. Reist, S. Geinoz, P. A. Carrupt, and B. Testa. Evaluation and prediction of drug permeation. *Journal of Pharmacy and Pharmacology*, 51:1339–1357, 1999.
- K. Palm, P. Stenberg, K. Luthman, and P. Artursson. Polar molecular surface properties predict the intestinal absorption of drugs in humans, 1997.
- K. Palm, K. Luthman, J. Ros, J. Grasjo, and P. Artursson. Effect of molecular charge on intestinal epithelial drug transport: pH-dependent transport of cationic drugs. *Journal of Pharmacology and Experimental Therapeutics*, 291:435–443, 1999.
- T. Parasassi, A. M. Giusti, M. Raimondi, and E. Gratton. Abrupt modifications of phospholipid bilayer properties at critical cholesterol concentrations. *Biophysical Journal*, 68:1895–1902, 1995.

Bibliography

- W. M. Pardridge. Transport of small molecules through the blood-brain barrier: Biology and methodology. *Advanced Drug Delivery Reviews*, 15:5–36, 1995.
- S. Paula, A. Volkov, and D. Deamer. Permeation of halide anions through phospholipid bilayers occurs by the solubility-diffusion mechanism. *Biophysical Journal*, 74:319–327, 1998.
- G. M. Pauletti and H. Wunderli-Allenspach. Partition coefficients in vitro: Artificial membranes as a standardized distribution model. *European Journal of Pharmaceutical Sciences*, 1:273–282, 1994.
- T. J. T. Pinheiro. The role of rafts in the fibrillization and aggregation of prions. *Chemistry and Physics of Lipids*, 141:66–71, 2006.
- M. Ptak, M. Egret-Charlier, A. Sanson, and O. Bouloussa. A NMR study of the ionization of fatty acids, fatty amines and N-acylamino acids incorporated in phosphatidylcholine vesicles. *Biochimica et Biophysica Acta*, 600:387–397, 1980.
- R Development Core Team. *R: A Language and Environment for Statistical Computing*. R Foundation for Statistical Computing, Vienna, Austria, 2006. URL <http://www.R-project.org>.
- J.-L. Rigaud, B. Pitard, and D. Levy. Reconstitution of membrane proteins into liposomes: Application to energy-transducing membrane proteins. *Biochimica et Biophysica Acta (BBA) - Bioenergetics*, 1231:223–246, 1995.
- J. A. Ruell, K. L. Tsinman, and A. Avdeef. PAMPA—a drug absorption in vitro model: 5. Unstirred water layer in iso-pH mapping assays and pKaflux-optimized design (pOD-PAMPA). *European Journal of Pharmaceutical Sciences*, 20:393–402, 2003.
- S. M. Saparov, Y. N. Antonenko, and P. Pohl. A new model of weak acid permeation through membranes revisited: Does overton still rule? *Biophysical Journal*, 90:L86–88, 2006.
- European Pharmacopoeia Secretariat. *European Pharmacopoeia*. Strasbourg, 1997.
- D. Seebach, P. E. Ciceri, M. Overhand, B. Jaun, D. Rigo, L. Oberer, U. Hommel, R. Amstutz, and H. Widmer. Probing the helical secondary structure of short-chain beta-peptides. *Helvetica Chimica Acta*, 79:2043–2066, 1996.
- D. Seebach, K. Namoto, Y. R. Mahajan, P. Bindschädler, R. Sustmann, M. Kirsch, N. S. Ryder, M. Weiss, M. Sauer, C. Roth, S. Werner, H.-D. Beer, C. Munding, P. Walde, and M. Voser. Chemical and biological investigations of beta-oligoarginines. *Chemistry and Biodiversity*, 1: 65–97, 2004.
- P. R. Selvin and J. E. Hearst. Luminescence energy transfer using a terbium chelate: Improvements on fluorescence energy transfer. *Proceedings of the National Academy of Sciences of the United States of America*, 91:10024–10028, 1994.
- P. A. Shore, B. B. Brodie, and C. A. Hogben. The gastric secretion of drugs: a pH partition hypothesis. *Journal of Pharmacology and Experimental Therapeutics*, 119:361–369, 1957.
- A. Sigler, P. Schubert, W. Hillen, and M. Niederweis. Permeation of tetracyclines through membranes of liposomes and escherichia coli. *European Journal of Biochemistry*, 267:527–534, 2000.

- M. Silvander, M. Johnsson, and K. Edwards. Effects of PEG-lipids on permeability of phosphatidylcholine/cholesterol liposomes in buffer and in human serum. *Chemistry and Physics of Lipids*, 97:15–26, 1998.
- K. Simons and R. Ehehalt. Cholesterol, lipid rafts, and disease. *Journal of Clinical Investigation*, 110:597–603, 2002.
- K. Simons and D. Toomre. Lipid rafts and signal transduction. *Nature Reviews Molecular Cell Biology*, 1:31–39, 2000.
- S. J. Singer and G. L. Nicolson. The fluid mosaic model of the structure of cell membranes. *Science*, 175:720–731, 1972.
- R. Singh, M. Ajagbe, S. Bhamidipati, Z. Ahmad, and I. Ahmad. A rapid isocratic high-performance liquid chromatography method for determination of cholesterol and 1,2-dioleoyl-sn-glycero-3-phosphocholine in liposome-based drug formulations. *Journal of Chromatography A*, 1073:347–353, 2005.
- W. D. Stein. *Transport and Diffusion across Cell Membranes*. Academic Press, inc., Orlando, 1 edition, 1986.
- W. D. Stein. Kinetics of the multidrug transporter P-glycoprotein and its reversal. *Physiological Reviews*, 77:545–590, 1997.
- R. M. Straubinger, K. Hong, D. S. Friend, and D. Papahadjopoulos. Endocytosis of liposomes and intracellular fate of encapsulated molecules: encounter with a low pH compartment after internalization in coated vesicles. *Cell*, 32:1069–1079, 1983.
- K. Sugano, H. Hamada, M. Machida, H. Ushio, K. Saitoh, and K. Terada. Optimized conditions of bio-mimetic artificial membrane permeation assay. *International Journal of Pharmaceutics*, 228:181–188, 2001.
- K. Takacs-Novak and G. Szasz. Ion-pair partition of quaternary ammonium drugs: The influence of counter ions of different lipophilicity, size, and flexibility. *Pharmaceutical Research*, 16:1633–1638, 1999.
- H. Takanaga, I. Tamai, and A. Tsuji. pH-dependent and carrier-mediated transport of salicylic acid across Caco-2 cells. *Journal of Pharmacy and Pharmacology*, 46:567–570, 1994.
- B. Testa, P. A. Carrupt, P. Gaillard, F. Billois, and P. Weber. Lipophilicity in molecular modeling. *Pharmaceutical Research*, 13:335–343, 1996.
- I. V. Tetko. Virtual Computational Chemistry Laboratory, July 2006. URL <http://www.vcclab.org/>.
- I. V. Tetko, J. Gasteiger, R. Todeschini, A. Mauri, D. Livingstone, P. Ertl, V. A. Palyulin, E. V. Radchenko, N. S. Zefirov, A. S. Makarenko, V. Y. Tanchuk, and V. V. Prokopenko. Virtual computational chemistry laboratory—design and description. *Journal of Computer-Aided Molecular Design*, 19:453–463, 2005.

Bibliography

- A. V. Thomaе, H. Wunderli-Allenspach, and S. D. Krämer. Permeation of aromatic carboxylic acids across lipid bilayers: the pH-partition hypothesis revisited. *Biophysical Journal*, 89: 1802–1811, 2005.
- A. V. Thomaе, T. Koch, C. Panse, H. Wunderli-Allenspach, and S. D. Krämer. Comparing the lipid membrane affinity and permeation of drug-like acids: The intriguing effects of cholesterol and charged lipids. submitted.
- H. Ti Tien and A. Ottova-Leitmannova. *Membrane biophysics*, volume 5 of *Membrane Science and Technology Series*. Elsevier, Amsterdam, 2000.
- University of Georgia. Sparc, July 2006. URL <http://ibmlc2.chem.uga.edu/sparc/>.
- J. A. Urbina, S. Pekerar, H. B. Le, J. Patterson, B. Montez, and E. Oldfield. Molecular order and dynamics of phosphatidylcholine bilayer membranes in the presence of cholesterol, ergosterol and lanosterol: a comparative study using ²h-, ¹³c- and ³¹p-nmr spectroscopy. *Biochimica et Biophysica Acta*, 1238:163–176, 1995.
- H. van de Waterbeemd, G. Camenisch, G. Folkers, J. R. Chretien, and O. A. Raevsky. Estimation of blood-brain barrier crossing of drugs using molecular size and shape, and H-bonding descriptors. *Journal of Drug Targeting*, 6:151–165, 1998.
- W. L. Vaz. Percolation properties of two-component, two-phase phospholipid bilayers. *Molecular Membrane Biology*, 12:39–43, 1995.
- D. F. Veber, S. R. Johnson, H. Y. Cheng, B. R. Smith, K. W. Ward, and K. D. Kopple. Molecular properties that influence the oral bioavailability of drug candidates. *Journal of Medicinal Chemistry*, 45:2615–2623, 2002.
- J. N. Weinstein, S. Yoshikami, P. Henkart, R. Blumenthal, and W. A. Hagins. Liposome-cell interaction: Transfer and intracellular release of a trapped fluorescent marker. *Science*, 195: 489–492, 1977.
- J. Wilschut, N. Duzgunes, R. Fraley, and D. Papahadjopoulos. Studies on the mechanism of membrane fusion: Kinetics of calcium ion induced fusion of phosphatidylserine vesicles followed by a new assay for mixing of aqueous vesicle contents. *Biochemistry*, 19:6011–6021, 1980.
- M. A. Wilson and A. Pohorille. Mechanism of unassisted ion transport across membrane bilayers. *Journal of the American Chemical Society*, 118:6580–6587, 1996.
- S. Winiwarter, N. M. Bonham, F. Ax, A. Hallberg, H. Lennernäs, and A. Karlen. Correlation of human jejunal permeability (in vivo) of drugs with experimentally and theoretically derived parameters. A multivariate data analysis approach. *Journal of Medicinal Chemistry*, 41:4939–4949, 1998.
- D. Winne. Shift of pH-absorption curves. *Journal of Pharmacokinetics and Biopharmaceutics*, 5:53–94, 1977.
- T. Xiang, Y. Xu, and B. D. Anderson. The barrier domain for solute permeation varies with lipid bilayer phase structure. *Journal of Membrane Biology*, 165:77–90, 1998.

- M. Yazdanian, S. L. Glynn, J. L. Wright, and A. Hawi. Correlating partitioning and Caco-2 cell permeability of structurally diverse small molecular weight compounds. *Pharmaceutical Research*, 15:1490–1494, 1998.
- P. L. Yeagle, W. C. Hutton, C. Huang, and R. B. Martin. Phospholipid head-group conformations; intermolecular interactions and cholesterol effects. *Biochemistry*, 16:4344–4349, 1977.
- Y. H. Zhao, M. H. Abraham, J. Le, A. Hersey, C. N. Luscombe, G. Beck, B. Sherborne, and I. Cooper. Rate-limited steps of human oral absorption and QSAR studies. *Pharmaceutical Research*, 19:1446–1457, 2002.
- R. Zhu and W. T. Kok. Determination of catecholamines and related compounds by capillary electrophoresis with postcolumn terbium complexation and sensitized luminescence detection. *Analytical Chemistry*, 69:4010–4016, 1997.

Acknowledgements

To my experience, a Ph.D. thesis is a daily adventure, which can not be undertaken alone. A lot of people contributed to this thesis.

First of all, I would like to express my thanks to my supervisor Prof. Dr. Heidi Wunderli-Allenspach. She led my Ph.D. studies with a lot of experience through the storms, low tides and downwinds. I am grateful for her encouraging and critical advise.

My co-referee Dr. Stefanie D. Krämer was a continuous support through all the years, and our discussions helped a lot to illuminate a number of problems. Her enthusiasm and helpfulness at any day- or nighttime was always a big motivation. Many thanks.

I am very grateful to Prof. Dr. Karl-Heinz Altmann for his friendly acception to be my co-referee and for his valuable advice.

Maja Günthert was not only an expert in organizing everything at the right time, but was a big help for me in conducting the permeation experiments and introducing me in the tricky language of Schwyzerdütsch.

Tamara Koch was my Diploma student in the summer term of 2005 and she did an excellent work investigating the influence of cholesterol on membrane permeation.

I shared a project with Prof. Dr. Dieter Seebach and Dr. James Gardiner and I am grateful to them for their introduction into the world of peptide synthesis. James synthesized a battery of different peptides and gave me the possibility to learn peptide synthesis on my own, which was a precious experience for me.

Many thanks to Dr. Peter Ertl, Novartis for our discussions concerning the multivariate analysis results. I am grateful to Dr. Bernhard Pfeiffer, who spent a lot of time with me setting up the NMR pilot experiments and who taught me the usage of the instrument. Many thanks also to Dr. Manuel Morillas, who introduced me into the stopped-flow technique.

Special thanks are due to my daily labmates. My time at the ETH Zurich will be unforgettable due to the interesting people from all over Europe I met here. Thanks to all of them for sharing the everyday joy and sorrows as well as scientific discussions. Thanks to Jiří Hofmann, for his continous support with delicious Czech cookies. Thanks to Marco Marenchino, for teaching me the art of liposome preparation and italian cooking. Thanks to Karsten Bucher, "the other German" in the lab, for his precious advise especially in the beginning of the Ph.D. Thanks to Sara Belli, for transferring her passion for classical music to me. Thanks to Dario Lombardi, who joined into the permeation project, for the nice discussions and his grandmother's recipes. Also, I would like to wish good luck to my new colleagues Samuel Murri and Denise Ilgen.

I am grateful to my friends from the Martin-Luther-University Halle, Marian Brandau and Knud Zabrocki, as well as Frank Potthast, Zurich, who initialised the PermSim solution.

Certainly, I would also like to thank Rene Bemsel and his team from the PharmaShop as well as our IT group Tanasis Galicidasis, Tibor Kovacs and Monika Langfritz for their efforts.

Finally, I am grateful to my family for their support, encouragement and understanding during the last years. Christian Panse was especially patient in sharing the everyday trouble and solved many problems with his careful advise. I am also happy about our PermSim project which we completed together and I am looking forward to our future projects.

Curriculum vitae

Biographical data

Name Anita Verena Thomae
Date of birth 06. 05. 1979
Place of birth Dohna, Germany

Education and Professional Experience

02/2003 – 12/2006 Ph.D. Studies in Biopharmacy, Department of Chemistry and Applied Biosciences, ETH Zurich, Switzerland
12/2002 – 01/2003 Pharmacy “Park-Apotheke” Wörlitz, Sachsen-Anhalt, Germany
04/2002 – 10/2002 Pharmacy “Hof-Apotheke” Meersburg, Baden-Württemberg, Germany
10/2001 – 03/2002 Diploma Thesis (Title: ”Characterization of interactions between Hyaluronic acid and Lidocaine”) at the Martin-Luther-University Halle-Wittenberg, Germany
10/1997 – 10/2002 Studies in Pharmaceutical Sciences, Martin-Luther-University Halle-Wittenberg, Germany
07/1997 Final school exams, Latina “August-Hermann-Francke”, Halle, Germany

Publication list

Journal Articles

- T. Shimanouchi, P. Walde, J. Gardiner, Y. R. Mahajan, D. Seebach, A. V. Thomae, S. D. Krämer, M. Voser and R. Kuboi. Permeation of a beta-heptapeptide derivative across phospholipid bilayers. *manuscript in preparation*.
- A. V. Thomae, T. Koch, C. Panse, H. Wunderli-Allenspach and S. D. Krämer. Comparing the lipid membrane affinity and permeation of drug-like acids: The intriguing effects of cholesterol and charged lipids. *manuscript submitted*.
- J. Gardiner, A. V. Thomae, R.I. Mathad, D. Seebach and S. D. Krämer. Comparison of permeation through phosphatidylcholine bilayers of N-dipicolinyl-alpha- and beta-oligo-peptides. *Chemistry and Biodiversity*, 3:1181-1201, 2006
- A. V. Thomae, H. Wunderli-Allenspach and S. D. Krämer. Permeation of aromatic carboxylic acids across lipid bilayers: the pH-partition hypothesis revisited. *Biophysical Journal*, 89:1802-1811, 2005.
- H. Wunderli-Allenspach, K. Bucher, J. Hofmann, M. Marenchino, A. V. Thomae, M. Günthert, S. D. Krämer. Exploring barrier mechanisms relevant for drug therapy. *Chimia*, 58:681-683, 2004

Oral communications

- *4th Symposium on Engineering Science of Liposomes*. Zurich, Switzerland, 2006: Bilayer permeation of aromatic carboxylic acids in liposomes: Influence of pH and lipid composition.
- *LogP2004*. Zurich, Switzerland, 2004: Influence of Solute Properties and Membrane Composition on Lipid Bilayer Permeation.

Posters

- *Conference on Optimisation of Drug-Like Properties of Leads in Discovery: Fine-Tuning the PhysChem-Biopharmaceutical-ADME-Tox Profile*. Zurich, Switzerland, 2006: Comparing the lipid membrane affinity and permeation of drug-like acids: the intriguing effects of cholesterol and charged lipids.
- *International Biophysics Congress.*, Montpellier, France, 2005: Influence of pH and lipid composition on lipid bilayer permeation of small aromatic carboxylic acids.
- *Mechanisms of Carrier-Mediated Intracellular Delivery of Therapeutics*. Montpellier, France, 2006: A liposomal assay to study lipid bilayer permeation of cell penetrating peptides.

Publication list

- *LogP2004*. Zurich, Switzerland, 2004: Lipid Bilayer Permeation: Influence of Solute Properties and Membrane Composition